RESONANT INDUCTIVE WIRELESS POWER TRANSFER SYSTEM FOR WIRELESS CAPSULE ENDOSCOPY APPLICATION

MD. RUBEL BASAR

FACULTY OF ENGINEERING
UNIVERSITY OF MALAYA
KUALA LUMPUR

2017

University of Malaya

RESONANT INDUCTIVE WIRELESS POWER TRANSFER SYSTEM FOR WIRELESS CAPSULE ENDOSCOPY APPLICATION

MD. RUBEL BASAR

THESIS SUBMITTED IN FULFILMENT OF THE REQUIREMENTS FOR THE DEGREE OF DOCTOR OF PHILOSOPHY

FACULTY OF ENGINEERING
UNIVERSITY OF MALAYA
KUALA LUMPUR

2017

University of Malaya

UNIVERSITY OF MALAYA

ORIGINAL LITERARY WORK DECLARATION

Name of Candidate: Md. Rubel Basar

Matric No: KHA130118

Name of Degree: Doctor of Philosophy (PhD)

Title of Thesis:

RESONANT INDUCTIVE WIRELESS POWER TRANSFER SYSTEM FOR WIRELESS CAPSULE ENDOSCOPY APPLICATION

Field of Study: Biomedical Instrumentation

I do solemnly and sincerely declare that:

(1) I am the sole author/writer of this Work;
(2) This Work is original;
(3) Any use of any work in which copyright exists was done by way of fair dealing and for permitted purposes and any excerpt or extract from, or reference to or reproduction of any copyright work has been disclosed expressly and sufficiently and the title of the Work and its authorship have been acknowledged in this Work;
(4) I do not have any actual knowledge nor do I ought reasonably to know that the making of this work constitutes an infringement of any copyright work;
(5) I hereby assign all and every rights in the copyright to this Work to the University of Malaya ("UM"), who henceforth shall be owner of the copyright in this Work and that any reproduction or use in any form or by any means whatsoever is prohibited without the written consent of UM having been first had and obtained;
(6) I am fully aware that if in the course of making this Work I have infringed any copyright whether intentionally or otherwise, I may be subject to legal action or any other action as may be determined by UM.

Candidate's Signature Date:

Subscribed and solemnly declared before,

Witness's Signature Date:

Name:

Designation:

University of Malaya

ABSTRACT

Resonant inductive wireless power transfer (WPT) system is regarded as a promising way to overcome high power demand for future wireless capsule endoscopy (WCE). Despite much attentions in this area, aspects such as overall power transfer efficiency (PTE) and received power stability (RPS) remain suboptimal and therefore investigation for further improvement is still required. Thus, this thesis presents several techniques to improve the PTE and RPS of WPT system for WCE application. In order to improve the PTE and RPS, three new power transmission coils (PTCs) are proposed which are named as PTC-I, PTC-II, and PTC-III. The proposed PTCs are mainly differed by the number of coil segments used, separation and number of turn ratio among the coil segments. The design parameters of proposed PTCs have been rigorously analyzed with complete mathematical models and computer simulations. The improvement in the power receiving side is contributed by the optimization of number of strands in the power receiving coil (PRC), incorporation of high permeability ferrite core, mixed resonance scheme, and power combining technique with 2-3 D PRC. For the overall inductive link, a multi-coils link approach is analyzed in WCE platform and an optimized 3-coils link is proposed to minimize effect of load resistance to the PRC. Finally, the PTC is designed in wearable form for compact portable WPT system. The results of analysis and experimental test indicate a remarkable improvement of PTE and RPS. The PTE obtained by the proposed optimal design is 8.12% when 758 mW of power being transferred. This PTE is remarkably higher than the PTE of 3.55% obtained by the best existing design in literature. The optimum proposed design also attained overall RPS of 79.2% whereas only 33.9% of RPS obtained by the best existing design. In addition, an electromagnetic effect analysis is performed with incorporation of PRC and high permeability ferrite core in a multi-layer homogenous body model. Results from this analysis indicate that 200 mW power can be transferred safely based on the guidelines provided by the ICNIRP.

University of Malaya

ABSTRAK

Pemindahan tenaga tanpa wayar sistem induktif (WPT) dianggap sebagai cara yang dijanjikan dapat mengatasi permintaan tenaga yang tinggi untuk kegunaan kapsul endoskopi tanpa wayar (WCE) masa depan. Walaupun banyak kajian dalam bidang ini telah dan sedang dijalankan, aspek-aspek seperti keseluruhan kecekapan pemindahan kuasa (PTE) dan kestabilan penerimaan kuasa (RPS) masih berada pada tahap suboptimal dan oleh itu siasatan terperinci untuk penambahbaikan masih diperlukan. Oleh itu, tesis ini membentangkan beberapa teknik untuk meningkatkan PTE dan RPS sistem WPT untuk applikasi WCE. Dalam usaha untuk meningkatkan PTE dan RPS, tiga gegelung penghantaran kuasa (PTC) baru dicadangkan yang dinamakan sebagai PTC-I, PTC-II, dan PTC-III. PTCs unit-unit PTC yang dicadangkan ini memiliki perbezaan dari segi jumlah segmen gegelung yang digunakan, jarak pemisahan antara segmen gegelung dan bilangan nisbah lingkaran antara segmen gegelung. Parameter reka bentuk PTCs yang dicadangkan telah dianalisis dengan berhati-hati menggunakan model matematik yang lengkap dan simulasi komputer. Peningkatan prestasi pada bahagian penerima tenaga telah disumbangkan oleh pengoptimuman bilangan lilitan dalam gegelung kuasa menerima (PRC), penggunaan skim salunan campuran, dan teknik gabungan kuasa menggunakan 2-3 D PRC. Untuk rangkaian induktif keseluruhan, teknik rangkaian multi-gegelung telah dianalisa dalam platform WCE dan rangkaian optimum 3-gegelung telah dicadangkan untuk mengurangkan kesan beban rintangan pada PRC. Untuk sistem WPT mudah alih compak, analisis dan ujian eksperimen menunjukkan peningkatan yang luar biasa ke atas PTE dan RPS. Peratusam PTE yang diperolehi oleh reka bentuk optimum yang telah dicadangkan adalah pada 8.12% apabila 758 mW tenaga dipindahkan. Pencapaian PTE ini adalah lebih tinggi sebanyak 3.55% berdanding reka bentuk yang terbaik sedia ada. Hasil reka bentuk optimum juga telah mencapai RPS keseluruhan sebanyak 79.2% berbanding 33.9% daripada RPS dari reka bentuk yang terbaik sedia ada.

University of Malaya

Tambahan pula, analisis kesan elektromagnet turut dilakukan dengan gabungan PRC menggunakan teras besi berketelapan tinggi yang diuji pada model badan yang mempungai lapisan homogenous. Dapatan menunjukkan kuasa sebanyak 200mW dapat dipindahkan secara tanpa wayar dengan selamat dan ini memenuhi garis panduan oleh ICNIRP yang melibatkan ketumpatan arus teraluh.

University of Malaya

ACKNOWLEDGEMENTS

All praises and glory to Allah Subhanahu Wa Taalaa (Almighty, the most Gracious, the most Merciful…) who gave me ability to carry out this work. Then, I would like to express my deepest thank to my supervisors Dr. Mohd Yazed Ahmad and Professor Ir. Dr. Fatimah Ibrahim for their valuable, constructive, and consistent supervision to this work. I am very much indebted for their tireless support and critical comments that extremely helped me to reach my goals and produce this thesis. My deepest thank also to Professor Dr. Jongman Cho for his constructive comments, suggestion, and guideline on my works. I also express my gratitude to the Ministry of Higher Education, Malaysia, and University of Malaya for providing financial support for this work through the University of Malaya Research Grant (UMRG: RP009D-13AET) and Postgraduate Research Grant (PPP: PG138-2015B). I would like to thank to all the member of Bio-Sensors and Embedded System Lab. and Centre for Innovation in Medical Engineering (CIME), along with all the staffs of Department of Biomedical Engineering, Dean Office, IPPP, and IPS for their cooperation during my PhD candidature. I would like to share this moment of contentment and express the appreciations to my parents and family members who encouraged me at every steps of my life.

Finally, I thank everyone else who has facilitated the making of this thesis.

University of Malaya

TABLE OF CONTENTS

Abstract iii

Abstrak iv

Acknowledgements vi

Table of Contents vii

List of Figures xii

List of Tables xvii

List of Symbols and Abbreviations xviii

CHAPTER 1: INTRODUCTION 1

1.1 Overview 1

1.1.1 Limitation of current wireless capsule endoscopy 2

1.1.2 Future capsules and power shortage problem 2

1.1.3 Wireless power transfer as a promising solution 4

1.2 Problem Statement 4

1.2.1 Inadequate design and analysis 5

1.2.2 Poor power transfer efficiency 5

1.2.3 Poor received power stability 6

1.2.4 Inadequate safety analysis 6

1.3 Aim and Objective of This Research 7

1.4 Brief Description of Methodology 7

1.5 Organization of This Thesis 9

CHAPTER 2: LITERATURE REVIEW 11

2.1 Introduction 11

2.2 Methods of Wireless Power Transfer 11

University of Malaya

2.3 Basic Block Diagram of Inductive WPT System 15

2.4 Overview of Inductive WPT System for WCE 15

2.5 Current Issues in Design of WPT System for WCE Application 16

2.6 State-of-art in Design of WPT System for WCE Application 17

2.6.1 Available design of power transmitter 18

2.6.1.1 Design of DC-AC inverter/power amplifier 18

2.6.1.2 Design consideration for PTC 20

2.6.1.3 Existing PTC design 21

2.6.2 Available design of power receiver 24

2.6.2.1 Design consideration for PRC 24

2.6.2.2 Design specification of existing PRC 24

2.6.2.3 Power conversion circuit 26

2.7 Specifications of Existing WPT System for WCE 28

2.7.1 Transferred power and efficiency 28

2.7.2 Received Power Stability 32

2.7.3 Effect of WPT system on body tissues 34

2.7.3.1 Standard limit on electromagnetic exposure 35

2.7.3.2 Electromagnetic exposure effect observed in existing studies .. 36

2.7.4 Effect of biological tissues on the WPT system 37

2.8 Summary 39

2.8.1 Design and optimization of WPT system 40

2.8.2 Stability of received power 41

2.8.3 Analysis of biological tissues safety 42

CHAPTER 3: EFFICIENCY IMPROVEMENT OF WPT SYSTEM 43

3.1 Introduction 43

3.2 Literature Review 43

University of Malaya

3.3 Materials and Methods 45
3.3.1 WPT system overview in WCE platform 45
3.3.2 PTC configuration 46
3.3.2.1 Configuration of existing PTCs 46
3.3.2.2 Configuration of proposed PTC 48
3.3.3 Mathematical modeling of inductive link 49
3.3.3.1 Modeling of link efficiency 49
3.3.3.2 Modeling of coupling coefficient 51
3.3.3.3 Modeling of quality factor 52
3.3.4 Performance analysis of the PTCs 55
3.3.4.1 *H*-field intensity and uniformity 55
3.3.4.2 Coupling Characteristics 57
3.3.4.3 Quality Factor 58
3.3.4.4 Variation of the link efficiency and field uniformity with PTC diameter 59
3.3.5 Implementation of PTC-I and 1D PRC based inductive link 60
3.3.5.1 Implementation of PTC 61
3.3.5.2 Implementation of 1D PRC 61
3.4 Results and Discussion 63
3.4.1 Measurement of k and Q_t 63
3.4.2 Measurement of the link efficiency 65
3.4.3 Effect of biological tissues on the η 67
3.4.4 Overall power transfer efficiency from source to load 68
3.4.5 Effect of WPT system on body tissues 69
3.4.5.1 Simulation setup 69
3.4.5.2 Induced current density 70

University of Malaya

3.5 Conclusion 71

CHAPTER 4: IMPROVEMENT OF RECEIVED POWER STABILITY 73

4.1 Introduction 73

4.2 Literature Review 73

4.3 Materials and Methods 75

4.3.1 Schematic of WPT System 75

4.3.2 Configuration of the proposed PTC-II 78

4.3.3 Optimization of *s* and *g* of the proposed PTC-II 79

4.3.3.1 Analysis of *H*-field and its uniformity 80

4.3.3.2 Analysis of quality factor 82

4.3.4 Analysis of Mixed Resonance Scheme 85

4.3.5 Implementation of the Proposed PTC-II and MRS based WPT System 87

4.3.5.1 Implementation of the PTC-II 88

4.3.5.2 Implementation of the PRC with MRS 89

4.3.5.3 Implementation of the PTC Driver 91

4.4 Results and Discussion 91

4.4.1 Experimental results on the PTC-II and MRS based WPT system 91

4.4.1.1 Output power with variation of PRC position 92

4.4.1.2 Stability of output power with variation of PRC position 93

4.4.1.3 Performance comparison 94

4.5 Conclusion 96

CHAPTER 5: OVERALL PERFORMANCE IMPROVEMENT OF WPT SYSTEM 98

5.1 Introduction 98

5.2 Literature Review 98

University of Malaya

5.3 Materials and Methods 99

5.3.1 Configuration of PTC-III 99

5.3.2 Performance Comparisons of PTC-I, PTC-II and PTC-III 102

5.3.3 Overview of multi-coil inductive power link in WCE platform 103

5.3.4 Improved Power Receiving Scheme and Orientation Stability 105

5.3.5 Prototype Implementation 109

5.3.5.1 Implementation of Wearable PTCs 109

5.3.5.2 Implementation of improved power receiving system 110

5.3.5.3 Driving circuit with fine tuning capability 112

5.4 Results and Discussion 113

5.4.1 Experimental test of implemented WPT system 113

5.4.2 Experimental test of with orientation of 2-3D PRC 114

5.4.3 Experimental test of WPT system in saline water 114

5.4.4 Electromagnetic exposure effect 115

5.5 Conclusion 117

CHAPTER 6: CONCLUSIONS AND RECOMMENDATIONS 118

6.1 Introduction 118

6.2 Conclusions 118

6.3 Summary of Major Contributions 119

6.4 Limitation of the Study 123

6.5 Recommendations for Future Works 123

References 125

List of Publications and Papers Presented 134

University of Malaya

LIST OF FIGURES

Figure 1.1: An overview of: (a) a typical wired endoscopy (adopted from online: http://www.acgaec.com/upper-endoscopy), and (b) a wireless capsule endoscopy system (adopted from Adler & Hassan, 2013; Ghoshal, 2013). 1

Figure 1.2: The CWC and hypothetical prototype of future capsules: HRVC, RCE, and MMR (Carta *et al.*, 2010; Pan *et al.*, 2011)..... 3

Figure 1.3: Estimated power budget for different type of existing and future capsule endoscopes. 4

Figure 1.4: Flow chart of research methodology. 8

Figure 2.1: WPT methods for application in different frequency range and transmission distance (Jusoh *et al.*, 2015)..... 12

Figure 2.2: The basic operation principle of near field short distance WPT system: (a) Acoustic power transfer (Roes *et al.*, 2013), (b) Capacitive power transfer (Aldhaher, 2014), and (c) Inductive power transfer (Aldhaher, 2014). 13

Figure 2.3: The number of articles published in: (a) IEEE explore: journal and magazine only, and (b) web of science. (This search sets with the keywords “wireless power transfer”, OR “inductive wireless power transfer”, NOT “Acoustic”, NOT “capacitive”). 14

Figure 2.4: Basic block diagram of WPT system for biomedical devices. 15

Figure 2.5: Overview of the inductive WPT system for WCE application. 16

Figure 2.6: Batteryless wirelessly powered WCE system developed by RF system lab Japan..... 18

Figure 2.7: Schematic of class E power amplifier loaded with PTC (Jourand & Puers, 2012; B. Lenaerts & Puers, 2007)..... 19

Figure 2.8: Schematic of full bridge class D power amplifier/driving/inverter circuit (Xin *et al.*, 2010; Yadong *et al.*, 2013a)..... 20

Figure 2.9: Design consideration for PTC adopted from (Sun *et al.*, 2013)..... 20

Figure 2.10: Common structures of PTC: (a) single solenoid; (b) pair of solenoid; (c) pair of double layer solenoid; (d) segmented solenoids; (e) Helmholtz coil. (PA = power amplifier)..... 22

Figure 2.11: Configuration of orthogonal 3D-PRC (Xin *et al.*, 2010)..... 24

University of Malaya

Figure 2.12: Configuration of half-wave rectifier circuit to rectify alternating current received by 3D PRC to a direct load current (Lenaerts & Puers 2007). 27

Figure 2.13: Configuration of full-wave rectifier circuit to rectify alternating current induced in 3D PRC to a direct load current (Pan *et al.* 2011)..... 28

Figure 2.14: Model of relative alignment between PTC and PRC (Pan *et al.* 2011)..... 32

Figure 3.1: Schematic of a WPT system with a PTC fixed around the patient body and a WCE consists of a PRC and a receiver circuit located in the human GI tract (Basar *et al*., 2016a)..... 45

Figure 3.2: Schematic configuration of the existing PTCs: (a) typical solenoid coil (TSC); (b) typical Helmholtz coil (THC); and c) segmented solenoid coil (SSC). The number of segments has been denoted by "nos" (Basar *et al*., 2016a)..... 47

Figure 3.3: Schematic of the proposed PTC-I: (a) basic structure and (b) enlargement of the axial region with an additional middle coil. The outer and middle coils have been represented by "OC" and "MC," respectively (Basar *et al*., 2016a)..... 48

Figure 3.4: Simplified circuit model of the resonant inductively coupled wireless power transfer system (Basar *et al*., 2016a)..... 49

Figure 3.5: Coupling model between PTC-PRC (adopted from Basar *et al*., 2016a)..... 51

Figure 3.6: (a) lumped equivalent circuit model of a tightly would single solenoid segment of the PTC, and (c) simplified lumped equivalent circuit model (Basar *et al*., 2016a). . 52

Figure 3.7: Color map of the *H*-field distribution in: a) TSC, b) THC, c) SSC with segment 3 has been excited, and d) PTC-I. The field has been shown on the *yz* plane at $x = 0$ for a coil radius of 20 cm, excitation power of 5 W, frequency of 300 kHz, and coil inductance of ~460 µH (Basar *et al.*, 2016a)..... 56

Figure 3.8: Variation of the coupling coefficient along the radial axis: a) without axial distance (at $z = 0$) and b) with axial distance (at $z = h/2$). The coupling coefficient has been calculated for $\mu_{eff} = 210$, $S_r = 9.5*10^{-5}$ m^2, L_t ~460 µH, and $L_r = 426$ µH (Basar *et al*., 2016a) 58

Figure 3.9: Unloaded quality factor of the PTCs over the frequency (Basar *et al*., 2016a). 59

Figure 3.10: Variation of the minimum *H*-field uniformity and link efficiency with the diameter of the PTCs (Basar *et al*., 2016a). 60

Figure 3.11: Experimental setup for the measurement of the coupling coefficient (*k*) and the unloaded quality factor (Q_t) of the implemented PTCs (Basar *et al*., 2016a). 61

University of Malaya

Figure 3.12: Received power by the 1D PRC with different number of strands of Litz wire for a constant level of *H*-field (105 A/m) generated by the PTC (Basar *et al*., 2014b)..62

Figure 3.13: Comparison of the measured coupling coefficient (*k*) with that of the calculated. Both of the PTCs having equal radius and inductance, the PRC specification was: μ_{eff} = 210, $S_R = 9.5 * 10 - 5$ m^2, and L_r = 426 µH (Basar *et al.*, 2016a).....64

Figure 3.14: Comparison of measured and calculated Q_t of PTC-I and SSC when both of the coils had equal radius and inductance (Basar *et al*., 2016a). 65

Figure 3.15: Measurement of PTE of the WPT system: (a) circuit diagram of the measurement; (b) experimental setup (Basar *et al*., 2016a).....66

Figure 3.16: Comparison of the measured efficiency with that of calculated (Basar *et al*., 2016a).....66

Figure 3.17: Testing of WPT system's performance in tissues environment: (a) fresh biological tissues of a slaughtered goat torso with a PRC inside the tissues, and (b) measurement setup in the biological tissues environment (Basar *et al*., 2016a).....67

Figure 3.18: Overall PTE and received power.....68

Figure 3.19: Evaluation of the current density: a) analytical model of the simulation setup with homogeneous multi-layer tissues, PTC-I, PRC, and excitation source; b) simulated induced current density for 0.5 A of coil current and 146 mW of output power (Basar *et al*., 2016a). 70

Figure 3.20: Limit on the coil current (I_t) and output power for the different PTCs to fulfill the safety guideline provided by the ICNIRP (Basar *et al*., 2016a).....71

Figure 4.1: Schematic of a WPT system for RCE: (a) sketch of the WPT system, and (b) circuit model (Basar *et al*., 2017).....75

Figure 4.2: *H*-field distribution in a typical Helmholtz coil (THC) perpendicular to the *z*-axis and co-centric with Cartesian coordinate system, the *H*-field has been generated with 26 Ampere-turns (Basar *et al*., 2015).....77

Figure 4.3: Variation of inductive link efficiency and magnetic field uniformity with the radius *r* of the PTC, uniformity was considered within a region of Ø 30 cm x height 20 cm inside the PTC (Basar *et al*., 2017). 77

Figure 4.4: Crossectional view with desing specification of: (a) typical Helmholtz coil (THC), and (b) the proposed PTC-II (Basar *et al*., 2017).....78

Figure 4.5: Variation of $\gamma PTC - II(s, g)$ with the: a) separation *sr* between outer to middle coil, and b) turn ratio *g*: within the region $-15cm \leq y \leq 15$ cm and $-10\ cm \leq z \leq 10$ cm inside the PTC (Basar *et al*., 2017).....80

University of Malaya

Figure 4.6: Comparison of normalized *H*-field (on *y*-*z* plane at $x = 0$) generated by the proposed PTC-II and the conventional THC: $n = 6$ and $r = 20$ cm are used for both of the coils (Basar *et al*., 2017). 81

Figure 4.7: Comparison of *H*-field uniformity of THC and PTC-II along the radial axis at $z = 0$ and $z = r/2$ (Basar *et al*., 2017). 81

Figure 4.8: (a) Modified Helmholtz coil based PTC, (b) lumped model, and (c) simplified lumped model (Basar *et al*., 2017). 82

Figure 4.9: The Q_t of the PTC-II over the frequency and the number of turns. Coil specification: $r = 20$ cm, coil conductor was AWG 42 Litz wire with 270 strands (Basar *et al*., 2017). 83

Figure 4.10: The Q_t of THC and PTC-II for different *n*. Coil specification: $r = 20$ cm, coil conductor is AWG 42 Litz wire with 270 strands (Basar *et al*., 2017). 84

Figure 4.11: PRC resonance scheme: (a) PRS, (b) SRS, and (c) MRS (Basar *et al*., 2017). 85

Figure 4.12: Simulation model of WPT system to verify the performance of MRS, SRS and PRS (the connection of CP and CS were adjusted for SRS and PRS) (Basar *et al*., 2017). 87

Figure 4.13: Power delivery to the load by the MRS, SRS and PRS for the WPT setup shown in Figure 4.12 (Basar *et al*., 2017). 87

Figure 4.14: A prototype of the proposed WPT system: (a) proposed PTC-II, (b) 3D PRC with mixed resonance scheme (MRS) and power conversion circuitry (PCC), and (c) class E driving amplifier circuit (Basar *et al*., 2017). 88

Figure 4.15: Output power measured at the different position of PRC inside the PTCs: the positon of PRC varies along *y*-axial lines through at $z = 0$ and $z = r/2$ with 1 cm interval (Basar *et al*., 2017). 93

Figure 4.16: Received power stability over the positions of PRC varies along *y*-axial lines through at: a) $z = 0$, and b) $z = r/2$ (Basar *et al*., 2017). 95

Figure 4.17: Comparison of PTE attained by the PTC-II and THC_2 under two resonance schemes (MRS and SRS) with PRC: position of PRC varies in *y* direction where $x = 0$ and $z = 0$ (Basar *et al*., 2017). 96

Figure 5.1: Design specification of PTC-III: (a) schematic view and (b) cross sectional view (Basar *et al.*, 2016b). 100

Figure 5.2: Comparison of calculated normalized *H*-field intensity generated by the proposed PTC-III and: a) THC (Basar *et al.*, 2016b), and b) PTC-II. 101

University of Malaya

Figure 5.3: Simplified 4-coil based inductive link: (a) schematic view, and (b) lumped element model. 103

Figure 5.4: Comparison of simulated link efficiency of 2-coils, 3-coils, and 4-coils based inductive link in WCE platform. 105

Figure 5.5: Typical configuration of power receiver. 106

Figure 5.6: Relative orientation (misalignment) model between PRC and PTC axis... 106

Figure 5.7: (a) configuration of 2-3D PRC, (b) power combining configuration of 2-3D PRC. 108

Figure 5.8: Variation of load power P_L with the relative orientation of PRC in conventional parallel configuration and power combining configuration used in this study. 108

Figure 5.9: (a) Experimental setup for measurement of power and efficiency, (b) PTC-I, and (c) PTC-III set with the free size mannequin. 109

Figure 5.10: Implemented: (a) 1D PRC, (b) 2-3D PRC, (c) power conversion circuit loaded with LEDs, (d) power receiving circuit with 30 Ω load, (e) custom made 2-3D PRC orientation controller, (f) calibrated coaxial cable for power measurement..... 111

Figure 5.11: Class E driver with improved tuning circuit: (a) schematic diagram, and (b) implemented driver. 112

Figure 5.12: Measured P_L and PTE of implemented 3-coils WPT system with PTC-I and PTC-III. 113

Figure 5.13: Variation of received power with the orientation of the PRC. 114

Figure 5.14: Comparison of transfer power in air (left) and in saline water (right) through the LED intensity. 115

Figure 5.15: Comparison of measured PTE in air and in saline water. 116

Figure 5.16: Simulated induced current density (J, A/m^2) in the biological tissues for the WPT system with PTC-I (left) and PTC-III (right). 116

University of Malaya

LIST OF TABLES

Table 2.1: Specification of existing power transmission coils those were used in previous studies. 23

Table 2.2: Specification of existing 1D power receiving coil used in previous study. 25

Table 2.3: Specification of existing 3D power receiving coil used in existing study. 26

Table 2.4: Design specification and performance indices of related WPT systems in the literature. 31

Table 2.5: Overview of existing WPT system stability. 34

Table 2.6: Reference level of electromagnetic exposure limit. 35

Table 2.7: Basic safety limitation for human body tissues by ICNIRP and JSMEBE. 36

Table 2.8: Overview of electromagnetic safety of existing WPT system. 37

Table 2.9: Effect of biological tissues on the performance of WPT system. 39

Table 3.1: Specification of the implemented power transmission coils (Basar *et al*., 2016a). 62

Table 3.2: Specification of the implemented power receiving coil (Basar *et al*., 2016a). 63

Table 4.1: Electrical Specification of the PTCs (Basar *et al*., 2017). 90

Table 4.2: Specification of the PRCs and resonance circuit. 91

Table 4.3: Performance comparison of WPT system based THCs, PTC-II, SRS and MRS (Basar *et al*., 2017). 94

Table 4.4: Performance comparison of the proposed WPT systems with existing system (adopted from Basar *et al*., 2017). 96

Table 5.1: Performance comparison of proposed PTCs. 102

Table 5.2: Specification of implemented wearable PTCs 110

Table 5.3: Specification of 2-3D PRC. 112

Table 6.1: Comparison of received power stability. 121

Table 6.2: Comparison of PTE attained by the proposed and existing system. 122

University of Malaya

LIST OF SYMBOLS AND ABBREVIATIONS

CMOS	:	Complementary Metal–oxide–semiconductor
CWC	:	Commercial wireless capsule
GI	:	Gastrointestinal
HRVC	:	High resolution video capsule
ICNIRP	:	International Commission on Non-Ionizing Radiation Protection
PTC-I	:	Power Transmission Coil I (Improved power transmission coil)
LED	:	Light Emitting Diode
PTC-II	:	Power transmission coil II (PTC based on modified Helmholtz coil)
MMR	:	Multifunctional medical robot
PRC	:	Power receiving coil
PTC	:	Power transmission coil
PTE	:	Power transfer efficiency
RCE	:	Robotic capsule endoscopy
RPS		Received power stability
SAR	:	Specific Absorption Rate
SCC	:	Standards Coordinating Committee
SSC	:	Segmented solenoid coil
THC	:	Typical Helmholtz coil
TSC	:	Typical solenoid coil
WCE	:	Wireless capsule endoscopy
WPT	:	Wireless power transfer
α_o		Pitch misalignment
a		Radius of Litz wire

University of Malaya

d_0		Axial misalignment
d_{uv}		Distance between the turn u and v in the coil
r_0		Lateral misalignment
r		Radius of coil
Ø		Diameter of the coil
C_{stray}		Stray capacitance in the inductive coil
f		Frequency
M		Mutual inductance between two coils
N		Total number of turn in the coil
n		Number of turn in the single coil segment
L		Self inductance of single turn
L_{self}		Self inductance of single coil segment
$L_{i \in (t, r)}$		Effective self inductance of coil t: transmission coil, r: receiving coil
$R_{i \in (t, r)}$		Effective series resistance of coil
R_{ac}		AC resistance of coil due to skin and proximity effect
Q		Quality factor
$Q_{i \in (t, r)}$		Unloaded quality factor of coil
$Q_{i,L}$ $i \in (t, r)$		Loaded quality factor of coil
$I_{i \in (t, r)}$		Current through the coil
α	:	Load factor
ε	:	Permittivity
η	:	Inductive link efficiency
ρ	:	Weight density of biological tissues
σ	:	Electrical conductivity of biological tissues
φ_{yz}	:	Magnetic flux density on the yz plane
μ_0	:	Magnetic permeability

University of Malaya

μ_{eff}	:	Effective magnetic permeability
H	:	Magnetic field strength
h	:	Coil height
J	:	Current density
P_L		Load or received power
$P_{L,S}$		Received power stability
$P_{L,PS}$		Position stability of received power
$P_{L,OS}$		Orientation stability of received power
R_L		Load resistance
S_r	:	Area enclosed by the power receiving coil
V_L		Load voltage
Vs	:	Input supply voltage

University of Malaya

CHAPTER 1: INTRODUCTION

1.1 Overview

The gastrointestinal (GI) or digestive system extracts the essence of our diet and keeps our body active, but nowadays an increasing number of people are being affected by GI disorders due to malignant diseases like gastric cancer, tumors, and bleeding to name a few (Myer *et al.*, 2013; Yu & Zhang, 2013). Early detection of these diseases is important for effective prevention and treatment that can avoid subsequent complications or diseases. In this regards, wireless capsule endoscopy (WCE) is a promising technology for direct visualization of the entire GI path (Iddan *et al.*, 2000). An overview of a typical wired endoscopy and a WCE system is shown in Figure 1.1. In comparison to the typical wired endoscopy, the WCE can provide comfortable, painless diagnosis to the patient and may reduce the time span for the patient to stay in a health care facility without significant interruption of the patient's daily activities. In addition, the WCE is able to travel in entire small bowel area where the typical endoscopes fail to reach such as small bowel area, and this can be accomplished without full supervision by a specialist (Mustafa *et al.*, 2013).

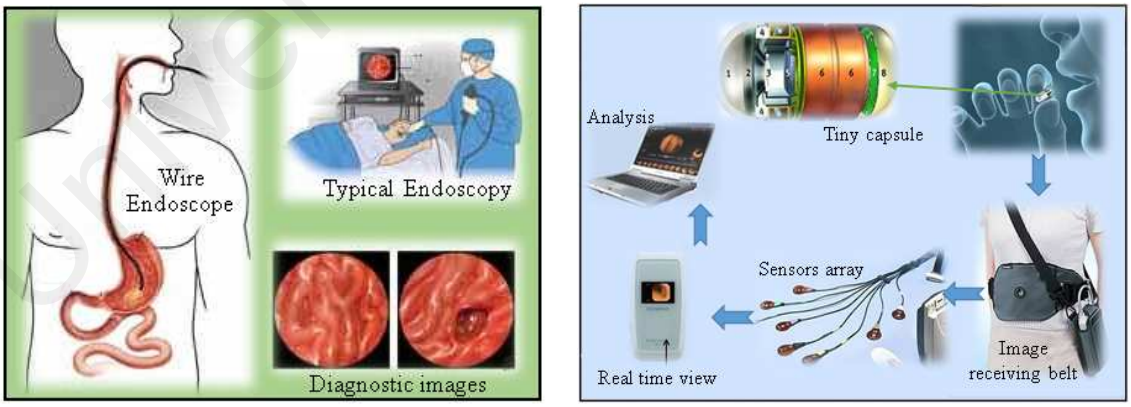

(a) **(b)**

Figure 1.1: An overview of: (a) a typical wired endoscopy (adopted from online: http://www.acgaec.com/upper-endoscopy), and (b) a wireless capsule endoscopy system (adopted from Adler & Hassan, 2013; Ghoshal, 2013).

University of Malaya

However, in the view of specialist, WCE is still a premature technology that requires improvement (Koulaouzidis & Dabos, 2013; Mavrogenis *et al.*, 2011).

1.1.1 Limitation of current wireless capsule endoscopy

In comparison with the conventional wired endoscopies, WCE system is superior in identifying abnormalities in the GI tract (Drug, 2002; Ge *et al.*, 2003; Moglia *et al.*, 2009). As a result, several clinical products of WCE system have been developed with different specifications. Even so, the diagnostic yield (DY) of current WCE remains the main issue that causes the conventional wired endoscopes being still in used in many clinics (Koulaouzidis & Dabos, 2013; Mavrogenis *et al.*, 2011; Moglia *et al.*, 2009; Westerhof *et al.*, 2012). The DY is poor mainly due to limited visual field, low image resolution, lower frame rate, and inconsistent movement of capsule (Ghotbi *et al.*, 2015). To obtain a better DY, important features such as image resolution, frame rate, working time, and view angle of the existing WCE need to be improved (Swain, 2008). In addition, another concerning limitation is the limited control of the movement of the capsule. The movement of the existing capsule depends on the natural transit of the bowel, which makes the system incapable to re-examine certain areas due to incapability of moving backward or maintain its location for a certain period of time. The inconsistence of bowel transit (slow or fast) increases the likelihood the important information not to be properly captured.

1.1.2 Future capsules and power shortage problem

Suboptimal image quality of the existing commercial wireless capsule (CWC) can be overcome by employing high resolution video capsule (HRVC) (Lenaerts & Puers, 2005; Zhu *et al.*, 2012) which utilizes a higher resolution imaging/video device, a higher light intensity, and a RF transmitter capable of transmitting high quality image data. Moreover,

University of Malaya

additional features such as miniaturized active control system, capsule's actuation and locomotion mechanism, can provide a better generation of WCE devices whereby a robotic type of capsule endoscopy (RCE) can be made possible (Swain, 2008). In addition, some of the advanced features including microsurgery, drug delivery, biopsy, and micro-syringe are also anticipated for future multifunctional tiny medical robot (MMR). All of these current and future capsules are illustrated in Figure 1.2.

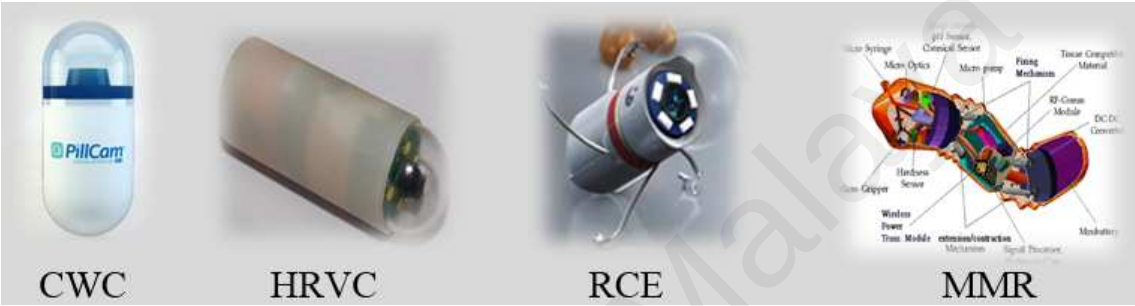

Figure 1.2: The CWC and hypothetical prototype of future capsules: HRVC, RCE, and MMR (Carta *et al.*, 2010; Pan *et al.*, 2011).

In order to realize these future capsules, the first and main challenge is the energy of onboard battery is not sufficient that needs to be resolved. The most basic CWC typically requires around 20 mW to 30 mW of electrical power (Shiba *et al.*, 2010; Xiang *et al.*, 2005). However, the power demand increases up to 93 mW to 150 mW for HRVCs as illustrated in Figure 1.3. The next generation of WCE known as RCE which will have additional sub-systems such as advanced control electronics, locomotion systems, auto focus systems, image compression and other sensors (Carta *et al.*, 2010; Carta *et al.*, 2011). Such RCEs demand a higher level of electrical energy that can reach up to 400 mW. The power demand increases more in MMR which can reach around 570 mW (Ye *et al.*, 2008). Based on the anticipated features and power budget for future capsules, it is noted that there is a large gap between the available battery power (merely around 30 mW) and the power required for the next generation capsule.

University of Malaya

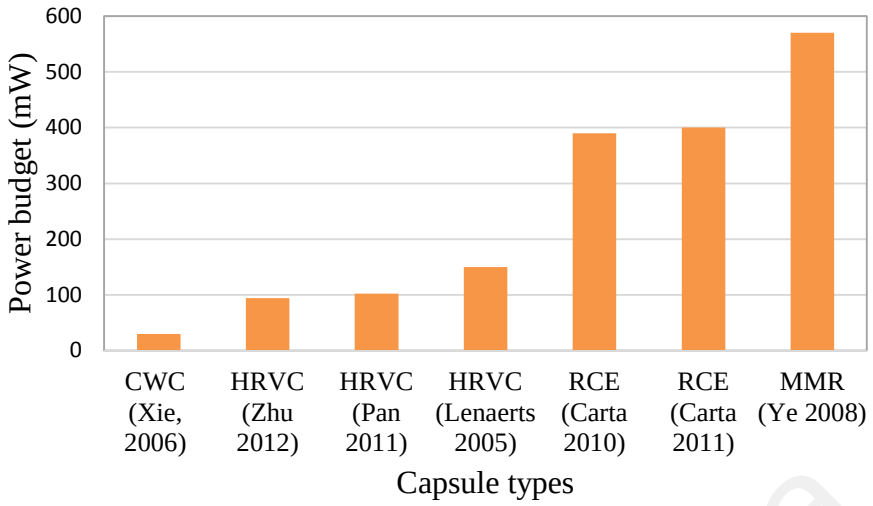

Figure 1.3: Estimated power budget for different type of existing and future capsule endoscopes.

1.1.3 Wireless power transfer as a promising solution

In order to bridge this large power gap between the power required by the future capsules and power storage capacity of available battery, a wireless power transfer (WPT) system based on resonant inductive coupling method (Schuylenbergh *et al.*, 2009) would be a promising solution, since, it has been successfully experimented in transcutaneous energy transfer (TET) system for artificial heart (Arai *et al.*, 2005; Shibuya & Shiba, 2013). In the TET system, power transmission coil (PTC) and power receiving coil (PRC) are fixed at certain positions and power can be transferred within few tens millimeter distance. However, unlike the TET system for artificial heart (Arai *et al.*, 2005), and other biomedical devices such as neural implants (Jegadeesan *et al.*, 2015), retinal prosthesis (Wang *et al.*, 2005) etc. (where position and orientation of PTC and PRC are fixed), the PRC is freely moving inside the GI tract in WPT system for WCE application which causes continuous change in the position and orientation between PTC-PRC (Xin *et al.*, 2010). Thus, the design of WPT system for WCE application becomes more challenging.

1.2 Problem Statement

Several studies on WPT systems have been presented in open literature for WCE application (Carta *et al.*, 2011; Na *et al.*, 2015; Sun *et al.*, 2012; Xin *et al.*, 2010). At

University of Malaya

present, the available research works in this field indicated the common shortcomings and challenges. The current design challenges and shortcomings are discussed as follows:

1.2.1 Inadequate design and analysis

The available WPT systems for WCE application commonly consist of PTC and PRC with power amplifier and rectifier circuits. Generally, a Helmholtz coil (Jourand & Puers, 2012; Pan *et al.*, 2011; Xin *et al.*, 2010) or a solenoid pair (Jia *et al.*, 2012; Zhu *et al.*, 2012) are used as PTC and a miniaturized 3D orthogonal coil with ferrite core is used as PRC (Carta *et al.*, 2009). The PTC and PRC are implemented with arbitrarily considering the important design parameters such as coil configuration, coil dimension, total number of turns. Whereas the important performance indices such as magnetic field uniformity, coil's quality factor, coupling coefficient, power transfer efficiency (PTE) and received power stability (RPS) are not fully analyzed with adequate mathematical model or simulation (Carta *et al.*, 2011; Jia *et al.*, 2012; Xin *et al.*, 2010).

1.2.2 Poor power transfer efficiency

Considering the electromagnetic exposure of the human body tissues, the power transfer efficiency (PTE) of such system is an important concern. In addition, the high PTE is also important to enable the transmitter system to be powered by a battery rather than connecting it to the city power link which is necessary to improve portability thus patient can walk freely. Unfortunately, the PTE of such systems is poor due to weak coupling between the PTC-PRC mainly contributed by: i) tiny size of the receiver (i.e. the PRC); ii) misalignment between the PTC-PRC; and iii) large separation between the PTC and the PRC. For instance, Jourand *et al.* (2012) developed a WPT system with a PRC of 9 mm diameter. The PRC was small enough to be embedded in the existing capsule. The PTC was 75 cm in diameter and can cover the whole abdominal region. The

University of Malaya

PTE attained by this system was as low as ~0.33% at 37.5 cm transmission distance. In spite of numerous research in this field, the PTE of such system is still poor and within the range of 0.02% to 3.55% (Ke *et al.*, 2015; Na *et al.* 2015; Shi *et al.*, 2015).

1.2.3 Poor received power stability

While capsule is working, it is freely moving within the GI tract. The free movement and orientation of the capsule cause misalignment between the PTC and the PRC. This misalignment may result fluctuating or poor stability of received power level (Pan *et al.*, 2011). The overall stability of received power level can be classified into two types: i) position stability, and ii) orientation stability (Xin *et al.*, 2010). The position stability refers to the fluctuation of received power level due to changing in location/position of the PRC with respect to the PTC. Whereas, the orientation stability refers to the fluctuation of the received power level with respect to the misalignment between PRC-PTC (Xin *et al.*, 2010). The position stability is mostly correlated with the uniformity of *H*-field produced by the PTC. While the orientation stability is related to the configuration of the PRC. In order to cope with high fluctuation (poor stability) of the received power, the existing studies used typical Helmholtz coil (THC) as PTC to generate a uniform *H*-field and a 3D PRC to ensure a consistent level of received power at any orientation. However, the overall stability (position stability$\times$orientation stability) that attained by the existing studies is only 33.9% (Xin *et al.*, 2010). Thus, further study and investigation are required to improve this poor stability.

1.2.4 Inadequate safety analysis

The electromagnetic effect of WPT system to the patient body tissues are indexed by two parameters: i) specific absorption rate (SAR, W/kg), and ii) induced current density (J, A/m^2). In the existing research, the SAR and the J have been analyzed using a human body model set with a PTC (Xin *et al.*, 2010; Zhiwei *et al.*, 2011). In the existing analysis,

the effect of PRC and ferrite core have not been considered. The high permeability ferrite core and high quality PRC are expected to improve the coupling as well as PTE. However, the high permeability ferrite core and high quality PRC increase the magnetic flux density around it and may cause higher electromagnetic effect to the tissues around the PRC. To estimate this effect, safety analysis needs to be performed with incorporation of PRC and ferrite core.

1.3 Aim and Objective of This Research

The objective of this thesis is to design a WPT system with high power transfer efficiency and received power stability so that it is possible to continuously deliver adequate level of power to a WCE device. In order to achieve this objective, the following sub-objectives have been specified in this research:

i. To develop a complete mathematical model for design and optimization of a WPT system for WCE application.
ii. To design of a WPT system with investigation and implementation of new techniques to improve power transfer efficiency and received power stability.
iii. To test the design through fabrication of WPT system prototypes and perform rigorous experiments.
iv. To perform electromagnetic safety test of the designed WPT system on the biological tissues with incorporation of PRC and high permeability ferrite core materials.

1.4 Brief Description of Methodology

The overall methodology of this research on design of magnetic resonance-based inductively coupled WPT system for WCE application is shown in Figure 1.4. This research starts with in depth literature review and critical analysis on the existing WPT systems along with summarizing the existing potential research gaps.

University of Malaya

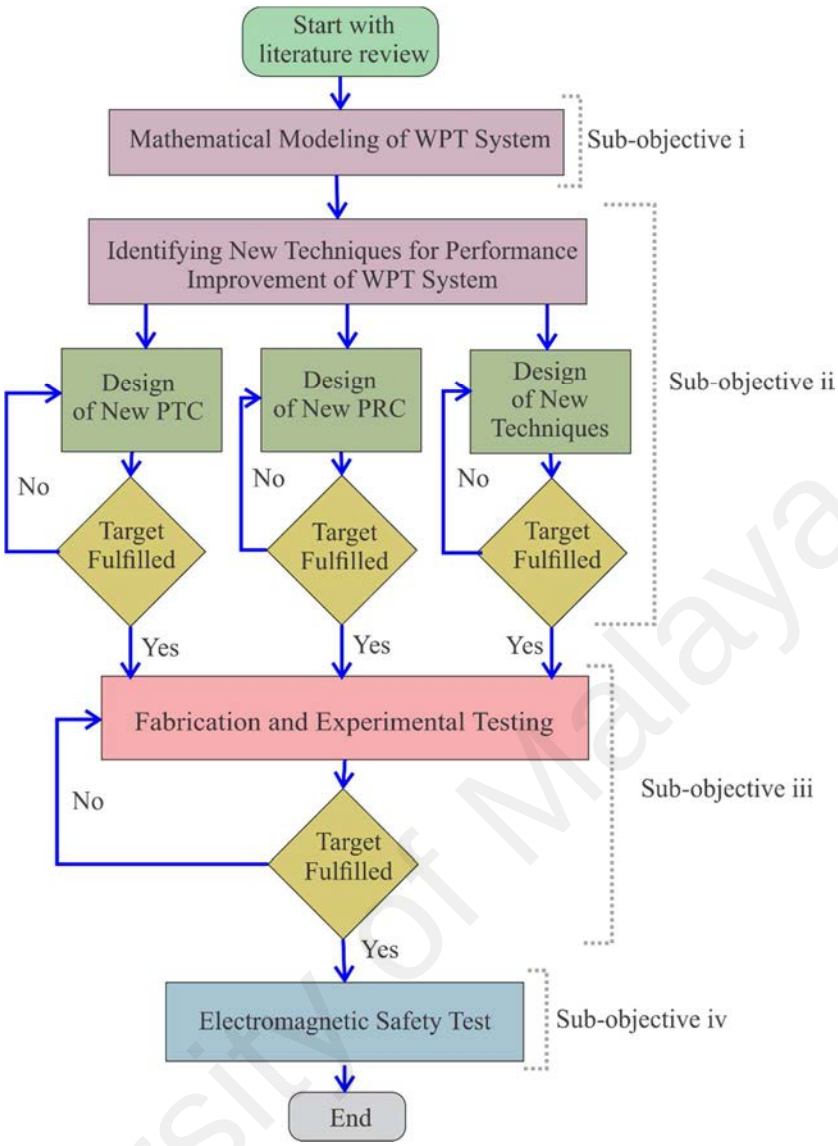

Figure 1.4: Flow chart of research methodology.

In order to design and optimize a WPT system, a complete mathematical model is developed which enables rigorous analysis and optimization of the important design parameters such as optimum coil configuration, quality factor, coupling coefficient, magnetic field uniformity and resonance frequency. The analysis is performed using a simulation tool "Mathematica" developed by Wolfram Research. In addition, the magnetic field uniformity is also observed using COMSOL Multiphysics simulation tool. Based on the mathematical model and simulation, new designs for PTC and PRC are proposed to improve the PTE and RPS. For further improvement, some other new techniques such as integration of high permeability ferrite core, use of multi-strands Litz

University of Malaya

wire, utilization of mixed resonance scheme, incorporation of full wave bridge rectifier with ultra low voltage Schottky diodes, use of 3-coils inductive link and power combining technique with 2-3D PRC have been considered. Rigorous analysis is performed to ensure whether the new designs fulfill the target. When the targeted performance of WPT system is achieved with new designs, several prototypes are fabricated. After that the fabricated prototype of proposed WPT system has been experimentally tested. Finally, the electromagnetic effect of the proposed WPT system is tested by analyzing the induced current density (*J*) with incorporation of PTC, biological tissues materials, PRC and high permeability ferrite core materials.

1.5 Organization of This Thesis

This thesis is organized into six distinct chapters and their contents are described as follows:

Chapter 1: This chapter provides an overview of WCE technology and a brief review of the state-of–the-art to highlight the shortcomings of the existing WCE and WPT technologies along with the current design challenges. Then, the aims and objectives of this thesis are listed, followed by a brief description of methodology and organization of this thesis.

Chapter 2: The detailed literature review on the various methods of WPT system and their suitability for particular applications, basic block diagram and working principle of resonant inductive power transfer, existing design of magnetic resonance based inductively coupled WPT system in WCE platform, their performance, critical analysis on the existing WPT system, potential gap for future research are presented in this chapter.

University of Malaya

Chapter 3: This chapter illustrates a complete mathematical model for design, analysis, and optimization of inductive link for WPT. This chapter also discusses the efficiency improvement of inductive link through the new configuration of power transmission coil-I (PTC-I). Rigorous analysis on the performance of PTC-I and its comparison with that of other existing PTCs are presented in this chapter. Finally, the implementation and experimental test of PTC-I and a 1D PRC based WPT are included at the end of this chapter.

Chapter 4: This chapter describes design, analysis, and optimization of another variant power transmission coil known as PTC-II that offers a better *H*-field uniformity with higher stability of received power level. Besides, the performance analysis on different resonance scheme on receiving coil side is also included. Then the implementation of WPT system with PTC-II and a mixed resonance receiver is presented along with the associated experiments.

Chapter 5: This chapter presents overall efficiency and stability improvement of WPT system through the configuration of PTC-III, analysis of multi-coil inductive WPT link in WCE platform, power combining technique with 2-3D PRC. The transformation of PTC in wearable form also presented. Then, implementation of compact WPT system with wearable PTC and its performance testing in air and in saline water are given in details. Finally, analysis of electromagnetic effect is also included in this chapter.

Chapter 6: This chapter summarizes the overall research outcomes and findings with highlighting the key contributions, and scope of future research.

References cited in this thesis and publications resulted from this research work are listed at the end of this thesis.

University of Malaya

CHAPTER 2: LITERATURE REVIEW

2.1 Introduction

Wireless power transfer (WPT) system is considered as a promising measure to overcome high power demand of future biomedical wireless capsule endoscopy (WCE) which cannot be mitigated by the onboard battery. As a consequence, the design of WPT system for WCE application has drowned tremendous attentions in current research. In this research, the main objectives are to obtain as much as possible high power transfer efficiency (PTE) and high received power stability. In addition, for the application of WPT system in WCE environment, the physical configuration of power transmitter system needs to be compatible to set with the patient body whereas the power receiving system must be compact enough to be embedded in the tiny biomedical capsule. Moreover, the safety of patient body tissues needs to be ensured for practical use of WPT system.

There are many research groups have been dedicated their research efforts with the aforementioned objectives and have resulted numerous number of publications in the open literature. Thus, this chapter aims to present a systematic review with emphasis on the aspects related to the important performance indices of WPT system. It is noted that, till now the development of WPT system for this WCE application is still in initial stage and there is still ample of room for improvements, especially involving system efficiency, stability, and the patient safety aspects.

2.2 Methods of Wireless Power Transfer

Currently, WPT system has received tremendous attention in research and it emerges as an alternative method for charging or direct powering of today's and future applications including vehicles, handheld electronics, and biomedical implantable devices (Barman *et al.*, 2015; Hui *et al.*, 2014). After many years of development, several methods such as

University of Malaya

acoustic, inductive, capacitive, microwave, and optical power transfer systems have been established by which power can be transferred from a source to a load wirelessly (Aldhaher, 2014; Sun *et al.*, 2013). Each of these methods has its suitability for a specific range of operating distance and frequency in a particular application. A survey on the applications of particular methods considering distance and frequency of operation is illustrated in Figure 2.1 (Jusoh *et al.*, 2015).

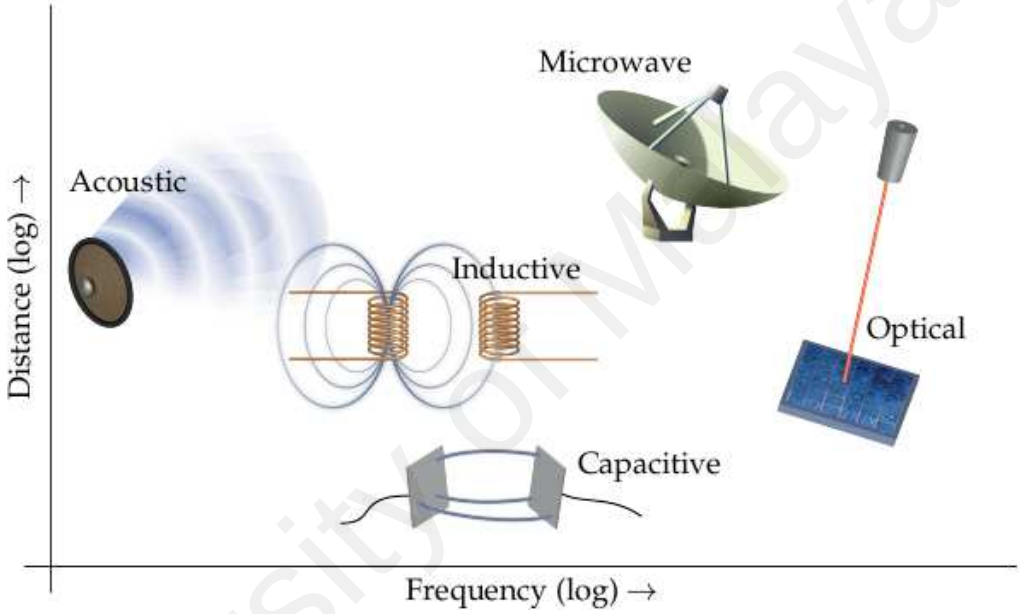

Figure 2.1: WPT methods for application in different frequency range and transmission distance (Jusoh *et al.*, 2015).

Depending on the operating distance, these methods can be classified into two categories: i) far-field power transfer methods which include microwave and optical transfer technique, and ii) near-field power transfer methods which include acoustic, inductive and capacitive transfer techniques (Sun *et al.*, 2013). Taking into account of PTE, the far-field technique is not commonly used for WPT; it is rather suitable for high speed and long distance data communication (Aldhaher, 2014; Sun *et al.*, 2013). In order to achieve high PTE for a short distance (within few tens millimeters or centimeters), the near-field transfer method is commonly chosen in most of the WPT research (Aldhaher, 2014). The schematic and basic working principle of available near-field wireless power

transfer i.e.: i) inductive power transfer (Aldhaher, 2014; Schuylenbergh *et al.*, 2009), ii) capacitive power transfer (Aldhaher, 2014), iii) acoustics power transfer (Roes *et al.*, 2013) are illustrated in Figure 2.2.

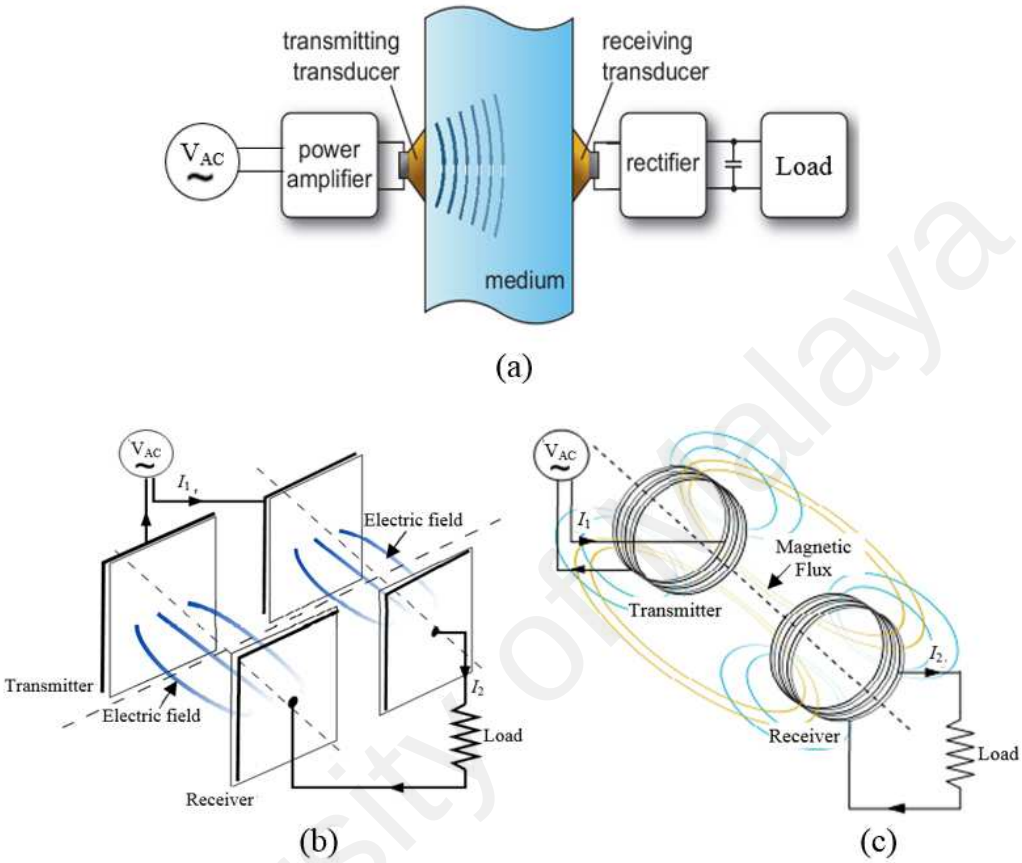

Figure 2.2: The basic operation principle of near field short distance WPT system: (a) Acoustic power transfer (Roes *et al.*, 2013), (b) Capacitive power transfer (Aldhaher, 2014), and (c) Inductive power transfer (Aldhaher, 2014).

All of these techniques have their own figure of merits and drawbacks. Acoustics power transfer is a relatively new form of WPT in which power is being transferred from source to load in the form of sound wave. This technique is suitable for power transfer over a longer distance taking account of transmitter and receiver dimension (Roes *et al.*, 2013). In addition, it has a good capability of misalignment (between transmitter and receiver) tolerance. However, complete performance index of this technique is still obscure such as reflection and attenuation loss in the power transfer through the multi-layer medium between transmitter and receiver spatially in deep tissues implant device.

University of Malaya

In the capacitive power transfer technique, power is transferred between a pair of parallel plates by means of the electric field. This is very less often used method due to strictly limited distance of power transfer. This is mainly because of inverse proportionality of capacitance over the distance between transmitter and receiver plates.

In inductive power transfer, the power is transferred from an inductive power transmission coil (PTC) to a power receiving coil (PRC) by the linkage of the magnetic field. Although, the PTE in this method is inversely proportional to the distance, but it is free from reflection by the medium (if the medium is non-magnetic), therefore it is the most commonly used technique for biomedical application even for deep tissues implants.

Unlike other WPT techniques, inductive technique can attain the PTE up to 95% at short distance (Aldhaher, 2014). In fact, the inductive power transfer is a fast growing research field where the number of publications is being increased almost exponentially (Figure 2.3). Thus, hereinafter this review mainly focused on inductively coupled WPT system.

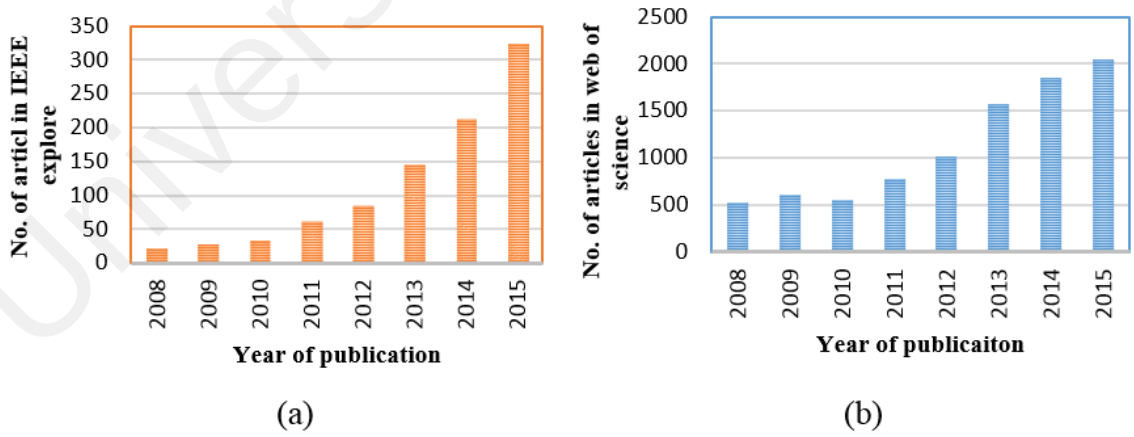

Figure 2.3: The number of articles published in: (a) IEEE explore: journal and magazine only, and (b) web of science. (This search sets with the keywords "wireless power transfer", OR "inductive wireless power transfer", NOT "Acoustic", NOT "capacitive").

University of Malaya

2.3 Basic Block Diagram of Inductive WPT System

The basic block diagram of two coils (PTC and PRC) inductive WPT system for application in the area of biomedical implantable device is shown in Figure 2.4 (Aldhaher, 2014). It consists of four main parts: i) a DC-AC inverter/driving circuit/power amplifier; ii) a PTC; iii) a PRC; and iv) an AC-DC rectifier/power conversion circuit. The DC-AC inverter generates high frequency and high amplitude AC current within the range 1A-8A. The high frequency AC signal is fed to the PTC to allow power to be delivered via inductive link. The inductive link refers to the inductively coupled PTC-PRC which works based on the Ampere's circuital law at the PTC and Faraday's law of induction at the PRC. Based on these two laws, the injection AC signal in the PTC produces high frequency alternating magnetic field (*H*-field). This field covers the PRC and thus induces AC voltage at PRC terminals. The received AC voltage is then converted into DC using AC-DC rectifier and some additional circuit such as voltage regulator and smoothing circuits.

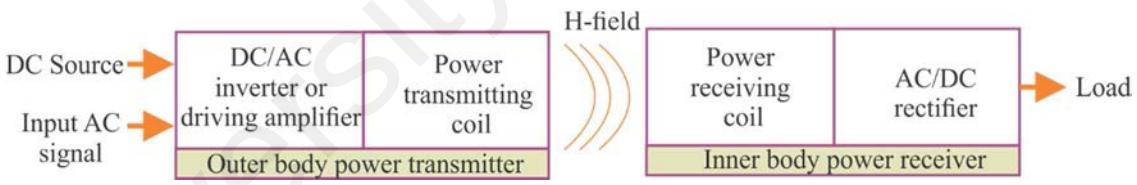

Figure 2.4: Basic block diagram of WPT system for biomedical devices.

2.4 Overview of Inductive WPT System for WCE

An overview of the inductive WPT system for WCE application is shown in Figure 2.5. In this system, the PTC is fixed with the patient body, whereas the PRC is made compact enough to be embedded in a tiny biomedical capsule having dimensions of 27 cm in length and 13 cm in diameter (Li *et al.*, 2008). The tiny size of capsule imposes strict size limitation of the PRC. Small size of PRC (~ 1 cm in diameter) and long distance between the PTC-PRC (15 cm -30 cm) cause the WPT system very weakly coupled. In order to improve the coupling coefficient between PTC-PRC, a high permeability ferrite core is

University of Malaya

used with the PRC. During the operation, the free movement of WCE causes continuous change in relative position and orientation between PTC-PRC and this free movement affects the received power level. In order to minimize the effect of relative position change, a PTC capable of generating uniform magnetic field within the capsule's working area is therefore required. In addition, an advanced 3D configuration of PRC is necessary to minimize the effect of misalignment due to changes in PTC-PRC orientation.

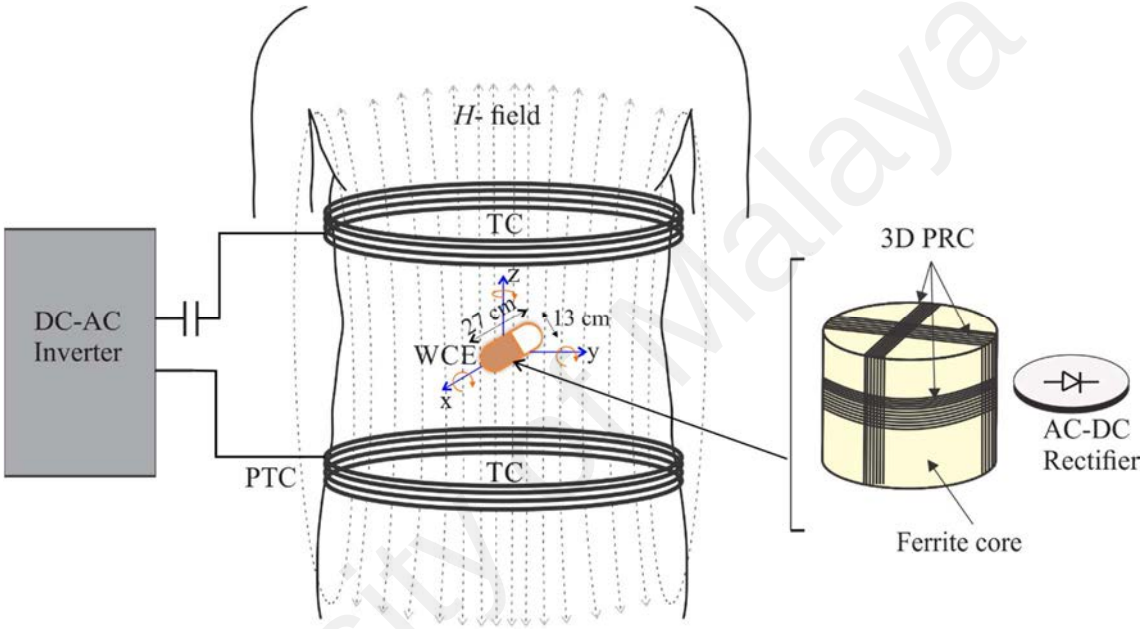

Figure 2.5: Overview of the inductive WPT system for WCE application.

2.5 Current Issues in Design of WPT System for WCE Application

The design of inductively coupled WPT system arises more challenges for the application in biomedical implants where miniaturization of the PRC and electromagnetic safety of biological tissues are highly important. In addition, the design becomes more critical when one of the coils (either PTC or PRC) is freely moving and there is no consistent alignment between these coils (Pan *et al.*, 2011). This happens in the WPT system for WCE application. Generally in the WPT system for WCE, the PTC can be made wearable and the PRC with a power conversion circuit (rectifier and regulator) can be embedded within the capsule. Unfortunately, the required large size of the PTC and

allowable small size of the PRC cause large air gap and very weak coupling between the PTC and PRC. As a result, the PTE becomes low. In addition, the coil misalignment due to the free movement and unpredictable orientation of PRC within 360^0 further reduce the coupling coefficient as well as PTE. In addition, this misalignment causes the received power fluctuating within a large range. Moreover, in real life application, the patient body tissues get exposed to the *H*-field generated by the PTC, therefore, a careful evaluation of the electromagnetic exposure effect is importantly required. Based on the aforementioned issues, the key challenges in the design of WPT system for WCE application can be pointed as below:

- To improve PTE by minimizing the weak coupling effect between the PTC-PRC.
- To improve the received power stability (RPS) with advanced configuration of PTC and PRC.
- To analyze and minimize the electromagnetic effect to the patient body tissues.

2.6 State-of-art in Design of WPT System for WCE Application

A team of RF System lab in Japan is among the pioneer working on WPT system's application for WCE. Their NORIKA project team disclosed their first battery-free microcapsule endoscope in 2003 (Uehara & Hoshina, 2003). This capsule is powered wirelessly from the outer body PTC attached in a coil vest. However, the WPT module in NORIKA system was premature with only one-dimensional PRC which was not capable to ensure received power in omnidirectional orientation of PRC. Later on, the NORIKA system is updated to SAYAKA capsule which includes 3D PRC to ensure omnidirectional PRC (Figure 2.6). The successful testing of this capsule opens extensive research in this field. As a consequence, there are many different designs have been published in academic journals.

University of Malaya

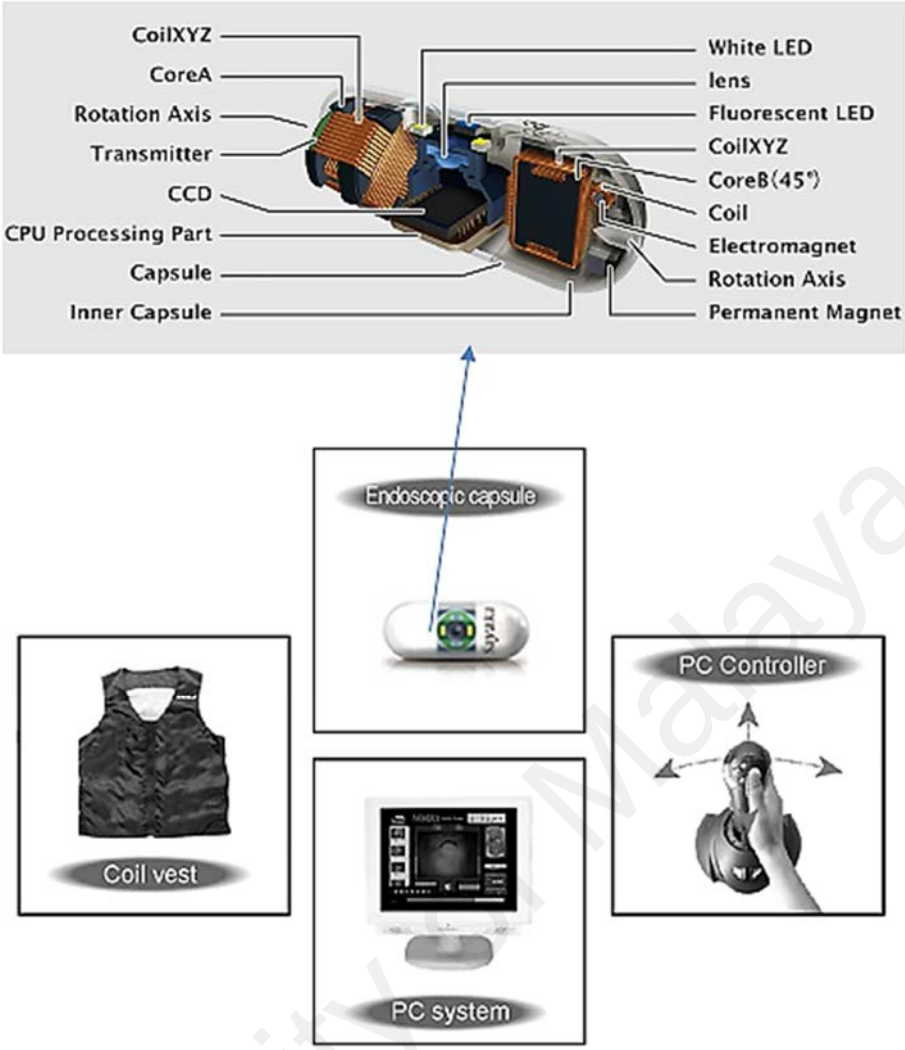

Figure 2.6: Batteryless wirelessly powered WCE system developed by RF system lab Japan.

The existing design of WPT systems can be represented by two main sections: i) power transmitter design, and ii) power receiver design. The power transmitter design includes the design of: a) power amplifier/inverter circuit, and b) PTC. While power receiver design includes the design of: a) PRC, and b) power conversion circuit.

2.6.1 Available design of power transmitter

2.6.1.1 Design of DC-AC inverter/power amplifier

In order to generate a strong alternating magnetic field, the transmitting coil needs to be powered with high alternating current. Because of this requirement, a driving circuit capable of generating high output alternating current is required which convert DC supplied power to AC power and amplifies it up to the desired level. In the power

amplifier, the typical mode of amplifications includes class E or class D amplifier (Jourand & Puers, 2012; Xin *et al.*, 2010). The basic circuit configuration of class E and class D power amplifiers are shown in Figure 2.7 and Figure 2.8, respectively. Although both the class E and class D amplifiers are able to amplify the driving signal, nonetheless, the class E amplifier is widely used due to its advantage in size, cost, and efficiency (Liu *et al.*, 2016). Theoretically, the efficiency of class E amplifier can reach up to 100% (Lenaerts & Puers, 2007; Jourand & Puers, 2012; Narendra *et al.*, 2014a). However, the performance of class E amplifier is highly sensitive to the parameters of the load network (inductance of PTC and resonating capacitor). Due to the environmental effects on the inductance of PTC (L_{coil}) and changing the value of resonating capacitance ($C_{res.}$) with temperature, it is difficult to maintain load impedance with constant value and this lead to utilization of class D amplifiers in some studies (Xin *et al.*, 2010; Yadong *et al.*, 2013a). In both of the cases, the selection of C_{res} should consider its voltage tolerance and its effective series resistance (ESR). The high quality factor (Q) of a PTC generates very high voltage up to several kilovolts across the C_{res}. Thus, the C_{res} is required to be able to cope with this high voltage. On the other hand the high ESR of C_{res} remarkably reduces the overall Q as well as efficiency of the transmitter.

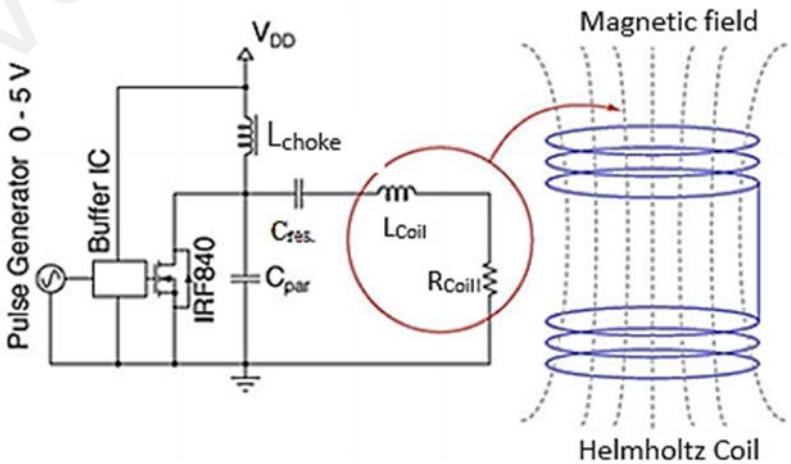

Figure 2.7: Schematic of class E power amplifier loaded with PTC (Jourand & Puers, 2012; B. Lenaerts & Puers, 2007).

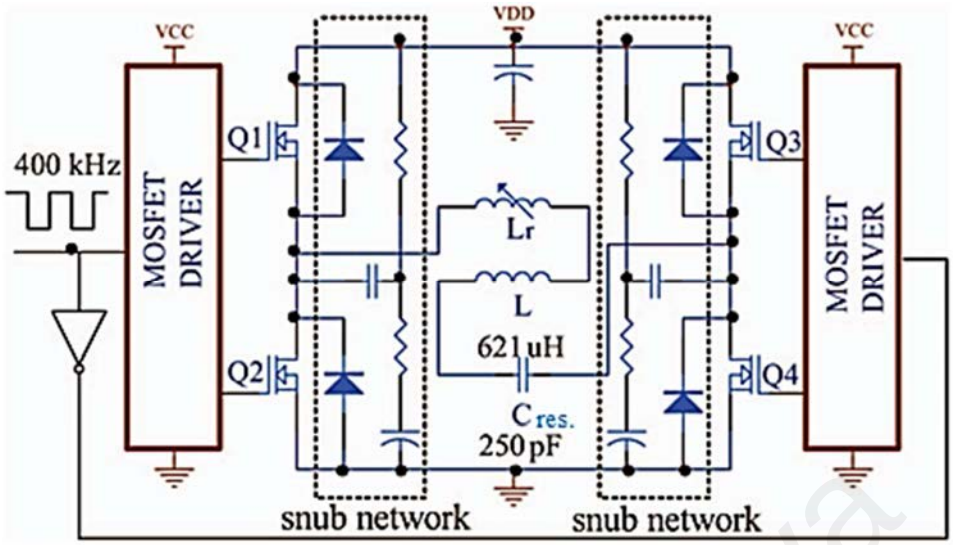

Figure 2.8: Schematic of full bridge class D power amplifier/driving/inverter circuit (Xin *et al.*, 2010; Yadong *et al.*, 2013a).

2.6.1.2 Design consideration for PTC

Five common indexes which need to be in considerations to design the PTC for WPT system are: i) PTC size, ii) H-field distribution, iii) Quality factor, iv) Coupling coefficient, and v) Operating frequency and they are shown in Figure 2.9.

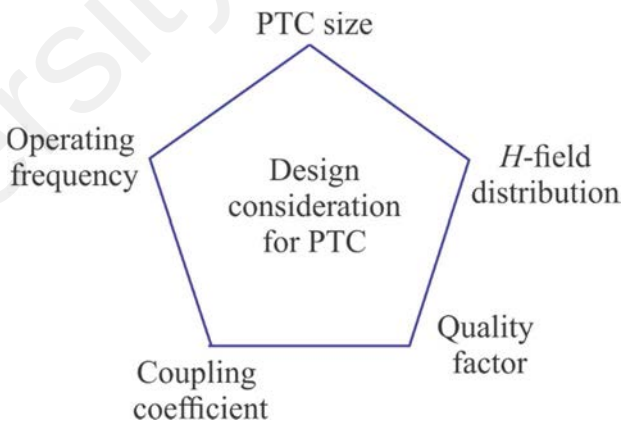

Figure 2.9: Design consideration for PTC adopted from (Sun *et al.*, 2013).

i) PTC size: the PTC size should be compatible to be set with the patient body with sufficient optimization to obtain optimal *H*-field uniformity and PTE. Notably, the large size is good to attain higher *H*-field uniformity but the use of larger size will abruptly reduce system efficiency.

University of Malaya

ii) H-field distribution: this is one of the important goals of PTC design where it is expected as much as possible to be uniform within the possible working region of the capsule. The uniform distribution of *H*-field can ensure stable level of received power irrespective of capsule movement. The *H*-field distribution is mostly related to the size and configuration of the coils used in the PTC such as number of coil segments, their relative separation, turns ratio, etc.

iii) Quality factor: the quality factor (*Q*) of the PTC must be high as much as possible. The high *Q* minimizes resistive loss in the PTC and thus maximizes the efficiency. The *Q* is related to the coil size, coil conductor type, number of turns, and operating frequency.

iv) Coupling coefficient: this is related to the configuration and effective self inductance of the PTC. To obtain maximum PTE, the coupling coefficient is needed to be optimum. The weak coupling causes the PTE low.

v) Operating frequency: all of the design parameters are needed to be optimized so that the coil is able to attain the best performance at the operating frequencies. The operating frequency needs to set in the range of few hundreds kHz (200 kHz – 500 kHz) to maximize the system performance and minimize the electromagnetic effect on patient body tissues (Shiba *et al*., 2008; Xin *et al*., 2010; Ke *et al.* 2016).

2.6.1.3 Existing PTC design

i) *Configuration of existing coil:* In order to obtain a better performance, several types of PTC configurations have been used in the existing design. In general, the available configurations of PTC can be classified into two types which include solenoid coils (Zhiwei *et al.*, 2011; Zhiwei *et al.*, 2012; Yadong *et al.*, 2013a) and Helmholtz coils (Carta & Puers, 2011; Pan *et al.*, 2011). The solenoid coil can be arranged in four different forms: i) single solenoid (Ma *et al.*, 2007); (ii) a pair of solenoids (Xuelin *et al.*, 2011); (iii) a pair of double layer solenoids (Zhiwei *et al.*, 2012) and (iv)

University of Malaya

segmented solenoids (Yadong *et al.*, 2013a). The generalized structures of these coils are shown in Figure 2.10.

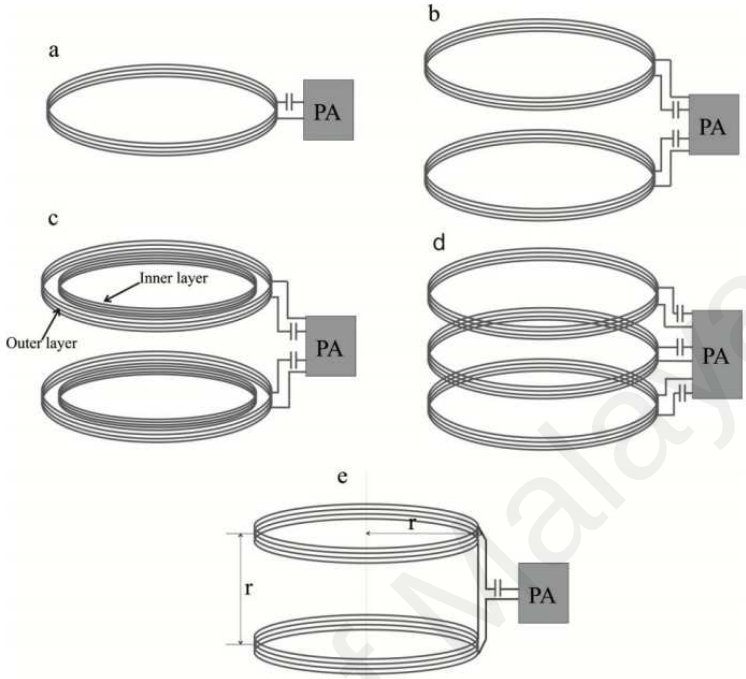

Figure 2.10: Common structures of PTC: (a) single solenoid; (b) pair of solenoid; (c) pair of double layer solenoid; (d) segmented solenoids; (e) Helmholtz coil. (PA = power amplifier).

ii) *Design specification of Existing PTC:* The goal of the PTC design is to obtain high performance indices such as *Q*, coupling coefficient, and uniformity of the generated magnetic field. However, there is lack of effective analysis and optimization to improve the performance indices of PTC. Selection of the existing design parameters such as coil diameter (Ø), number of turns (*n*), and operating frequency (*f*) in different coil configurations such as solenoid coil and Helmholtz coil were not fully discussed. The important design parameters used to construct the PTC in existing studies are summarized in Table 2.1. Ma *et al.* (2007) implemented a tightly wounded small size solenoid PTC of Ø 30 cm and 25 turns of AWG 16 solid copper wire. The *Q* of their implemented coil was measured to be 70 at 58.42 kHz frequency. A larger PTC with a higher number of turns was developed by (Ye *et al.*, 2008). In this study (Ye *et al.*, 2008), the *Q* of the coil was not observed whereas the total coil inductance was

University of Malaya

measured 3476 µH for 66 turns of Ø 40 cm. For AWG 16 solid copper wire, the calculated DC resistance of this coil was 1.06 Ω. In order to generate uniform magnetic field, a large Helmholtz coil of Ø 64 cm was used by (Pan *et al.*, 2011). To minimize skin and proximity effect loss, this coil was constructed with Litz wire which contains 180 strands of AWG 38 enamel wire. The same type of wire was used by (Puers *et al.*, 2011), and (Jourand & Puers, 2012) to construct 12 turns Helmholtz coil of Ø 75 cm. With that wire Liu *et al.* (2015) constructed 25 turns solenoid pair of Ø 40 cm. Puers *et al.* and Journad *et al.* did not report the *Q* of their coils but Liu's coil attained the *Q* as high as 560 at the frequency of 218 kHz. Moreover, the impedance of PTC for different configurations such as Helmholtz, solenoid pair, and double layer solenoid was reported by Jia *et al.* (2012) for a different number of turns from 20 to 40 with an increment of 2 turns. This study also did not report the *Q* of coil and changes of impedance with frequency.

Table 2.1: Specification of existing power transmission coils those were used in previous studies.

Study	PTC Type	Ø (cm)	N	Strands, AWG	L_{eff} (µH)	ESR (Ω)	Q, f (MHz)
Ma (2007)	Solenoid	Ø 30	25	1, 16	368.7	1.8	75, 0.058
Ye (2008)	Solenoid	Ø 40	66	1, 16	3476	DC: 1.1	NA
Pan (2011)	Helmholtz	Ø 64	26	180, 38	631	DC: 5	<143, 181
Puers (2011)	Helmholtz	Ø 75	12	180, 38	187.5	NA	NA
Jourand (2012)	Helmholtz	Ø 75	12	180, 38	147	1.5	615.44, 1
Liu (2015)	Solenoid	Ø 40	25	180, 38	1359	3.3	560, 0.218

The above reported coils were designed with arbitrarily selection of coil parameters such as number of turns, coil diameter, and configuration in which no systematic mathematical modeling and/or optimization techniques were used. However, an analytical model has been developed by Ke *et al.* (2015) to approximate the *Q* of the PTC. This study analyzed the *Q* of PTC with *n*, Ø, and *f*, however, the optimum values were

not recommended. Moreover, this model did not include analysis of overall system efficiency and variation of efficiency with *Q*.

2.6.2 Available design of power receiver

2.6.2.1 Design consideration for PRC

Like the PTC, the *Q*, coupling coefficient and size of PRC need to be optimized. In addition, the dimensions of the coil is constrained to be fitted within a typical capsule, at the same time it is important to ensure maximum received power in any orientation of the capsule. In existing design, an orthogonal structure of 3D PRC is used where three individual coils are orthogonally wound around a high permeability ferrite core as shown in the Figure 2.11 (Xin *et al.*, 2010). In this configuration, the electrical parameters of the coils need to be identical so that the received power by each coil becomes almost equal under similar orientation.

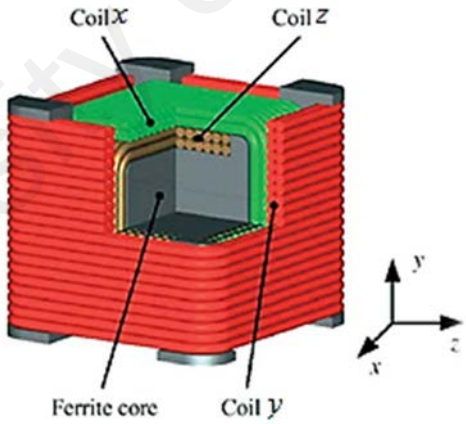

Figure 2.11: Configuration of orthogonal 3D-PRC (Xin *et al.*, 2010).

2.6.2.2 Design specification of existing PRC

The existing WPT systems published in the open literature were experimentally tested through the design of two types of PRC: i) 1D PRC and ii) 3D PRC. Although, the one dimensional coil does not guarantee that the PRC can receive power at all possible orientation of the coil, nonetheless it was used to test the power transfer capability and

University of Malaya

efficiency of the overall system. The specifications of one dimensional power receiving coils are listed in Table 2.2. In earlier design, a ferrite core based PRC with 220 turns of solid copper wire of AWG 35 was implemented by Ma *et al.* (2007). The inductance and *Q* of that implemented coil were 1439 µH and 40, respectively at the frequency 58.42 kHz. Same type of coil was also implemented by Ye *et al.* (2008) with slightly larger diameter and higher number of turns. The *Q* of this coil was not reported but based on the measured inductance and DC resistance it was lower than 34.4 at 36 kHz operating frequency.

Table 2.2: Specification of existing 1D power receiving coil used in previous study.

Study	AWG	*Ø, h* (mm)	*n*	L_{eff} (µH)	ESR (Ω)	Q, *f* (kHz)
(Ma Guanying *et al.*, 2007)	35	Ø 10, h: 8	220	1439	13.11	40@58.42
(Ye *et al.*, 2008)	35	Ø 11.5	232	1340	DC 8.8	<34.4@36

The specification of existing 3D PRCs is summarized in Table 2.3. Carta *et al.* 2009 have investigated four different sets of 3D PRCs with different number of turns, and coil with and without core (Carta *et al.*, 2009). They achieved the *Q* around 35 for the ferrite core coil of 9 mm diameter. The *Q* was further increased up to around 40 using higher number of turns in the PRC (Carta *et al.*, 2010). The *Q* was significantly increased by Xin *et al.* (2010) using multi-stands Litz wire, where around 140 turns with 4 strands of AWG 44 Litz wire was used. The variation of *Q* over the frequency was analyzed in this study which resulted the best *Q* nearly at 75. The *Q* attained by Pan *et al.* (2011) was quite low, perhaps due to the measurement error. A higher strands of Litz wire was used by Jia *et al*. (2012) to improve the *Q*, but the improvement was not significant. The highest *Q*, around 133, was obtained by Liu *et al.* (2015) where they used maximum 11 mm diameter of PRC with 90 turns using 10 strands of AWG 44 wire.

University of Malaya

2.6.2.3 Power conversion circuit

The AC–DC converter or the rectifier is one of the most important blocks in power transfer system. It converts the AC energy received by the receiving coils to DC power for loads. The received power has to pass through this block.

Table 2.3: Specification of existing 3D power receiving coil used in existing study.

Study	AWG, Strands	Coil no	*n*	L_{eff} (μH)	ESR (Ω)	*Q*	*Ø, h* (mm)	*f* (kHz)
Carta (2009)	10, NA	1	33	43.2	7.98	34	Ø 9, h: 9	1000
		2	33	43.7	7.62	36		
		3	33	44.3	7.56	36.8		
Carta (2010)	40, NA	1	45	97.1	13.61	44.8	Ø 9, h: 7	1000
		2	45	99.8	15.47	40.5		
		3	45	97.1	15.21	40.1		
Xin (2010)	44, 4	1	150	478.5	16	75.3	Ø 9.6, h: 9.6	400
		2	140	404.5	13.3	76.7		
		3	130	390.9	13.5	72.4		
Pan (2011)	33, NA	1	150	0.257	DC: 10	<0.029	Ø 9.5, h: 8.9	181
		2	150	0.090	DC: 1	<0.027		
		3	150	0.235	DC: 2	<0.024		
Jia (2012)	44,12	1	160	286	DC: 6.6	<59.32	Ø 13, h: 13	218
		2	160	279	DC: 5.2	<73.45		
		3	160	278	DC: 5.4	<70.48		
Liu (2015)	44, 10	1	90	308.7	3.18	132.9	Ø 11, h: 10	218
		2	90	323.8	3.21	133.5		
		3	90	303.4	3.13	132.7		

Thus the overall PTE is affected by the efficiency of rectifier. The CMOS differential rectifier has good compactness (Sun *et al.*, 2013). However, the threshold voltage of CMOS limits its power conversion efficiency. Several approaches such as low-dropout techniques like the threshold voltage cancellation (Nakamoto *et al.*, 2006), the adaptive threshold (Long *et al.*, 2009), and switch-mode rectifiers (Poon *et al.*, 2009) were utilized to improve the efficiency. But the efficiency was still below of that in Schottky diode rectifier. The majority of AC/DC rectifiers that have been used in recent publications on wireless power transmission systems were either traditional half-wave rectifiers or full wave bridge rectifiers (Lenaerts & Puers, 2007; Pan *et al.*, 2011). The main losses that

University of Malaya

occur in the rectifiers were due to the forward voltage drop of the rectifying elements (diodes) and their switching losses.

Since an AC voltage signal alternately changes its polarity between positive voltage value and a negative voltage value, a half wave rectifier simply allows the positive part of the AC voltage signal to pass to the load while blocking the negative part, or alternatively, passing the negative part and blocking the positive part. The classical half wave Schottky diode rectifier has shown in Figure 2.12. It requires only two diodes for each of the coil thus the less space on the circuit board but it utilized only half cycle of the received signal and results low output power.

Instead of blocking the negative part of the AC voltage signal, a full-wave rectifier not only passes the positive part but also converts the negative parts into a positive voltage. Consequently, the full-wave rectifier needs a higher number of components compared to that of the half-wave rectifier. The unwanted voltage ripples from this approach are smaller. The use of classical full wave bridge rectifier (Figure 2.13) provides the highest efficiency. However, the efficiency of this rectifier relies much on the selection of the Schottky diode, where the lowest threshold voltage at the high forward current is most preferable.

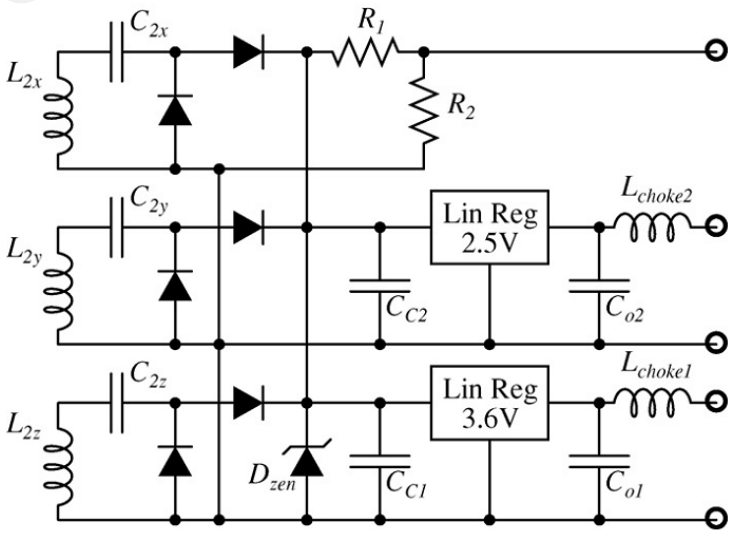

Figure 2.12: Configuration of half-wave rectifier circuit to rectify alternating current received by 3D PRC to a direct load current (Lenaerts & Puers 2007).

2.7 Specifications of Existing WPT System for WCE

The performance of WPT system for WCE is assessed by few parameters such as transmitting and receiving coil size, amount of transferred power, power transfer link

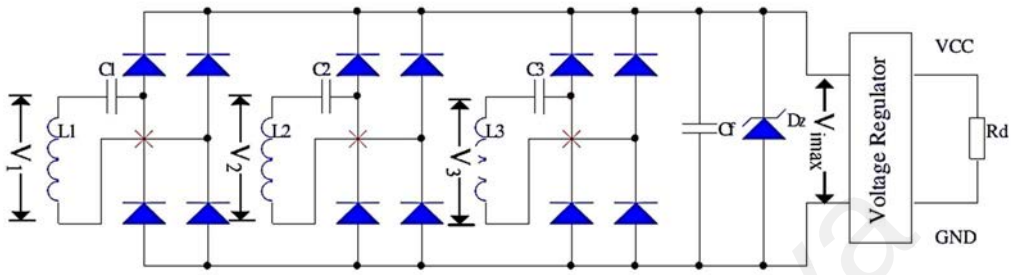

Figure 2.13: Configuration of full-wave rectifier circuit to rectify alternating current induced in 3D PRC to a direct load current (Pan *et al.* 2011).

efficiency, and stability of the transferred power and electromagnetic safety of nearby biological tissues. For an ideal system transmitting coil size should be optimized to fit patient body, receiving coil size should be small enough to be embedded in the capsule, the transferred power must be adequate and the PTE should be high as much as possible while received power level need to be stable with respect to the misalignment of the coil. In addition, the electromagnetic safety is the prerequisite for practical application, where safety indices such as current density (J, A/m^2) and specific absorption rate (SAR, W/kg) are needed to be below of the standard limits. All of the aforementioned parameters of existing systems are summarized in the sections below.

2.7.1 Transferred power and efficiency

The specification of existing WPT systems and attained link efficiency for desired received power have been summarized in Table 2.4. An initial design of WPT system for capsule endoscopy was proposed by Lenaerts *et al.* in (2007). That system used solenoid type transmitting coil and moderate size of transmitting and receiving coil. Prototype of that system was capable of transferring 150 mW power at the 1% dc-dc efficiency. In the same year, Guanying *et al.* (2007) reported that their system attained the efficacy of 1.3

University of Malaya

%. The transmitting coil diameter of Guanying's system was lower than that of Lenaerts's system which reduced the transfer distance; perhaps that was the factor to improve the link efficiency. Ryu *et al.* (2007) miniaturized the receiving coil size up to Ø 8 mm and *h* of 5 mm while enlarging the transmitting coil up to Ø 60 cm but the efficiency of this study was not reported in the paper. Ye *et al.* (2008) tested their developed WPT system by transferring 480 mW power at the link efficiency of 1.6%. But the size of Ye's receiving coil was larger than that of all earlier developed WPT systems. Two years later, Xin *et al.* (2010) proposed Helmholtz coil based WPT system which could transfer at least 310 mW power, however, the link efficiency did not improve by that system since the transmitting coil was relatively large. Carta *et al.* (2010) and Pan *et al.* (2011) also developed large Helmholtz coil based WPT systems which were capable of transferring 300 mW and 136 mW power. In addition, Jourand *et al.* (2012) investigated on the inductive power delivery system with very large transmitting coil of 75 cm diameter to cover entire upper body of the patient and powering multiple devices. The large transmitting coil results the link efficiency as low as 0.33%. A two hop WPT system was presented by Sun *et al.* (2012) in which an end field helical power transmitter coil transferred the power from floor to a power relay in the patient jacket by strong coupling and then power was delivered to a capsule by a loosely coupled open end helical power relay. There was no wire connection between the power relay and city power supply and this allows the patient walk freely. This system was able to transfer an average power of 24 mW with the maximum efficiency of 3%. This high efficiency was mainly contributed by a highly efficient switch-mode rectifier circuit which minimized the power conversion loss in the power link. In addition, a mathematical programming model is proposed by Jia *et al.* (2012) to improve the power transmission link efficiency. To verify the feasibility this model, various transmitting and receiving coils with different coil impedance are designed and evaluated in this thesis. Finally, a double layer solenoid pair

University of Malaya

transmitting coil of Ø 40 cm and relatively large 3D receiving coil of Ø 13 mm and *h* 13 mm were used in their optimum system. The optimal system had capability of continuously transferring 500 mW power at 4.08% link efficiency. Adding to this, Na *et al.* (2015) presented a theory for tracking the optimal efficiency of magnetic resonance based WPT system. Based on that theory a WPT system was implemented with four coils (power, transmitting, receiving and load coils) where the receiving coil was Ø 9 mm and helical transmitting coil was Ø 22 cm. In this system the small transmitting coil plane to set with the patient body with coronal orientation which results the link efficiency as low as 0.02%. Also Liu *et al.* (2015) presented a WPT system for dual head WCE designed with a new type of receiving coil to maximize the uniformity of received power with coil orientation. The new receiving coil was designed with three coils reeled on a ferrite ring with 120^0 apart. The implemented coil's diameter and height were 10 mm and 11 mm respectively. The final design attained the RPS 78.3% and link efficiency 3.51% when transfer minimum 108 mW of power. Moreover, Ke *et al.* (2015) incorporated an analytical model for optimization of *Q* of PTC. For optimal performance they implemented a solenoid pair transmitting coil of 69 cm diameter and constructed with Litz wire. However, the link efficiency did not improve significantly with this large transmitting coil even through this coil had high *Q*.

University of Malaya

Table 2.4: Design specification and performance indices of related WPT systems in the literature.

Systems	Tx-coil	Tx coil Ø (cm)	Rx coil Ø, *h* (mm)	*f* (in MHz)	*d* (cm)	Rx-Power (mW)	Link η (%)
Lenaerts (2007)	Solenoid	Ø 41	Ø 10, h: 13	1.056	20.5	150	1
Ma (2007)	Solenoid	Ø 30	Ø 10, h: 8	0.058	15	170	1.3
Ryu (2007)	Helmholtz	Ø 60	Ø 8, h: 5	0.125	5	300	NA
Ye (2008)	Solenoid	Ø 40	Ø 11.5	0.036	20	480	1.6
Xin (2010)	Helmholtz	Ø 64	Ø 10, h: 12	0.400	32	≥310	1.24
Carta (2010)	Helmholtz	Ø 60	Ø 9.5, h: 7	1.000	30	300	NA
Pan (2011)	Helmholtz	Ø 64	Ø 9.5, h: 8.9	0.181	32	136	NA
Jourand (2012)	Helmholtz	Ø 75	Ø 9	1.00	37.5	300	0.33
Sun (2012)	Helix	Ø 31	Ø 11	13.56	15.5	24	3
Jia (2012)	Solenoid pair	Ø 40	Ø 13, h: 13	0.218	20	≥500	4.08
Na (2015)	Helical	Ø 22	Ø 9	16.47	7	300	0.02
Liu (2015)	Solenoid pair	Ø 40	Ø 10 ,h: 11	0.218	20	108	3.51
Ke (2015)	Solenoid pair	Ø 69	Ø 9.5, h: 10	0.22	34.5	Max: 750	3.55

University of Malaya

2.7.2 Received Power Stability

The stability of received power highly depends on the alignment between power transmitting coil, receiving coil and their relative position when one of the coils is freely moving. For the application in the WCE, the PTC is fixed to the patient's body, but the PRC has freedom of motion which may cause misalignment between the PTC and PRC, and as a result the received power at the load varies. Referring to Figure 2.14, there are three kinds of misalignment: (i) axial misalignment (d_0); (ii) lateral misalignment (r_0); and (iii) pitch misalignment (α_0) as indicated in Figure 2.14 (Pan *et al.* 2011).

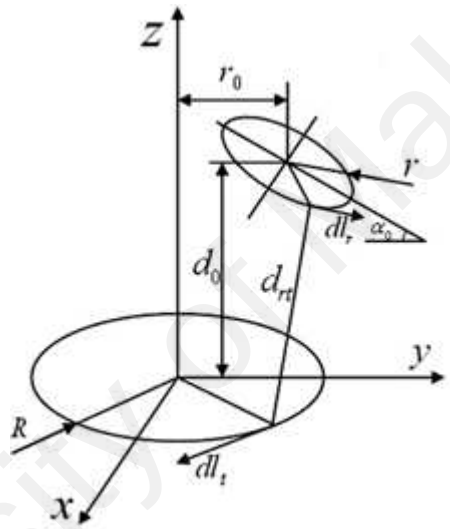

Figure 2.14: Model of relative alignment between PTC and PRC (Pan *et al.* 2011).

The effect of misalignment between PRC and PTC in WPT system can also be seen in different parameters such as coupling coefficient, efficiency, and received power of WPT system. The stability of received power, in terms of observed parameters, has been approximated based on the formula given in (2.1), where, "Max" and "Min" were the maximum and minimum values of the observed parameters within the possible misalignment. The d_o and r_o misalignment are considered within ± 10 cm and ± 15 cm, respectively, while the α_0 is considered within ± 90^0. During practical operation, the misalignment of capsule can occur within this range. The effects of d_0 and r_0 depend on the uniformity of *H*-field generated by the PTC while the effect of α_0 relies on the design of PRC.

University of Malaya

$$\text{Stability} = \left(1 - \frac{Max - Min}{Max}\right) \times 100\% \tag{2.1}$$

The power transfer stability against the misalignment of the coils' has been reported in Table 2.5 from the existing WPT system. Lenaerts *et al.* (2007) observed the misalignment effect by looking at the variation of efficiency. According to their measurement, the 3D receiving coil was able to deliver 55% stable power with respect to the orientation of coil. Ma *et al.* (2007) analyzed the misalignment effect by the variation of coupling coefficient. For their solenoid coil based system, the coupling coefficient was 38% and 43% stable against axial and radial misalignment, respectively. In addition, Li *et al.* (2008) conducted experiment with three sets of Helmholtz coils as PTC and compared their results with that obtained by single Helmholtz coil set. The results showed that three sets of Helmholtz coil have better stability than single Helmhotz coil. The stability obtained by this three Helmholtz coils system was approximately 60% and 56% with axial and pitch misalignment. Besides, Xin *et al.* (2010) used a large Helmholtz transmitting coil and improved the stability up to 82.1% with axial and radial misalignment, however, their 3D receiving coil still resulted in 41.3% stability with pitch misalignment. Additionally, Pan *et al.* (2010) reported large Helmholtz coil resulted the stability of coupling coefficient 74% and 83% with axial and radial misalignment, respectively. Carta *et al.* (2010), observed stability of received power (for 3D receiving coil) with variation of pitch misalignment. According to their experimental results, the received power was 78% stable. However, in spite of using 3D receiving coils (three coils are orthogonal to each other), Jia *et al.* (2012) and Shiba & Higaki (2009) could attain the stability of received power 35% and 22.8%, respectively. As the results shown by Jia *et al.* (2012), their received power varied within a large range from 526mW to 1502mW. While as reported in Shiba's work, the variation of received power ranged from 80mW to 350mW. Liu *et al.* (2015) used new type of 3D receiving coil in which three receiving

University of Malaya

coils were wounded on a ferrite ring with 120^0 apart. This design of receiving coil obtained 61.3% stability of received power.

Table 2.5: Overview of existing WPT system stability.

Study	Coil Type (PTC, PRC)	Observed Parameter	Approximate Stability
Lenaerts (2007)	solenoid, 3D	Efficiency	55% with α_0
Ma (2007)	Single solenoid, 1D	Coupling coefficient	38% with d_0, 43% with r_0
Li (2008)	Helmholtz, 1D	Efficiency	60% with d_0, 56% with α_0
Xin (2010)	Helmholtz, 3D	Received power	82.1% with r_0, 41.3% with α_0
Pan (2011)	Helmholtz, 3D	Coupling coefficient	74% with d_0, 83% with r_0
Carta (2011)	Helmholtz, 3D	Received power	78% with α_0
Jia (2012)	Solenoid pair, 3D	Received power	35% with α_0
Shiba (2009)	Solenoid pair, 3D	Received power	22.8% with α_0
Liu (2015)	Solenoid pair, new 3D	Received power	61.3% with α_0

2.7.3 Effect of WPT system on body tissues

Improper configuration of a WPT system for powering an implantable biomedical device may cause unnecessary effects due to exposure of patient body to a strong electromagnetic energy (Shiba *et al.*, 2008a). Therefore, concern of electromagnetic effect on patient body tissues must not be avoided. At the frequencies of 100 kHz-10 MHz, the effects include: i) stimulus action due to induced current within the tissues, and ii) rising temperature due to the absorption of electromagnetic energy by the tissues (Jia *et al.*, 2012). Those effects are often indexed by current density (J, A/m^{-2}) and specific absorption rate (SAR, W/kg), respectively which can be expressed by:

$$J = \pi C f \sigma \mu H, \text{and } SAR = \frac{J^2}{\sigma \rho} \tag{2.2}$$

University of Malaya

where C, μ and H are the hypothetical loop radius of the currents in the exposed tissues, magnetic permeability and H-field intensity, σ and ρ are the electrical conductivity and the weight density of the biological tissues respectively (Christ *et al.*, 2013; Shiba *et al.*, 2008a).

2.7.3.1 Standard limit on electromagnetic exposure

To guard against undesirable electromagnetic exposure effects, several scientific committees and organizations have developed exposure guidelines. Generally, the guidelines standardized the basic restrictions on induced J and SAR, above which the electromagnetic effects are expected. However, in many situations, direct measurement of J and SAR are technically impractical. Therefore, the guideline also defines reference level of maximum allowable exposure limit of electromagnetic fields. Where, the basic restrictions are presumed to be fulfilled if the exposure is below of the reference level. Table 2.6 shows the reference levels defined by most of the prominent groups such as International Commission on Non-Ionizing Radiation Protection (ICNIRP) and IEEE Standards Coordinating Committee 28 (SCC28). The reference level is different for the general and occupational public. Normally, the occupational population consists of adults who are trained to be aware of the potential risk. Since the WPT system for biomedical device operates with reactive near fields, in many cases application of reference level most probably gives over conservative result.

Table 2.6: Reference level of electromagnetic exposure limit.

Standardized by	f_M	H-field (A/m)		E-field (V/m)	
		GP	OP	GP	OP
ICNIRP (1998)	0.15-1	$0.73/f_M$	$1.6/f_M$	87	610
IEEE (2005)	0.1-1	$16.3/f_M$	$16.3/f_M$	614	1842
ICNIRP (2010)	0.003-10	21	80	83	170
NB: f_M, GP and OP are used to denote the frequency in MHz, general public and occupational public, respectively.					

Thus, according to the guideline probably there is no harm to exceed the reference level if the SAR and J are still below of basic safety level. On the other hand, temperature

of the nearby tissues could increase due to the overheating of PRC when excessive power required to be regulated. According to the Japan Society of Medical Electronics and Biological Engineering (JSMEBE), the temperature in the tissues cannot be exceeded 42.5 °C (JSMEBE, 2002). The safety specifications for WPT systems, standardized by ICNIRP and JSMEBE are given in Table 2.7.

Table 2.7: Basic safety limitation for human body tissues by ICNIRP and JSMEBE.

	By ICNIRP				By JSMEBE
Frequency Range	**Localized SAR (W/kg)**		**Average SAR (W/kg)**	**Current Density (mA/m²)**	**Temperature of RC**
	Head and Trunk	**Limb**			
1 kHz–100 kHz	—	—	—	<f (Hz)/100	<42.5 °C
100 kHz–10 MHz	<10	<20	<0.4	<f (Hz)/100	
10 MHZ–10 GHz	<10	<20	<0.4	—	

2.7.3.2 Electromagnetic exposure effect observed in existing studies

The electromagnetic safety of existing WPT systems are evaluated by observing SAR and *J*. Since the direct measurement of SAR and *J* are very difficult and almost impractical, these parameters were analyzed using numerical simulations with a computer based human body models. The outcomes of available analysis on SAR and *J* of the WPT system for WCE are summarized in Table 2.8 with corresponding ICNIRP limit.

Xin *et al.* (2010) evaluated the SAR and *J* in a computer based on high resolution human body model with 56 different kinds of tissues. The SAR and *J* were computed using finite integration technique based numerical simulation. In the simulation, a PTC of Ø 64 cm was excited by 78 amp-turn at 400 kHz. With this excitation, the computed average SAR and *J* were 0.392 W/kg and 3.82 A/m^2, which are close to the ICNIRP limits 0.4 W/kg and 4 A/m^2 respectively at 400 kHz.

Jia *et al.* also used same kind of simulation scheme and observed the whole body SAR 8 W/kg and *J* 1.8 A/m^2 in comparison to the limits of 10 W/kg and 2.18 A/m^2 at 218 kHz.

In addition, the SAR and *J* were found to be below the safety limit in (Li *et al.*, 2008; Sun *et al.*, 2012). The ESR-based SAR evaluation in (Lenaerts & Puers, 2007) showed that in the patient's hands down condition, 7 A PTC current at 1 MHz frequency results in 1.16 W/kg average SAR where the ICNIRP limit is 0.4 W/kg. Copper shielding of the inner and outer transmitting coil was used to control the excessive SAR, but this detunes the resonance frequency from 1 MHz to 1.4 MHz. Moreover, the SAR and *J* were analyzed by Shiba *et al.* (2008b) for the range of frequency from 100 kHz to 700 kHz and the results indicated that the *J* was less influential between 300 kHz to 400 kHz. In another study, Shiba *et al.* indicated that at 50 kHz, *J* greatly exceeded the restriction when the input current to the PTC was 1.94 A.

Table 2.8: Overview of electromagnetic safety of existing WPT system.

Study	**PTC Type, Ø** cm	**Input Power**	**f(kHz)**	**SAR (W/kg)**		***J* (A/m^2)**	
				Observed	**limit**	**Observed**	**limit**
Xin (2010)	Helmholtz, 64	78 amp-turn	400	0.392	**10**	3.82	**4**
Jia (2012)	Solenoid, 40	1.8 A	218	8	10	1.8	2.18
Lenaerts (2007)	Solenoid, 41	7 A	1056	1.16	0	NA	NA
Sun (2012)	Power relay, 31	8 W	1356	< 0.1(av)	NA	NA	NA
Li (2008)	Helmholtz, 32	35 W	50	NA	NA	0.47	0.5

2.7.4 Effect of biological tissues on the WPT system

A big size of biological tissues close proximity to the WPT coils may have some effect to change the system performance. Tissues located close to the coil may change the self-inductance and/or stray capacitance of the coil. Since the biological tissues have frequency dependent high permittivity, slightly conductivity and constant permeability, therefore, capacitive interaction is predominant over the inductive. Thus, the resonance frequency of WPT coils operating close proximity to the biological tissues may detune

University of Malaya

by changing the stray capacitance between the turns in the coil, as a consequence, system performance can be improved.

In the existing literature, there were several studies that investigated the effect of biological tissues proximity to the inductive coils for WPT. The methods and key observations of these investigations are summarized in Table 2.9. In order to analyze this effect, the impedance of resonant primary coil was evaluated in air and with a real human subject (Lenaerts & Puers, 2007). It was observed that the primary coil has detuned, impedance and absorption loss were increased when the coil was parasitically coupled with human body. These effects moreover increased when the subject's hands were down in comparison to hands up. Pan *et al.* (2011) also observed this effect by looking at the transferring power. In their investigation, they observed that when the PRC was covered with a piece of pig fat (6 cm thick), the received power reduced from 150 mW to 136 mW (it is about 8% reduction). This was due to the absorption loss by the biological tissues. In addition, Ryu *et al.* (2007) evaluated the received power by putting the PRC in side of an animal body (pig). They observed the received power by the performance of the LED which was connected to the PRC. Finally, they concluded that the animal body did not affect the performance of WPT system perhaps this was due to the low frequency, 125 kHz, at what the WPT system was operated. Similar experiment also conducted by Shi *et al.* (2015) with a pig of 20 Kg weight. They observed the performance of WPT system by looking at PTE which was reduced from 3.5% (in air) to 2.8% (in pig). Moreover, Na *et al.* (2015) investigated the penetration of power through the real biological tissues. In their experiment, they used a spherical pork chop with radius of 7 cm where PRC was placed at the center of pork chop. From the measurement of PTE, they concluded that the presence of pork tissues reduced the PTE by 0.062% which was negligible.

University of Malaya

Table 2.9: Effect of biological tissues on the performance of WPT system.

Study	Experiments	Observation
Lenaerts (2007)	PTE was investigated by looking at the impedance of primary coil in air and in real human subject.	At around 1.056 MHz, the PTE was decreased.
Pan (2011)	Received power was measured in air and when PRC covered with a 6 cm thick slice of pig fat.	At 181 kHz, received power reduced by 8% when PRC covered with a pig fat.
Ryu (2007)	Received power was observed by the illumination of LED putting the PRC inside a pig body.	The power receiving performance was not affected at 125 kHz (perhaps due to low frequency)
Shi (2015)	PTE was observed setting the PTC around and PRC inside an anesthetized pig of 20 Kg weight.	At 208 kHz frequency, the PTE reduced from 3.5% in air to 2.8% in pig.
Na (2015)	PTE was measured in air and putting the PRC in a pork chop of spherical shape with 7 cm radius.	At 16.47 MHz, the presence of biological tissues reduces the PTE by 0.062%.

Finally, in above investigations few of them observed the significant effect (Pan *et al.*, 2011; Shi *et al.*, 2015) but other not (Na *et al.*, 2015; Ryu *et al.*, 2007). Therefore, it is difficult to conclude that biological tissues proximity to the WPT system would likely degrade the system's performance significantly or not.

2.8 Summary

Based on the existing literature, the most important performance indices of WPT system for WCE were PTE, received power stability, electromagnetic safety and miniaturization of the receiver unit. Whereas the important design parameters were dimension of inductive coils, number of turns in the coil, operating frequency, quality factor, coupling coefficient, and magnetic field uniformity. The existing studies have been accessed based on the method for the selection of these design parameters and resultant performance of the system.

University of Malaya

2.8.1 Design and optimization of WPT system

Proper design and optimization are important to trace the best performance of WPT system. Although many research have been conducted on the design and optimization of WPT system, nonetheless, most of the studies have arbitrarily selected the important design parameters such as coil diameter, number of turns, wire type, operating frequency (Liu *et al.*, 2015; Sun *et al.*, 2012; Yan *et al.*, 2015). These parameters are selected based on simple assumption rather than rigorous analysis. Jia *et al.* (2012) have simply investigated the impedance of the PTC by varying the number of turns in three different coil configurations including a Helmholtz coil, a pair of solenoid coil and a double layer solenoid coil. However, the effect of this impedance on the coils' quality factor as well as overall PTE was not indicated in that investigation. In addition, the investigation just simply implemented the PTCs with different number of turns and directly measured the impedance rather than providing any mathematical model. Another study, Ke *et al.*, (2015) provided an analytical model that accurately calculated the quality factor of PTC. Nonetheless, none of the existing studies have fully analyzed the overall system efficiency and optimum design parameters. Therefore, further research is still required to develop a complete mathematical model to analyze the optimum design parameters of a WPT system. Moreover, most of the existing studies merely tested the capability of the transferred power of their proposed WPT system in air medium (between PTC and PRC). However, the study in (Pan *et al.*, 2011) suggests that the transferred power may be significantly reduced by the presence of biological tissues between PTC and PRC, thus, a rigorous *in vitro* test is necessary to validate the actual performance of the WPT system in the WCE environments.

University of Malaya

2.8.2 Stability of received power

The self-directed movement and alignment of capsule in the GI path cause misalignment between the PRC and PTC resulting in fluctuation of the received power at the PRC, *i.e.*, the power at the receiver is not always stable. Two kinds of stabilities have been assessed in the literature, namely position stability (due to axial and lateral misalignment) and orientation stability (due to pitch misalignment). In terms of coupling coefficient, the misalignment analysis in (Pan *et al.*, 2011) showed that WPT link obtained 30% orientation stability and 63% position stability. The WPT system designed for the optimum power transmission in (Xin *et al.*, 2010) obtained an orientation stability of 41.3% and a position stability of 82.1%. The best orientation stability of 84% was obtained in (Carta *et al.*, 2011). However, the analysis by (Pan *et al.*, 2011; Xin *et al.*, 2010) showed that the orientation stability theoretically can reach up to 57.8% when three coils of 3D PRC having same power receiving capabilities. This analysis indicated that there might be some measurement error in the result of 84% orientation stability attained by Carta *et al.* (2011). In order to overcome the orientation misalignment problem, a 3D orientation insensitive power receiver is proposed by (Ghotbi *et al.*, 2013). The analysis and results showed that the 3D orientation insensitive coil could almost overcome the orientation misalignment problem.

On the other hand, the typical Helmholtz coil (THC) has commonly been deployed to overcome the position misalignment by generating uniform magnetic field. However, the region of uniform magnetic field was limited around the center of the THC. Deploying a large diameter of THC can overcome this problem but it remarkably reduces the PTE. In addition, the large THC was not compatible for portable/flexible transmitting system. Therefore, an investigation is importantly required to improve the magnetic field uniformity within a PTC of limited diameter.

University of Malaya

2.8.3 Analysis of biological tissues safety

Moreover, the safety is a major considering issue for the clinical use of WPT system and it must be ensured. According to the safety analysis, specific absorption rate (SAR) and current density (*J*) always should be within acceptable level (Shiba & Higaki, 2009; Shiba *et al.*, 2008a; Xin *et al.*, 2010; Zhiwei *et al.*, 2011). However, the current density may exceed the restriction standardized by ICNIRP under certain level of system frequency and driving current applied to the PTC. The current density increased along with increasing the system frequency and driving current which imposes the limit on the maximum system frequency and driving current to maintain the safety level (Shiba *et al.*, 2008; Zhiwei *et al.*, 2011). The studies in (Shiba & Higaki, 2009; Shiba *et al.*, 2008a) revealed that the SAR mostly depends on the terminal voltage of PTC but the current density varies according to the excitation current applied to the PTC. So, tuning of these two parameters may maintain the SAR and current density to be within the desired level. Alongside, as the safety indexes highly depend on the voltage/current applied to PTC, the improvement of power transmission efficiency can make easier to keep safety parameters well below of the standard limits. As for the problem associated with PRC temperature, this can be overcome by using multi-strands wire as suggested by (Zhiwei *et al.*, 2011).

University of Malaya

CHAPTER 3: EFFICIENCY IMPROVEMENT OF WPT SYSTEM

3.1 Introduction

Magnetic resonance-based inductively coupled wireless power transfer (WPT) system can be considered as a promising technology to address the power shortage problem that encountered by the next generation's biomedical wireless capsule endoscopy (Na *et al.*, 2015; Sample *et al.*, 2011). In this WPT system, high efficiency of inductive link is of great importance. With perfect tuning of power transmitting and receiving coils, the efficiency of such system mainly depends on the coupling coefficient (k) between the coils, the coils' quality factor (Q), and the load impedance matching with the internal resistance of the PRC (Ke *et al.*, 2015). Despite numerous research, the k and Q of coils have not been fully analyzed and optimized, as a consequence, the efficiency of the existing designs was still low which in the range of 0.02 - 3.04% (Sun *et al.* 2012; Na *et al.*, 2015). Thus, in this chapter, a new configuration of power transmission coil named PTC-I is proposed to improve the efficiency and received power stability (RPS) by the improvement of k, Q and H-field uniformity. The performance of the proposed PTC-I has been analyzed using a mathematical model. The analytical performance of the proposed PTC also has been compared with that of the three existing PTCs. Adequate analysis, optimization, and a comparative study have shown that the proposed PTC-I and an optimized power receiving coil (PRC) tremendously improved the efficiency.

3.2 Literature Review

The power transfer efficiency (PTE) of inductive link for WCE application was poor due to tiny size of the PRC and the large distance between the PTC and the PRC. For example, Jourand *et al.* (2012) developed a WPT system with a PRC of 9 mm diameter. The PRC system was small enough to be embedded in the existing capsule size. The typical Helmholtz coil (THC) based PTC was as larger as 75 cm in diameter which could

University of Malaya

cover the whole abdominal region. The PTE attained by this system was as low as ~0.33% at the 37.5 cm transmission distance. In the last few years, significant research efforts have been dedicated to the development of an efficient WPT system for WCE application (Carta *et al.*, 2011; Ma *et al.*, 2007; Jia *et al.*, 2012; Jourand & Puers, 2012; Ke *et al.*, 2015; Lenaerts & Puers, 2005; Lenaerts & Puers, 2007; Na *et al.*, 2015; Pan *et al.*, 2011; Shiba *et al.*, 2008b; Sun *et al.*, 2012; Xin *et al.*, 2010). However, the PTE of the existing designs remains low within the range from 0.02% to 3.55% (Sun *et al.*, 2012; Ke *et al.*, 2015; Na *et al.*, 2015; Shi *et al.*, 2015). Recently, Na *et al.* (2015) proposed four coils based resonant WPT system, in which the optimal efficiency tracking theory attained the overall PTE of 0.02% at a 7 cm distance. Shi *et al.* (2015) also proposed a portable WPT system for a video capsule endoscope, in which three different PTC configurations were discussed. Their optimal configuration attained a PTE of 2.8% at 20 cm transmission distance. Liu *et al.* (2015) designed a WPT system for WCE. Their design incorporated a new type of PRC, which improved the received power stability and attained the PTE of 3.51%. Ke *et al.* (2015) developed an analytical model to calculate the quality factor of the PTC. This design attained a PTE of 3.55% with an enlarged PTC of 69 cm in diameter. Some other studies on the wireless powered capsule endoscopy have been presented in (He *et al.*, 2015; Liang *et al.*, 2015). However, the important performance indices of the WPT system have not been discussed in detail. Furthermore, a complete modeling of the WPT system remains limited. The important performance indices, such as *Q*-factor, coupling coefficient, *H*-field uniformity, and efficiency, have not been thoroughly analyzed in the existing designs. Moreover, the electromagnetic effects on the biological tissues have not been investigated by incorporating the PRC with a high-permeability ferrite core. On the basis of the summary of existing design limitations, this chapter presents a WPT system for the capsule endoscope with a new PTC configuration to

University of Malaya

achieve higher coupling coefficient, quality factor, and magnetic field uniformity to improve the PTE, received power stability, and electromagnetic safety.

3.3 Materials and Methods

3.3.1 WPT system overview in WCE platform

Figure 3.1 has shown a schematic of the magnetic resonance-based inductively coupled WPT system in WCE platform. A PTC can be made wearable, and a PRC with a power conversion circuit (rectifier and regulator) can be embedded within the capsule. The PTC is excited by a time-varying current I_t (generated by the power amplifier) to produce a time-varying *H*-field. A part of the generated *H*-field interacts with the PRC and induces voltage. Hence, power is being transferred from the source to the load by the linkage of the *H*-field. In this setup, the power level at the load can be adjusted by exciting the PTC with a higher or lower level of power source. However, transferring a high amount of power with low efficiency does not only waste of power but also increases the effect of the electromagnetic field on the nearby tissues. This electromagnetic effect on the nearby body tissues increases with the non-uniformity of *H*-field generated by the PTC.

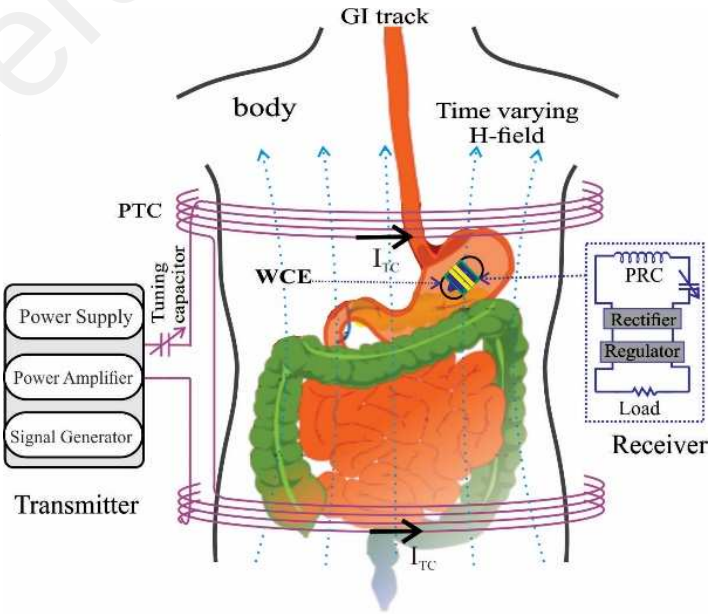

Figure 3.1: Schematic of a WPT system with a PTC fixed around the patient body and a WCE consists of a PRC and a receiver circuit located in the human GI tract (Basar *et al.*, 2016a).

Generally, *H*-field is not perfectly uniform in this type of non-radiating (near-field) PTC. The field is much stronger at the positions near the winding of the PTC and weaker at the positions a bit away from the PTC winding (Pan *et al.*, 2011). This field characteristic results in a very high power level and better efficiency in the strong field regions but a lower power level and lower efficiency in the weak-field regions (Na *et al.*, 2015; Pan *et al.*, 2011). As a consequent, the power received by the PRC becomes unstable when it moves within the non-uniform fields. In addition, the received power at the PRC in the weak-field regions might be insufficient to power up onboard circuitries. Although, the PTC can be excited with a higher power to boost up the received power level in the weak-field regions, however, a high excitation power at the PTC abruptly increases the intensity of the reactive field near the PTC over which the patient body tissues is exposed. Thus, the excitation power at the PTC should be within a limit satisfying the guideline provided by the International Commission on Non-Ionizing Radiation Protection (ICNIRP) and the Standards Coordinating Committee 28 (SCC28) of the IEEE. A regulator circuit can trim down the excessive power across the load when the received power is higher than the desired voltage. However, the regulator's input power (received voltage) must not be very high because excessive power may cause regulator breakdown. Therefore, the uniform *H*-field, along with the efficiency is also greatly important in the WPT system for capsule endoscopy and needs accurate modelling and intensive optimization.

3.3.2 PTC configuration

3.3.2.1 Configuration of existing PTCs

Three different PTC configurations have been found to be used in the existing WPT systems for capsule endoscopy. Figure 3.2 has depicted these PTC configurations. To simplify the analysis, these PTCs have been named as i) typical solenoid coil (TSC), shown in Figure 3.2a (Lenaerts & Puers, 2005); ii) typical Helmholtz coil (THC), shown

University of Malaya

in Figure 3.2b (Xin *et al.*, 2010); and iii) segmented solenoid coil (SSC), shown in Figure 3.2c (Yadong *et al.*, 2013b). These PTC configurations have mainly varied mainly due to different coil turn arrangements. The TSC has a loosely wound solenoid coil with *n* turns and overall height *h*, where the distance between the contagious turns is $h/(n-1)$. The THC has been configured with two tightly wound solenoid coils connected in series. These coils have been separated on a common axis by the distance of their identical radius (*r*). The SSC consists of a number of segments of a tightly wound solenoid coil. Each of the segment has been connected to an advanced switching system that can be activated and deactivated any particular segment depending on the PRC location.

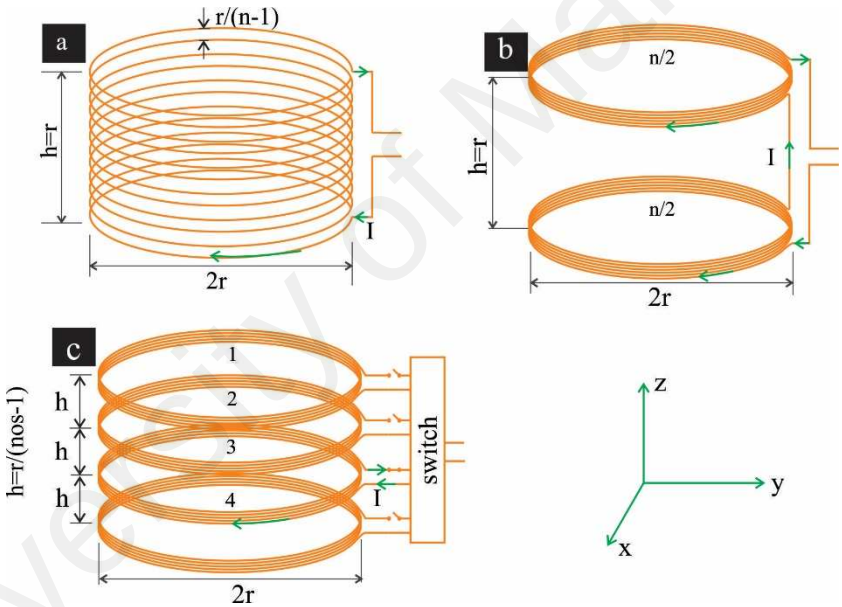

Figure 3.2: Schematic configuration of the existing PTCs: (a) typical solenoid coil (TSC); (b) typical Helmholtz coil (THC); and c) segmented solenoid coil (SSC). The number of segments has been denoted by "nos" (Basar *et al*., 2016a).

The quality factor and coupling coefficient are two important performance indices which have been used to access the performance of PTC. Nonetheless, the existing studies have not been fully accessed these indices to select any particular PTC configuration. Where the selection has mainly led by the index of the *H*-field intensity and uniformity. As such, the configurations of TSC and SSC have been preferred in the existing studies

University of Malaya

to increase the magnetic field intensity, whereas the THC has commonly been chosen to enhance the magnetic field uniformity.

3.3.2.2 Configuration of proposed PTC

Among the existing PTCs, the generated magnetic field was weak in the THC, whereas the uniformity was poor in the TSC and SSC. In addition, the uniformity of the field in the THC significantly decreased along with the radial (y-axial) distance beyond $r/2$ ($y > \pm r/2$). Therefore, PTC-I has been proposed to improve both H-field uniformity and intensity at once (within a large region inside the coil: $z \leq \pm h/2$ and $y \leq \pm 3r/4$). Figure 3.3 shows the design configuration of PTC-I. In this design, two outer and one middle coils are arranged so that they have the same radius (r). These coils are aligned in parallel. Their centers have been fixed at a common axis (Figure 3.3a). The separation and turn ratio between the outer coils and the middle coil for optimum H-field intensity and uniformity are set to $0.4r$ and 3:2, respectively.

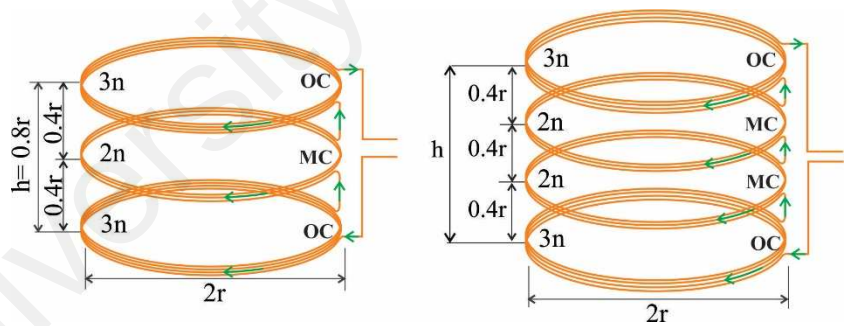

Figure 3.3: Schematic of the proposed PTC-I: (a) basic structure and (b) enlargement of the axial region with an additional middle coil. The outer and middle coils have been represented by "OC" and "MC," respectively (Basar *et al*., 2016a).

In this design, the overall coil height was $0.8r$. The coil height can be enlarged further along the axial distance with the inclusion of additional middle coil(s) to enlarge the area of the uniform H-field (Figure 3.3b).

University of Malaya

3.3.3 Mathematical modeling of inductive link

3.3.3.1 Modeling of link efficiency

The resonant inductive link can be simplified to a circuit model which is shown in Figure 3.4. In this model, L_t and L_r represent the effective self-inductances. R_t and R_r represent the effective series resistance of the PTC and PRC, respectively. C_t and C_r represent the tuning capacitors used to resonate both coils. M represents the mutual inductance between the coils.

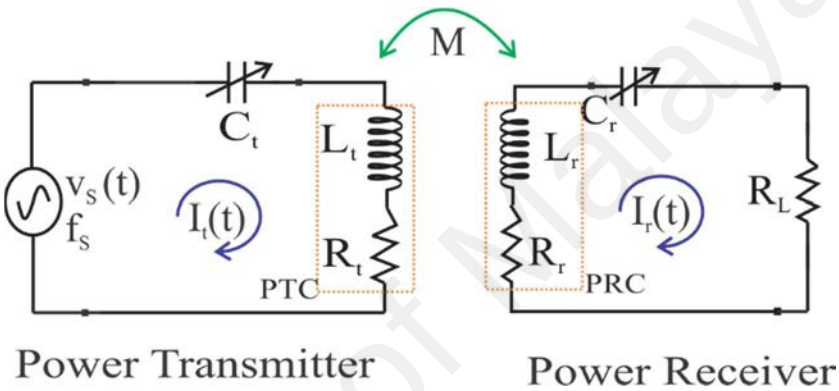

Figure 3.4: Simplified circuit model of the resonant inductively coupled wireless power transfer system (Basar *et al*., 2016a).

According to circuit theory, the relationship among the applied voltage to the PTC, $V_s(t)$, and current through the coils, $I_t(t)$ and $I_r(t)$ can be represented by the following matrix form (Yan *et al*., 2015):

$$\begin{bmatrix} V_s(t) \\ 0 \end{bmatrix} = \begin{bmatrix} Z_t & Z_m \\ Z_m & Z_r \end{bmatrix} \begin{bmatrix} I_t(t) \\ I_r(t) \end{bmatrix} \tag{3.1}$$

Where,

$$Z_t = R_t + j\omega L_t + 1/j\omega C_t, Z_r = R_r + R_L + j\omega L_r + 1/j\omega C_r, \text{and} Z_m = +j\omega M.$$

From (3.1):

$$V_s(t) + Z_m I_r(t) = Z_t I_t(t), \text{and} Z_m I_t(t) = Z_r I_r(t).$$

$$\rightarrow I_t(t) = \frac{V_s(t) + Z_m I_r(t)}{Z_t}$$

University of Malaya

$$\rightarrow I_r(t)=\frac{Z_m I_t(t)}{Z_r}=\frac{Z_m \dfrac{V_s(t)+Z_m I_r(t)}{Z_t}}{Z_r}=\frac{|Z_m| V_s(t)}{|Z_r||Z_t|-Z_m^2}.$$

$$\rightarrow I_t(t)=\frac{V_s(t)+Z_m I_r(t)}{Z_t}=\frac{V_s(t)+Z_m \dfrac{Z_m V_s(t)}{Z_r Z_t - Z_m^2}}{Z_t}=\frac{|Z_r| V_s(t)}{|Z_r||Z_t|-Z_m^2}$$

At the perfect resonance:

$$Z_t = R_t = |Z_t|, Z_r = R_r + R_L = |Z_r|, \text{and} Z_m = j\omega M; |Z_m| = \omega M.$$

Thus,

$$I_t(t)=\frac{(R_r+R_L)V_s(t)}{R_t(R_r+R_L)+\omega^2 M^2}, \text{and } I_r(t)=\frac{\omega M V_s(t)}{R_t(R_r+R_L)+\omega^2 M^2}. \tag{3.2}$$

Therefore, the inductive link efficiency (η) can be expressed as follows:

$$\eta=\frac{P_{out}}{P_{in}}=\frac{I_r^2(t)R_L}{I_t(t)V_s(t)}=\frac{\omega^2 M^2}{R_t(R_r+R_L)+\omega^2 M^2}\frac{R_l}{R_l+R_r}. \tag{3.3}$$

When $M = k\sqrt{L_t L_r}$ and k is the coupling coefficient between the coils, the η can be expressed as:

$$\eta = \frac{k^2 Q_t Q_t R_t}{R_L + R_r(1+k^2 Q_T Q_R)} * \frac{R_L}{R_r + R_L} \tag{3.4}$$

where $Q_t = \omega L_t / R_t$ and $Q_r = \omega L_r / R_r$ are the unloaded quality factors of PTC and PRC, respectively. For the optimum load transformation, $\alpha = R_L/R_r = 1$, the η is simplified as

$$\eta=\frac{k^2 Q_t Q_r}{\alpha+(1+k^2 Q_t Q_r)} * \frac{\alpha}{1+\alpha}=\frac{k^2 Q_t Q_r}{4(1+k^2 Q_t Q_r/2)}. \tag{3.5}$$

For a weakly coupled system, when $k^2 Q_t Q_r / 2 << 1$

$$\eta=\frac{1}{4}k^2 Q_t Q_r. \tag{3.6}$$

Modeling of k and Q are given below for analysis and optimization of η.

3.3.3.2 Modeling of coupling coefficient

For the inductive link, the coupling coefficient between PTC and PRC is denoted as (Na *et al.*, 2015)

$$k = \frac{M}{\sqrt{L_t L_r}}. \tag{3.7}$$

As it has been shown in Figure 3.5, the mutual inductance (M) between PTC-RPC for the PRC position at any coordinate (y, z) in a loosely coupled system can be expressed as

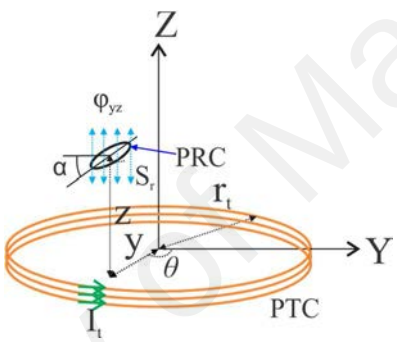

Figure 3.5: Coupling model between PTC-PRC (adopted from Basar *et al.*, 2016a).

$$M(y,z) = \frac{\varphi_{yz}}{I_t} = \frac{B(y,z)S_r\cos(\alpha)}{I_t} = \frac{\mu_0\mu_{eff}\,H(y,z)S_r\cos(\alpha)}{I_t}. \tag{3.8}$$

Where, φ_{yz} represents the magnetic flux density within the area enclosed by the PRC (S_r), and μ_{eff} represents the effective magnetic permeability of the core materials used in the PRC. The H-field generated by the PTC can be calculated at any point (y, z) using Biot–Savart's law as below (Beiranvand *et al.*, 2013)

$$H(y,z) = \frac{NI_t}{4\pi}\int_0^{2\pi}\frac{r - y\cos(\theta) + z\sin(\theta)}{\left[y^2 + z^2 + r^2 - 2yr\cos(\theta)\right]^{\frac{3}{2}}}\,d\theta. \tag{3.9}$$

Therefore, from (3.7), (3.8) and (4.2), the new expression of k is given as

$$k(y,z) = \frac{\mu_0 \mu_{eff} NS_R \cos(\alpha)}{4\pi\sqrt{L_t L_r}} \int_0^{2\pi} \frac{r - y\cos(\theta) + z\sin(\theta)}{\left[y^2 + z^2 + r^2 - 2yr\cos(\theta)\right]^{\frac{3}{2}}} d\theta \,. \tag{3.10}$$

The variation of $k(y,z)$ between PTC and PRC can be analyzed with respect to the variant of position and orientation of PRC using (3.10).

3.3.3.3 Modeling of quality factor

The lumped equivalent circuit based on LCR meter measurement of the single segment solenoid PTC is shown in Figure 3.6. In this model, the PTC comprises i) self-inductance (L_{self}), ii) series AC resistance (R_{ac}) caused by the skin and proximity effect, and iii) parallel stray capacitance (C_{stray}). Given that C_{stray} has very small (in few pico-farad) value and $\omega L_{self}\ R_{ac} C_{stray} \ll 1$, the simplified coil impedance is formulated as follows:

$$Z = \frac{R_{ac}}{(1-\omega^2 L_{self} C_{stray})^2} + j\frac{\omega L_{self}}{1-\omega^2 L_{self} C_{stray}}. \tag{3.11}$$

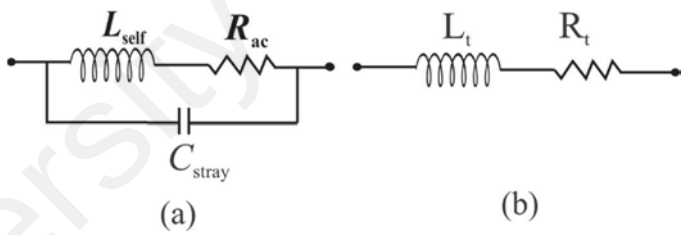

Figure 3.6: (a) lumped equivalent circuit model of a tightly would single solenoid segment of the PTC, and (c) simplified lumped equivalent circuit model (Basar *et al.*, 2016a).

The PTC model has been simplified with an effective series resistance R_t and effective self-inductance L_t as in Figure 3.6b. In that case, R_t and L_t are::

$$R_t = \frac{R_{ac}}{(1-\omega^2 L_{self} C_{stray})^2} \text{ and } L_t = \frac{L_{self}}{1-\omega^2 L_{self}\ C_{stray}}. \tag{3.12}$$

Therefore, the unloaded quality factor (Q_t) of the coil can be expressed as follows

$$Q_t = \frac{\omega L_t}{R_t} = \frac{\omega L_{self}}{R_{ac}}(1-\omega^2 L_{self} C_{stray}). \tag{3.13}$$

The quality factor of the PTCs are calculated using (3.13). For the PTC having number of coil segments b (i.e: b=3 for PTC-I, b=2 for THC) the Q_t can be given by.

$$Q_t = \frac{\omega \sum_{i=1}^{b} L_{t,i}}{\sum_{i=1}^{b} R_{t,i}}. \tag{3.14}$$

The L_{self}, R_{ac} and C_{stray} could be calculated according to the calculation given below.

i) **Calculation of self-inductance (L_{self}):** the L_{self} of individual coil is a summation of self-inductance of the individual turn (L) and mutual inductance among the turns (M) in the coil. The L of the turn with the coil radius r and wire radius a (assuming $a/r \ll 1$) has been approximated as (RamRakhyani *et al.*, 2011)

$$L\ (r,a) = \mu_0 \left[\ln\left(\frac{8r}{a}\right) - 2 \right]. \tag{3.15}$$

And the mutual inductance for perfectly aligned of two turns (u and v) with the radius of r_u and r_v are given by

$$M_{uv}(r_u, r_v, d_{uv}) = \mu_0 \sqrt{r_u r_v} \left[\left(\frac{2}{k_{uv}} - k_{uv} \right) K(k_{uv}) - \frac{2}{k_{uv}} E(k_{uv}) \right], \tag{3.16}$$

where $K(k_{uv})$ and $E(k_{uv})$ have represented the complete elliptical integrals of first and second kind, respectively, d_{uv} has represented the distance between the turns u and v, and

$$k_{uv} = \left(\frac{4 r_u r_v}{(r_u + r_v)^2 + d_{uv}^2} \right)^{1/2}. \tag{3.17}$$

Thus, the L_{self} of ith individual coil segment having n_i turns are given by

$$L_{self,i} = \sum_1^{n_i} L(r,a) + \sum_1^{n_i} M(r_u, r_v, d_{uv}) * (1 - \delta_{uv}). \tag{3.18}$$

where $d_{uv} = |u - v|d$, and d represents the diameters of Litz wire. δ_{uv} = 1 for the u = v, otherwise δ_{uv} = 0.

ii) **Calculation of AC resistance (R_{ac}):** due to the skin effect and proximity effect, the R_{ac} of a PTC increases with the operating frequency and the number of turns. It is desirable to reduce R_{ac} because this helps to increase the Q. The R_{ac} due to skin effect can be reduced by increasing the conductor surface area. One way to achieve this is by using multi-strand Litz wire (Ke *et al.*, 2015; Yang *et al.*, 2007).

According to the simplified model given in (RamRakhyani *et al.*, 2011; Yang *et al.*, 2007), the R_{ac} (including skin and proximity effect) of ith coil segment made of twisting multi-strand Litz wire is approximated as

$$R_{ac,i} = R_{dc,i}\left(1 + \frac{f^2}{f_{h,i}^2}\right) \tag{3.19}$$

where, f_h represents the frequency at which R_{ac}=2R_{dc} and it is calculated as

$$f_{h,i} = \frac{2\sqrt{2}}{\pi\mu_0\sigma r_s\sqrt{n_i n_s \eta_c \beta_w}} \tag{3.20}$$

where r_s, σ, n_s, η_c and β_w represent the radius of individual strands, conductivity of the conductor, number of strands in the Litz wire, area efficiency of the coil, and area efficiency of Litz wire, respectively.

The area efficiency of the coil can be obtained from Yang *et al.* (2007). For a single layer coil it can be approximated by $\eta_c = (99 - n)\times10^{-2}$. As for the area efficiency of Litz wire was equal to one when round Litz wire has been used (i.e. $\beta_w = 1$).

iii) **Calculation of stray capacitance (C_{stray}):** in practice, the inductive coil suffers from stray capacitance between the turns which determines the self-resonance frequency of the PTC and the stray capacitance limits the operating frequency range (RamRakhyani *et al.*, 2011). Neglecting the curvature of winding, for a tightly wound coil, the stray capacitance of a single layer coil has been approximated as (Ke *et al.*, 2015; Yang *et al.*, 2007)

$$C_{stray,i} = \frac{(n_i - 1)\varepsilon_0 \varepsilon_r}{n_i^2} * \int_0^{\frac{\pi}{4}} \frac{2\pi a r}{\varsigma + \varepsilon_r a(1 - \cos\theta)} d\theta, \tag{3.21}$$

where ε_0 has represented the permittivity of free space, $\varsigma$and ε_r have represented the thickness and relative permittivity of the strand insulation of the Litz wire.

3.3.4 Performance analysis of the PTCs

The key performance indices of different PTC configurations (i.e., *H*-field intensity and uniformity), coupling characteristics, and quality factor, and link efficiency are analyzed and compared in the following subsections.

3.3.4.1 *H*-field intensity and uniformity

The field distribution in different PTCs has been computed using the COMSOL Multiphysics computer simulation software to access the *H*-field intensity and uniformity. This software works based on partial differential equations. The simulation has been initially verified with the *H*-field intensity calculated using (4.2) which was adopted from the Biot–Savart's Law. An identical PTC radius of 20 cm and an excitation RF power of 5 W (at 300 kHz) are used in this simulation. All the PTCs are considered co-centric with the Cartesian coordinate system. The number of turns in each of the PTC are adjusted for an equal effective coil inductance L_t to minimize the effect of the tuning capacitor and the transmitting circuit.

University of Malaya

Figure 3.7 shows the color maps of the simulated *H*-field distribution in the PTCs. Within the region $y \leq \pm 3r/4$ and $z \leq \pm h/2$, the maximum and minimum field levels are noted with the coordinates. As shown in Figure 3.7, the peak intensity of the field in the TSC and SSC were relatively higher. However, the field intensity has abruptly increased with the radial (y-axial) distance and decreased with the axial (*z*-axial) distance. Therefore, the field intensity varies within a wide range resulting in poor uniformity.

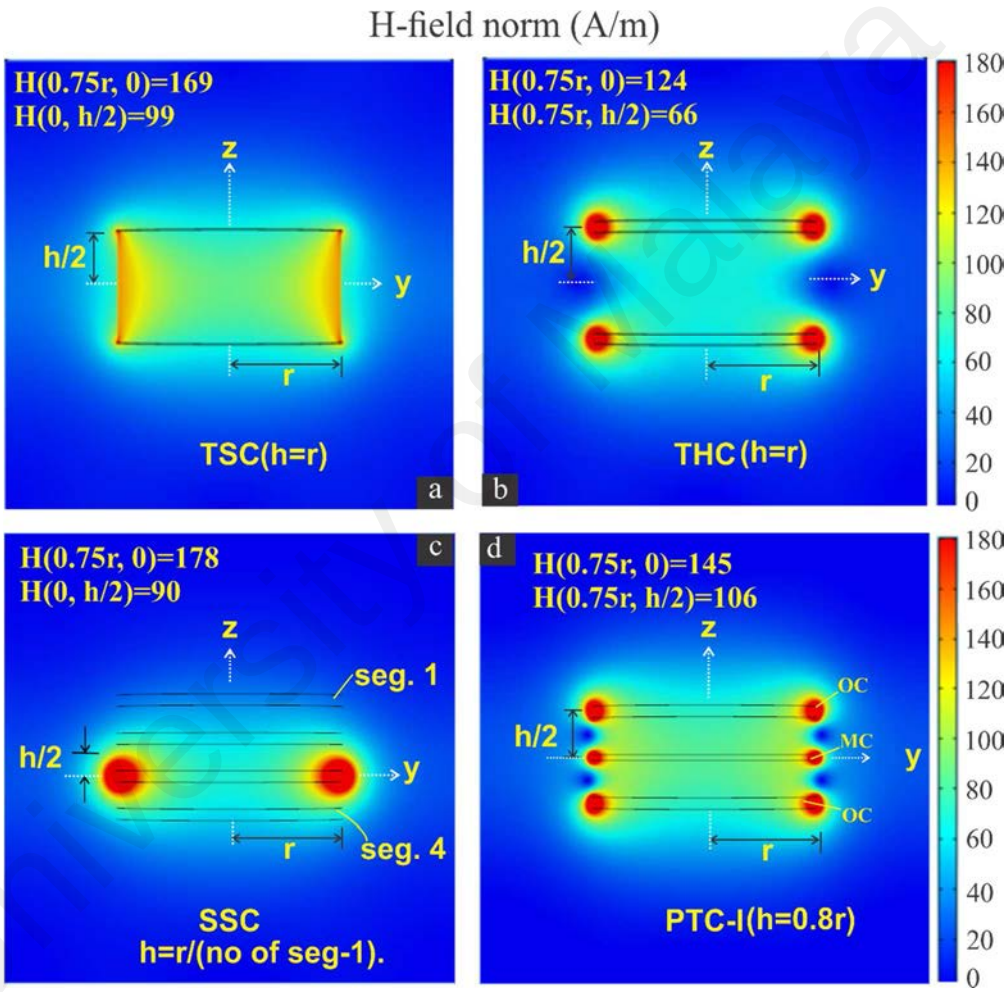

Figure 3.7: Color map of the *H*-field distribution in: a) TSC, b) THC, c) SSC with segment 3 has been excited, and d) PTC-I. The field has been shown on the *yz* plane at *x* = 0 for a coil radius of 20 cm, excitation power of 5 W, frequency of 300 kHz, and coil inductance of ~460 µH (Basar *et al*., 2016a).

In the THC, the field intensity was relatively lower and the uniformity was quite high within a limited region around the center ($y \leq \pm r/2$ and $z \leq \pm h/4$). Beyond this region, the field intensity has significantly dropped with the radial distance and sharply increased

toward the coil winding. Therefore, the uniformity within the large region was poor even in the THC. These problems have been overcome with the proposed PTC-I. The proper configuration of the middle coil in the PTC-I has compensated for the field reduction along the radial distance and overcome the excessive increase of the field toward the outer coil winding. Therefore, the variation of the maximum and minimum field intensities was minimized. Consequently, the proposed PTC-I has attained the three advantages over the existing PTCs: i) high field intensity, ii) high uniformity, and iii) lower peak electromagnetic exposure.

3.3.4.2 Coupling Characteristics

The coupling characteristics of the existing and proposed PTC configurations have been analyzed using (3.10). A PRC with high-permeability ferrite core, radius of 5.5 mm, S_R of $9.5 * 10^{-5}$ m^{-2}, L_r of 426μH, and μ_{eff} of 210 has been used in this analysis. The PRC are considered to be always perfectly aligned with the PTC. Based on this analysis, the variation of the coupling coefficient caused by the free movement of the PRC within the large region of the PTC ($y \leq \pm 3r/4$ and $z \leq \pm h/2$) has been compared in Figure 3.8. The comparison has shown that the minimum level of coupling is highest in the PTC-I. However, the coupling coefficient attained by the TSC was close to that of the PTC-I around the center region (Figure 3.8a). The coupling coefficient of the TSC has significantly decreased around the radial line along $z = h/2$. The coupling coefficient attained by the PTC-I along this line was significantly higher than any other PTCs Figure 3.8b. The coupling coefficient attained by THC was always the lowest. This coefficient further reduces along the radial distance of $z = 0$. The coupling coefficient of the SSC was moderate and varies within a wide range.

University of Malaya

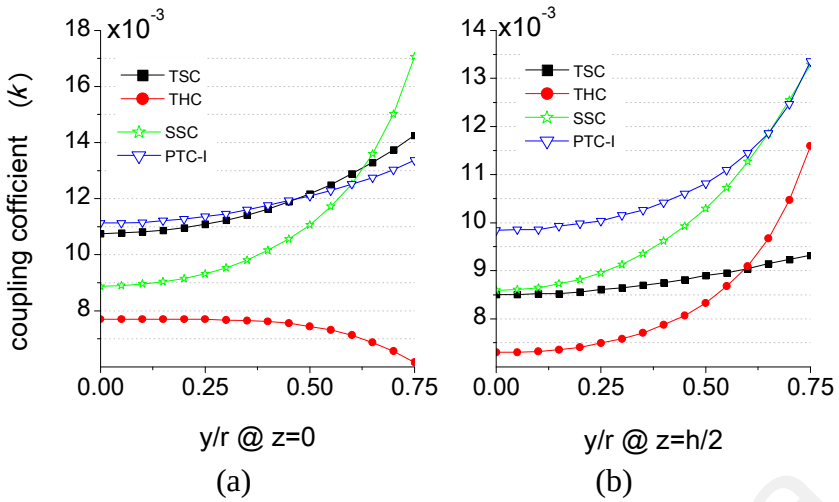

Figure 3.8: Variation of the coupling coefficient along the radial axis: a) without axial distance (at $z = 0$) and b) with axial distance (at $z = h/2$). The coupling coefficient has been calculated for μ_{eff} = 210, S_r =9.5*10^{-5} m^2, L_t ~460 µH, and L_r = 426 µH (Basar *et al*., 2016a) .

3.3.4.3 Quality Factor

The unloaded quality factor of the PTCs (Q_t) has been analyzed using the model given in (3.13) and (3.14). In this analysis, the number of turns in the different PTCs has been adjusted for almost to the equal value of coil inductance L_t ~460 µH. For this coil inductance, the number of turns obtained from the calculation were 30, 26, 22, and 32 for the TSC, THC, SSC, and PTC-I, respectively. The variations of the unloaded quality factor over the frequency are shown in Figure 3.9. Accordingly, each of the PTC exhibits a corresponding frequency at which the PTC has attained a maximum Q_t. The maximum Q_t and the corresponding frequency for a given coil diameter and number of turns depend on R_{ac}, L_{self} and C_{stray}, which vary with a gap between the contagious turns of the coil winding. The tightly wound solenoid coil in the THC and the SSC presents a relatively higher R_{ac} and C_{stray}, resulting in the lower maximum Q_t at a lower frequency. The loosely wound solenoid coil in the TSC has R_{ac}, and C_{stray} lower than that in the THC and SSC. Therefore, the TSC has demonstrated a relatively higher Q_t at a higher frequency. However, the excessive gap between the turns has reduced L_{self} by reducing the mutual inductance among the turns. Consequently, Q_t has reduced with an excessive gap between

University of Malaya

the turns. Therefore, an optimum gap equal to the radius of the wire was used in the PTC-I to obtain the maximum Q_t.

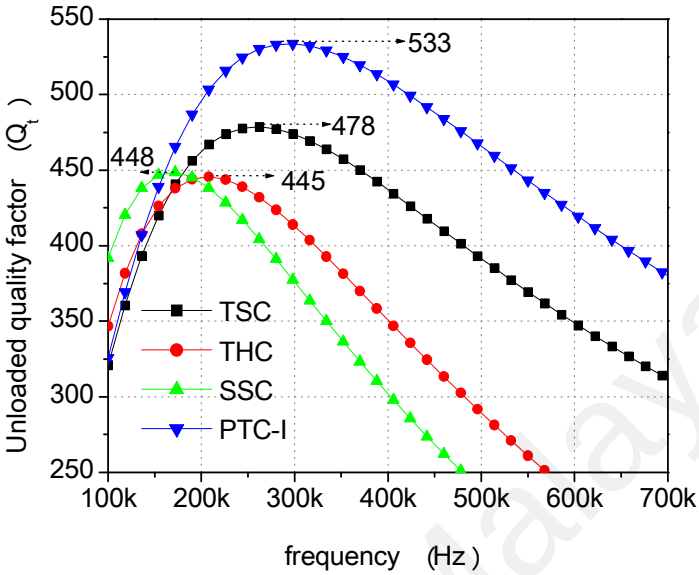

Figure 3.9: Unloaded quality factor of the PTCs over the frequency (Basar *et al.*, 2016a).

3.3.4.4 Variation of the link efficiency and field uniformity with PTC diameter

The field uniformity (γ) and the link efficiency (η) in the WPT system for WCE are expected to be high to minimize the instability of the received power and the electromagnetic exposure effect on the patient body tissues. Unfortunately, the η and the γ are opposite functions of the PTC diameter. In the existing studies, a PTC diameter has been chosen in between 40 cm and 75 cm with the medical viewpoint or seeking of higher γ, without proper investigation on the correlation of the η and the γ with the PTC diameter. The correlation between η and γ with the PTC diameter is illustrated in Figure 3.10. The η was calculated using (3.5), whereas the γ was calculated using

$$\gamma(y,z) = \left(1 - \frac{|H_z(0,0) - H_z(y,z)|}{H_z(0,0)}\right) \times 100\%. \tag{3.22}$$

where $H(0,0)$ and $H(y,z)$ have represented the magnetic field at the center and coordinate (y, z), respectively.

University of Malaya

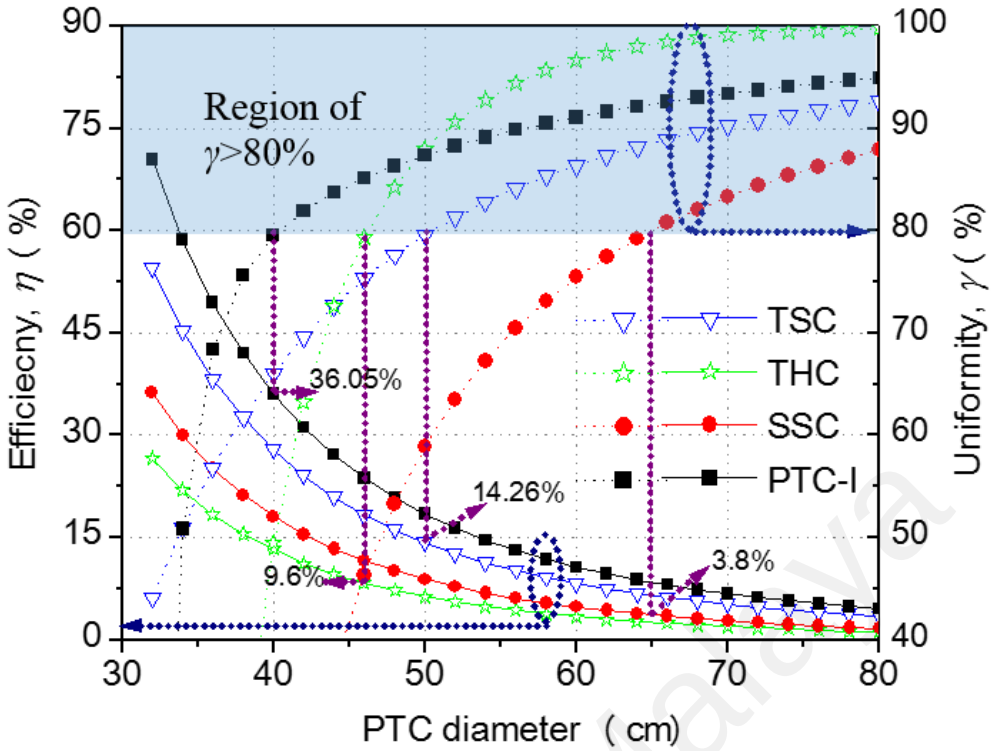

Figure 3.10: Variation of the minimum *H*-field uniformity and link efficiency with the diameter of the PTCs (Basar *et al*., 2016a).

As it has been shown in Figure 3.10, the η has decreased almost exponentially with the increase of the PTC diameter. The γ increases with the PTC diameter. This increment was abrupt within a certain range of the PTC diameter and then steady. Therefore, a possible minimum PTC diameter was 40 cm for the PTC-I, 45 cm for the THC, 50 cm for the TSC, and 65 cm for the SSC are required in order to attain the $\gamma > 80\%$ within the region inside PTC $y \leq \pm 15$ cm and $z \leq \pm h/2$. Given this PTC diameter, the maximum achievable η can be around 36.05% by the PTC-I, 9.6% by the THC, 14.26% by the TSC, and 3.8% by the SSC. The THC can attain the highest field uniformity with a larger diameter but may result in the sacrifice of a significant amount of η.

3.3.5 Implementation of PTC-I and 1D PRC based inductive link

Based on the design and analysis illustrated above, an inductive WPT link based on the proposed PTC-I, conventional PTC (SSC) and 1D PRC are shown in Figure 3.11 with an LCR meter for characterization of the coil performance.

University of Malaya

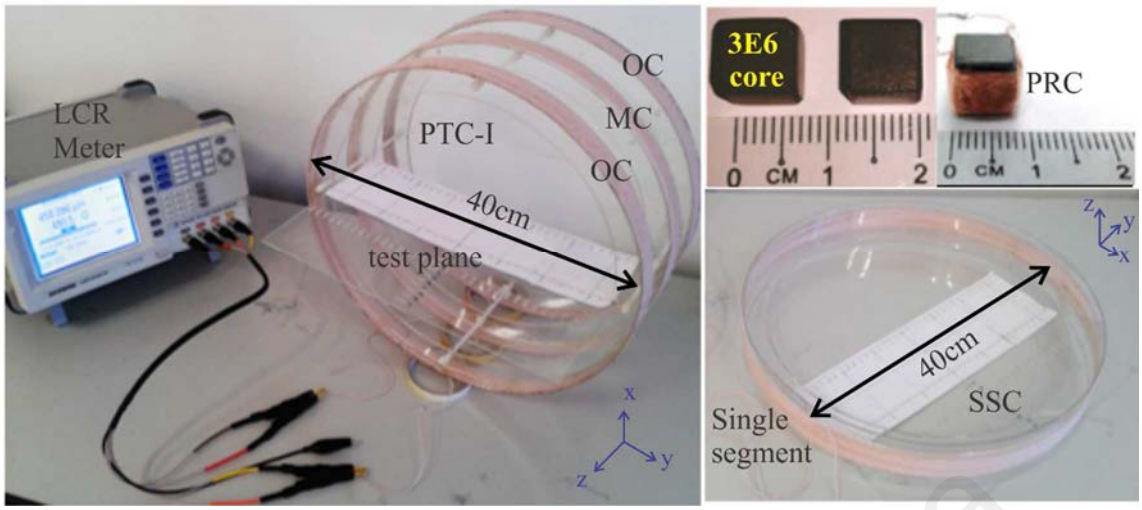

Figure 3.11: Experimental setup for the measurement of the coupling coefficient (*k*) and the unloaded quality factor (Q_t) of the implemented PTCs (Basar *et al*., 2016a).

3.3.5.1 Implementation of PTC

In order to implement the PTCs, a non-magnetic coil frame (using polymethyl methacrylate and polycarbonate sheet) has been fabricated using computer numerical control (CNC) machine where identical coil radius and coil separation were controlled precisely. For the purpose of measuring power and efficiency, a polymethyl methacrylate sheet has been used with the coil frame to indicate the measurement point on the *y*-*z* plane (named as Test Plane that can be removed). Considering system portability and optimally adjustable with the major patient group, a 40 cm coil diameter was chosen. In order to make it more comfortable to wear and improve patient's mobility, the PTC can be implemented on a flexible frame. In order to improve Q_t by minimizing the effective series resistance, a twisted round Litz wire with 270 strands of AWG 42 has been used as the coil conductor in the PTC. The details and specifications of the implemented PTCs are provided in Table 3.1.

3.3.5.2 Implementation of 1D PRC

A 1D PRC has been implemented to measure the coupling coefficient and link efficiency between PTC-PRC. The PRC has been implemented on a rounded cubic core

University of Malaya

with 8 mm side length. A ferrite core with high permeability (Feroxcube 3E6 material) has been used in the PRC.

Table 3.1: Specification of the implemented power transmission coils (Basar *et al.*, 2016a).

Parameters		PTC-I	SSC
Physical	Number of turns	32 (12 + 8 + 12)	22
	Coil diameter	40 cm	40 cm
	Wire diameter	1.5 mm	1.5 mm
	Wire type	AWG 42 Litz wire	AWG 42 Litz wire
	Strands	270	270
Electrical	R_{dc} (Ω)	0.886	0.623
	L_t (μH)	458.37	420.9
	R_t (Ω)	1.62	2.18
	Q_t	533.30	371.81
	**AC parameters are measured at 300 kHz		

The coil has been implemented with enamel coated multi-strands Litz wire. The number of strands has been optimized by implementing 7 individual PRCs with different number of strands from 4 to 10. With these different number of strands, the number of turns have been adjusted within the PRC diameter of 11.5 mm. The received power by the PRCs with different strands for a constant level of *H*-field generated by the PTC is shown in Figure 3.12. As it can be seen in the Figure 3.12, the PRC made with 8 strands Litz wire results the maximum received power.

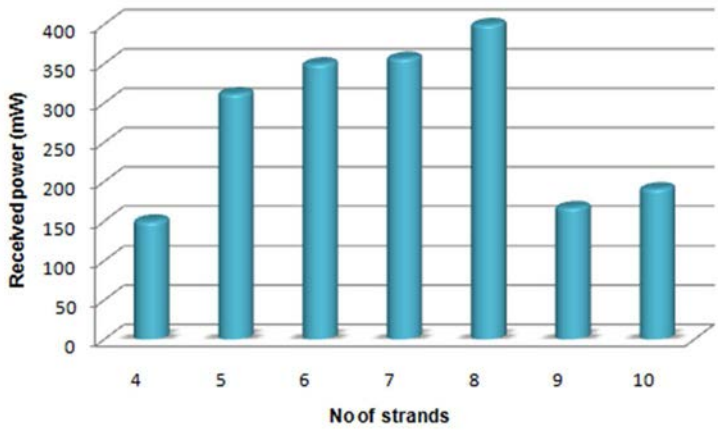

Figure 3.12: Received power by the 1D PRC with different number of strands of Litz wire for a constant level of *H*-field (105 A/m) generated by the PTC (Basar *et al.*, 2014b).

Thus, 8 strands Litz wire has been nominated for implementing the PRC. The details specifications of the implemented PRC made with 8 strands Litz wire have been provided in Table 3.2.

Table 3.2: Specification of the implemented power receiving coil (Basar *et al*., 2016a).

Parameters		Value
Physical	Number of turns	130
	Coil size	∅: 11.5 mm, h: 8 mm
	Core size (mm)	8 × 8 × 8
	Core materials	Mn–Zn, 3E6
	Wire type	AWG 44 Litz wire
	Strands	8
Electrical	R_{dc} (Ω)	4.48
	L_r (μH)	437.52
	R_r (Ω)	7.72
	μ_{core}	≈8000
	Q_r	107.1
	**AC parameters are measured at 300 kHz	

3.4 Results and Discussion

3.4.1 Measurement of *k* and Q_t

For the implemented PTCs, k and Q_t have been measured using an LCR meter (GW Instek LCR 8101G). The measurement setup is shown in Figure 3.11. With this setup, the effective self-inductance of the PTC and the PRC (i.e., L_t and L_r, respectively) have been measured. The mutual inductance between the PTC and the PRC has been measured by varying the PRC coordinates within the PTC. The measured mutual inductance and effective self-inductance of the coils were then converted to k by using (3.7). In addition, the unloaded quality factor of PTC (Q_t) has directly been measured using the LCR meter. The measurement has been conducted on a table top which was 1m above the floor and away from any metallic or conductive object to minimize metallic proximity effect. The measured k and Q_t were compared with the calculated values in Figure 3.13 and

University of Malaya

Figure 3.14, respectively. As shown in Figure 3.13, the measured *k* was in good agreement with the calculated values. The comparison of *k* attained by the PTC-I and SSC clearly indicated that the PTC-I has improved the minimum level of coupling along the both of the *y*-axial lines across *z*=0 and *z*=*h*/2.

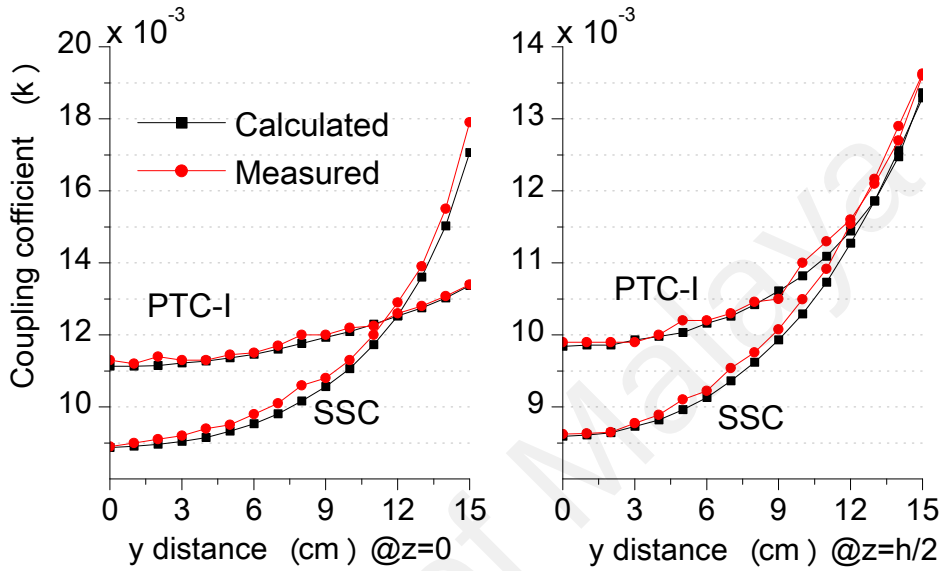

Figure 3.13: Comparison of the measured coupling coefficient (*k*) with that of the calculated. Both of the PTCs having equal radius and inductance, the PRC specification was: μ_{eff} = 210, $S_R = 9.5 * 10^{-5}$ m², and L_r = 426 µH (Basar *et al.*, 2016a).

Moreover, along both of the lines, the *k* attained by the PTC-I was more stable than that was attained by the SSC. Notably, the *k* of PTC-I along the *y*-axial line through *z*=0 was more stable than that through *z*=*h*/2. From the Figure 3.14, the measured Q_t has slightly differed from the calculated value because of the manual winding in the PTC. However, the graph shows that the maximum Q_t of PTC-I was higher than that of SSC. The maximum Q_t attained by the PTC-I was around 525 at 300 kHz whereas it was around 450 at 175 kHz for SSC.

University of Malaya

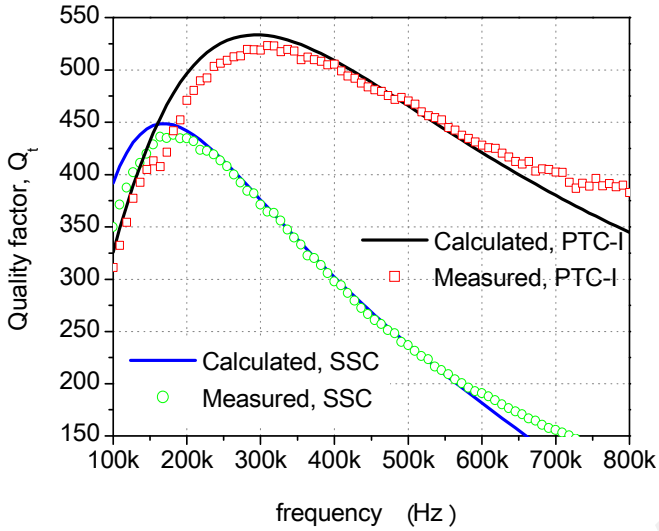

Figure 3.14: Comparison of measured and calculated Q_t of PTC-I and SSC when both of the coils had equal radius and inductance (Basar *et al.*, 2016a).

3.4.2 Measurement of the link efficiency

Figure 3.15 has shown the experimental setup for measuring the inductive link efficiency. In this experiment, both of the coils were resonated at 300 kHz with the tuning capacitor connected in the series. The PTC has been driven by a signal generator. An oscilloscope has been used to measure the output voltage (V_L) across the load (R_L) connected to the PRC. The input current through the PTC (I_t) has also been measured by measuring the voltage across a 1 Ω test resistor connected in series with the PTC. The measured power transfer link efficiency (varying the coordinate of the PRC within the PTC) has been calculated from the measured $V_L(y, z)$ and I_t as follows

$$\eta(y,z) = \frac{V_L^2(y,z)/R_L}{I_t^2 R_t}. \tag{3.23}$$

The measured and analytical efficiency and its variation with the position of the PRC have been compared in Figure 3.16. In comparison with the measured result, the analytical result has shown good acceptability of the given efficiency model. In addition, the proposed PTC-I configuration attained the PTE significantly higher than that of the existing PTC configuration. The minimum η attained by the PTC-I was around 36.5%, whereas the attained η by the SSC was nearly 24% when the equal radius has been used

for each of the coils. The equal radius in each of the coils causes the uniformity of magnetic field lower in SSC (see the Figure 3.10). However, the η attained by the SSC would be lower if the diameter of the SSC coil is adjusted for the magnetic field uniformity to be same to that of PTC-I.

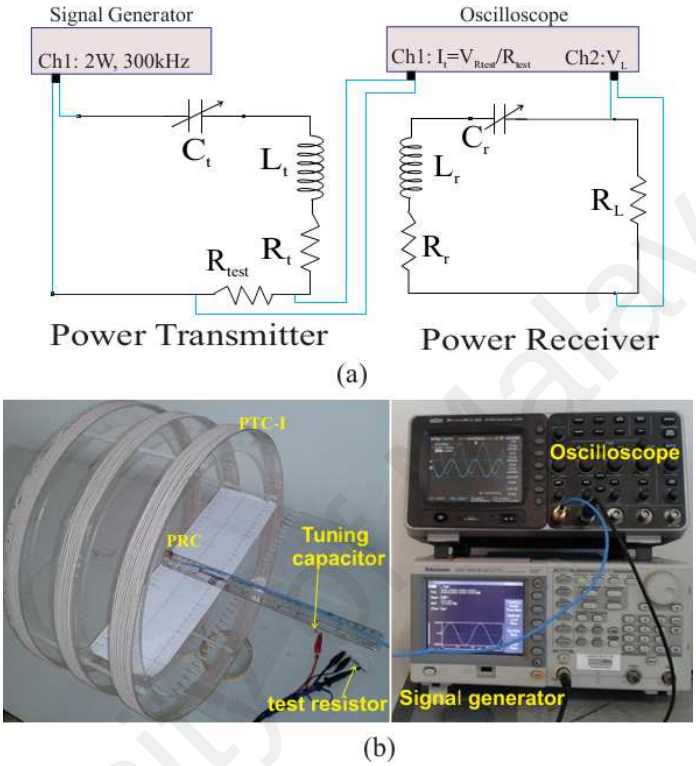

Figure 3.15: Measurement of PTE of the WPT system: (a) circuit diagram of the measurement; (b) experimental setup (Basar *et al*., 2016a).

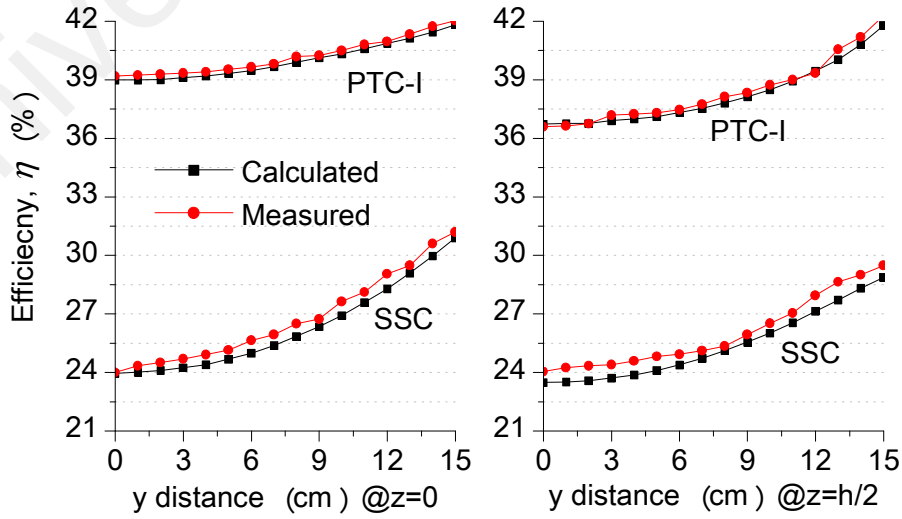

Figure 3.16: Comparison of the measured efficiency with that of calculated (Basar *et al*., 2016a).

3.4.3 Effect of biological tissues on the η

In this application, the PTC and the PRC work in close proximity of the human body tissues, therefore, an investigation on the effects of biological tissues on the performance of the WPT system has been provided in this subsection. In order to investigate this effect, the biological tissues from a slaughtered goat (*Capra aegagrus hircus*) torso of abdominal region including bone, muscle, fat and intestine have been used. The PRC covered with polyethylene film of 1 mm thickness has been placed inside the intestine in abdominal region as indicated in Figure 3.17a. Then the efficiency of the WPT system has been measured by placing the PRC surrounded with the biological tissues inside the PTC. The PRC has been set to be at the center of the PTC with its correctional area perpendicular to the direction of the generated *H*-field. The measurement setup is shown in the Figure 3.17b. The η obtained from this measurement was 33.18% whereas without the biological tissues (as the measurement setup is shown in Figure 3.15) the achieved η was 36.50%. The results indicated the presence of the biological tissues has slightly (around 3.32%) reduced the efficiency without much affecting the performance of WPT system.

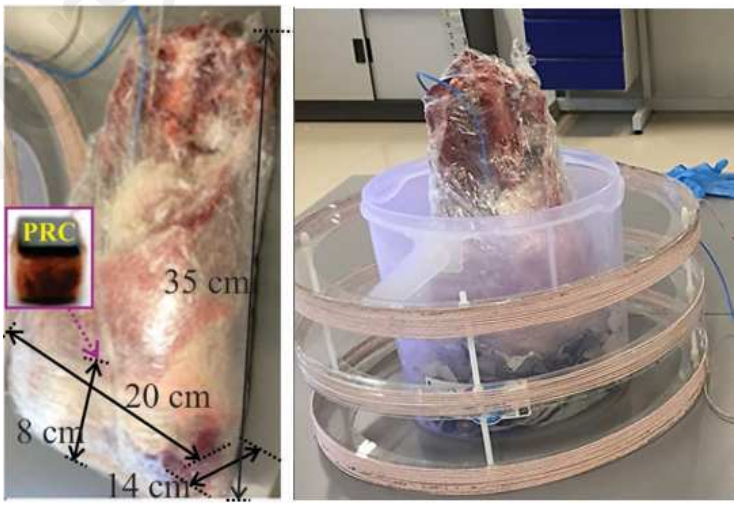

(a) (b)

Figure 3.17: Testing of WPT system's performance in tissues environment: (a) fresh biological tissues of a slaughtered goat torso with a PRC inside the tissues, and (b) measurement setup in the biological tissues environment (Basar *et al*., 2016a).

University of Malaya

This reduction was due to the slight conductivity of biological tissues that makes some power loss. Our finding complies with other similar studies in this area as reported in (Na *et al.*, 2015; Pan *et al.*, 2011; Shi *et al.*, 2015) which indicate slight reduction when the WPT system operating in biological tissues environments at this range of frequency.

3.4.4 Overall power transfer efficiency from source to load

In real field application to deliver required amount of power to the load, the PTC can be driven by a power amplifier (PA) or driving circuit, whereas PRC is connected to the power conversion (rectifier and regulator) circuit (PCC). In addition to cope with the high voltage that might raise across the high Q PTC, the PTC are resonated with the capacitor having high voltage tolerance. This capacitor adds some effective series resistance (ESR) with that of PTC. Therefore, voltage drops across all of these PA, PCC, and ESR contributed to the reduction of the overall power transfer efficiency (PTE) (considering power from the total DC source and the delivered DC power to the load). Thus, the PTE and the received power P_L of the proposed inductive link have also been tested by connecting with a PA, PCC, and high voltage capacitor. The details configuration of PA, PCC and high voltage capacitor are provided in next chapter (Chapter 4). The measured PTE and P_L across the y axial lines at z = 0 and z = h/2 are shown in Figure 3.18.

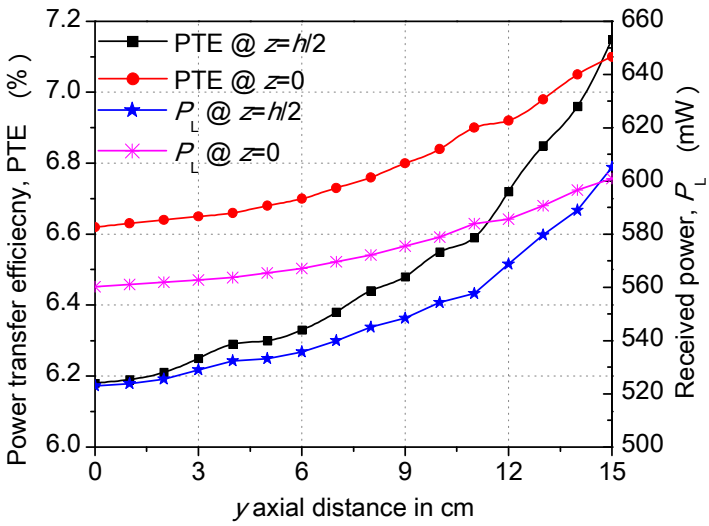

Figure 3.18: Overall PTE and received power.

As shown in the Figure 3.18, the minimum PTE obtained by transferring at least 523 mW of power was 6.18%. This minimum PTE was obtained when the PRC when it was located at $y = 0$, $z = 0$. This PTE was remarkably lower than the link efficiency, however, it was satisfactory in comparison to the PTE obtained by the existing system in the range of 0.02% to 3.55% (Sun *et al.*, 2012; Ke *et al.*, 2015; Na *et al.*, 2015; Shi *et al.*, 2015).

3.4.5 Effect of WPT system on body tissues

3.4.5.1 Simulation setup

The strong reactive field in the WPT system may exert some potential effects on the living body tissues. The effects include i) stimulus action caused by the induced current within the tissues and ii) rising temperature caused by the absorption of the electromagnetic energy by the tissues. These parameters are often indexed by the current density (J, A/m^{-2}) and specific absorption rate (SAR, W/kg). The SAR is not influential at a frequency lower than 10 MHz (ICNIRP, 1998). Therefore, J has been used as the safety analysis index. The J has been obtained by computer simulation based on partial differential equations. Figure 3.19a depicts the simulation setup. In this simulation, a body model of 30 cm in diameter has been used. This model has been built with multi-layer homogenous tissues materials, including the skin, muscles, bones, and intestines, which are the main parts of the abdominal region. The electrical properties of these tissues (i.e., conductivity (σ) and permittivity (ε)) were included in the 300 kHz frequency. The simulation setup with the PTC-I and the distribution of the induced J for the coil excitation current (I_t) of 0.5 A are shown in Figure 3.19b. The distributed J was relatively higher around the capsule when it was located within the intestine with a relatively higher σ than the skin, muscles, and bones. Moreover, J has increased with load reduction (R_L), which was kept at 20 Ω in this simulation. Current in the PRC has increased with the reducing R_L because it was related to $I_r(t) = \omega M I_t(t)/(R_r + R_L)$.

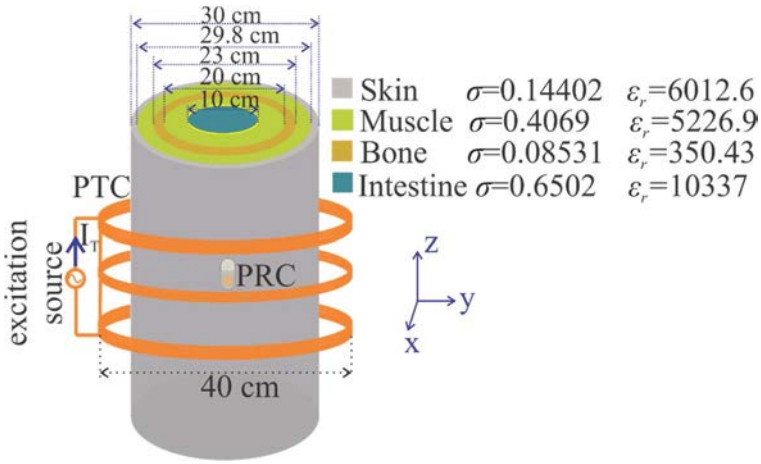

(a)

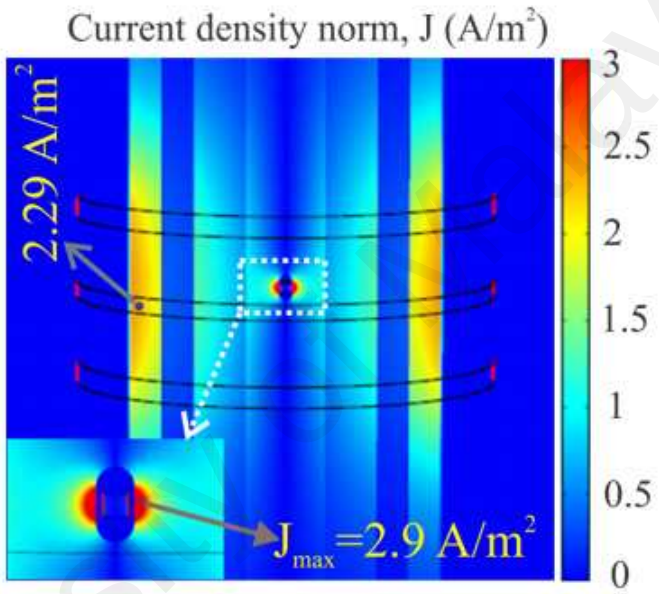

(b)

Figure 3.19: Evaluation of the current density: a) analytical model of the simulation setup with homogeneous multi-layer tissues, PTC-I, PRC, and excitation source; b) simulated induced current density for 0.5 A of coil current and 146 mW of output power (Basar *et al*., 2016a).

3.4.5.2 Induced current density

Considering this effect, a limit must be imposed on the allowable I_t in the PTCs and the maximum power that can be transferred following the ICNIRP guideline on J. The maximum allowable I_t, at which J exceeds the safety limit and the corresponding output power of different PTC configurations are shown in Figure 3.20. Both the PTC-I and the THC present a similar amount of maximum P_L for a common PRC location at the center of the PTC. Nevertheless, P_L has been reduced in the THC for the PRC location in the weak-field region (e.g., y = 0.75 r and z = 0).

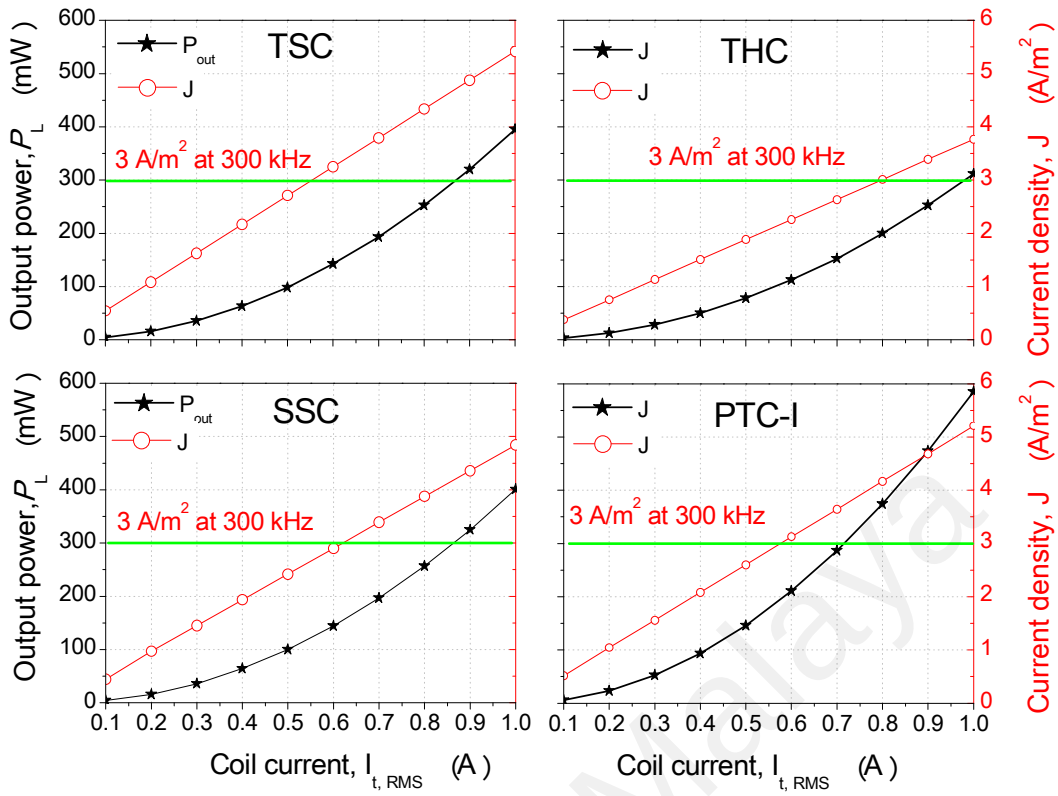

Figure 3.20: Limit on the coil current (I_t) and output power for the different PTCs to fulfill the safety guideline provided by the ICNIRP (Basar *et al.*, 2016a).

3.5 Conclusion

A complete model of a resonant inductive wireless power transfer system with an improved power transfer coil PTC-I has been presented in this chapter. The performances of the PTC-I and the inductive power link have been analyzed in detail by using a mathematical model. In comparison with the existing power transfer coil, the proposed PTC-I remarkably improves the quality factor and the coupling coefficient which increase the efficiency of the inductive link. In addition, the PTC-I has also resulted the *H*-field uniformity higher than that of existing PTCs. With a power receiving coil of Ø 11.5 mm × 8 mm, the minimum link efficiency attained by the PTC-I was 36.05%. The maximum efficiency attained by the existing PTCs was 14.26% while maintaining a similar *H*-field uniformity level. With a power amplifier circuit, power conversion circuit and high voltage capacitor, the proposed system has attained the overall PTE of 6.18% while transferring 523 mW of power. This PTE was satisfactory in comparison to that of the existing system. In addition, an electromagnetic safety analysis has been performed with

University of Malaya

a multi-layer homogenous body model and with incorporation of the high-permeability ferrite core receiving coil. The induced current density was higher around the high-permeability ferrite core than the other regions. The analyzed current density has indicated a power of 200 mW can be transferred in accordance with the electromagnetic safety guidelines.

University of Malaya

CHAPTER 4: IMPROVEMENT OF RECEIVED POWER STABILITY

4.1 Introduction

In order to improve the stability of received power and minimize the unexpected peak electromagnetic exposure, the *H*-field generated by the power transmission coil (PTC) needs to be as much as possible uniform. However, in reality, the *H*-field is not perfectly uniform within the PTC, and it is generally much stronger at the positions near the PTC and weaker at positions away of the PTC (Pan *et al.*, 2011; Xin *et al.*, 2010). As a result, the received power becomes unstable when the receiver moves within this non-uniform fields. Although a regulator circuit can be utilized to obtain a constant power by trimming excessive voltage. However, the induced voltage at the receiver has always to be equal or above the desired potential so it can continuously fulfill the power demand of the capsule. On the other hand, the induced voltage must not be too excessive from the desired level. However, over voltage may cause regulator breakdown and may increase heat at the receiver which can be harmful to the nearby tissues. Therefore, to overcome the aforementioned problems, a PTC capable of generating uniform magnetic field is of great importance to be investigated. Thus, this chapter mainly presents methods for improvement of the received power stability (RPS) by making the *H*-field uniform. This is achieved by proposing another new coil configuration which is named as PTC-II. The configuration of PTC-II is obtained from modified form of typical Helmholtz coil (THC), due to this fact, this PTC-II is also referred as modified Helmholtz coil (MHC). Besides that the performance of mixed resonance scheme (MRS) has been analyzed and adopted to ensure maximum power delivery to the load.

4.2 Literature Review

In the last few years, significant research efforts have been dedicated to develop an efficient wireless power transfer (WPT) system for wireless capsule endoscopy (WCE)

University of Malaya

application (Carta & Puers, 2011; Ma *et al.*, 2007; Zhiwei *et al.*, 2012; Lenaerts & Puers, 2005; Na *et al.*, 2015; Pan *et al.*, 2011; Shiba *et al.*, 2008b). So far, major development in this area includes: modeling of 3D power receiving coil (PRC) (Lenaerts & Puers, 2005; Ryu *et al.*, 2007), incorporation of ferrite core in 3D PRC (Carta *et al.*, 2009; Xin *et al.*, 2010), improving quality factors for the transmitting and the receiving coils (Zhiwei *et al.*, 2012; Ke *et al.*, 2016; Xin *et al.*, 2010), improving rectifier and driving circuits (Jourand & Puers, 2012; Sun *et al.*, 2012), efficiency optimization (Na *et al.*, 2015; Sun *et al.*, 2012) and analysis of electromagnetic effect on human tissues (Shiba & Higaki, 2009; Shiba *et al.*, 2008b).

However, the existing studies did not fully address the uniformity of magnetic field generated by PTC and the corresponding power stability within the possible working region of the capsule. Uniform magnetic field is of great importance so that exposure of human tissues to the peak electromagnetic field is minimized and at the same time the PRC could experience a consistent level of *H*-field thus producing a stable power within its working region. In the existing design, usually a solenoid coil or a THC has been employed as a PTC (Carta *et al.*, 2011; Ma *et al.*, 2007). The use of solenoid coil results relatively low uniformity of magnetic field (Na *et al.*, 2015; Shi *et al.*, 2012). In this regards a THC was therefore more preferable. However, uniformity of magnetic field in a THC is only within a limited region around the center of the coil (Beiranvand, 2013) and the uniform field does not cover the overall working region of the capsule. In order to address this problem, a larger dimension of THC has to be employed but this approach reduces power transfer efficiency (PTE) and it is undesirable for a portable system.

In addition, with an optimum coil design, the PTE further depends on the load factor which is the ratio of a load resistance to an effective series resistance of the PRC. For a maximum PTE, the load factor needs to be unity. In this regard, the resonance scheme

University of Malaya

used with the PRC has a significant effect on the PTE (Vandevoorde & Puers, 2001). In existing designs, where the load resistance was relatively low as few tens ohm or below, series resonance scheme was commonly used at the receiving side (Na *et al.*, 2015; Yan *et al.*, 2015) which improves the amount of transfer power by ensuring better load matching than that of the parallel resonance scheme (Ma *et al.*, 2007). However, the series resonance configuration could not always ensure unity load factor for optimum power delivery to the load even with high quality factor of the PRC. In order to address the aforementioned problems, PTC-II and MRS have been proposed in this chapter. The PTC-II tremendously improves the *H*-field uniformity and resultant received power stability, while, the MRS ensures the maximum power delivery to the load.

4.3 Materials and Methods

4.3.1 Schematic of WPT System

A schematic of a WPT system is illustrated in Figure 4.1. A PTC can be made wearable and a PRC with a power conversion circuit (PCC) can be embedded within the biomedical capsule endoscope.

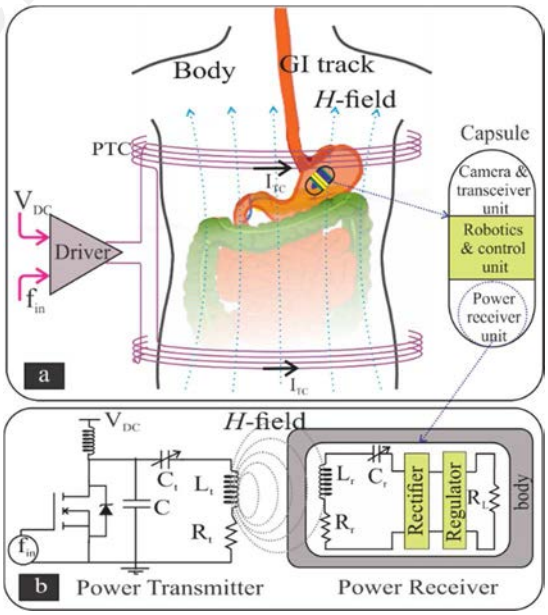

Figure 4.1: Schematic of a WPT system for RCE: (a) sketch of the WPT system, and (b) circuit model (Basar *et al.*, 2017).

Power can be transferred from PTC to PRC by the linkage of magnetic field. The transferred power is therefore adjustable by controlling the excitation source at the PTC. However, the excitation has to be limited so that *H*-field does not exceed a safety exposure limit (see Table 2.6) as suggested by the established standards such as ICNIRP and IEEE (ICNIRP guideline 1998; Lin, 2006). To achieve a higher PTE, the PTC and PRC must be resonated at the same operating frequency (f_{in}), where $f_{in} = 1/(2\pi\sqrt{L_t C_t}) = 1/(2\pi\sqrt{L_r C_r})$ (Ju *et al.*, 2015). The L_t and L_r represent the inductance of the PTC and the PRC, respectively. They are fixed for optimum quality factors. The C_t and C_r are tuning capacitors used to resonate both of the coils. Under the condition of perfect tuning, the PTE is further dependent on the three factors: i) coupling coefficient between the PTC-PRC, ii) quality factor (Q) of the coils, and iii) the load factor $\alpha = R_L/R_r$. In weakly coupled WPT system such as in WCE application, the link efficiency derived in section 3.3.3.1 can be rewritten with α as below

$$\eta = \frac{\alpha * k^2 Q_{TC} Q_{RC}}{(1+\alpha)^2}. \tag{4.1}$$

Unfortunately, the coupling coefficient k of such system is relatively low due to excessive distance between PTC-PRC and also due to small dimension of the PRC as compared to the PTC. Generally in a WPT system, $k = M/\sqrt{L_t L_r}$ (Pan *et al.*, 2011). For a loosely coupled system and considering a constant current in the PTC, the mutual inductance (M) is related by $M \propto HS\mu_{eff}$ (Liu *et al.*, 2015), where H, S, and μ_{eff} are the *H*-field strength generated by the PTC, projected area of the PRC in the magnetic field direction and the effective magnetic permeability of core material, respectively. The non-uniform *H*-field causes unstable k as well as received power. In real field application, the *H*-field generated by the PTC is not perfectly uniform. For better uniformity of *H*-field a THC has commonly been used in the existing studies (Carta *et al.*, & Xin *et al.*, 2010, Pan *et al.*, 2011). However, the *H*-field uniformity of the THC is high within a limited

region around the center of the coil as the distribution of field has been shown in Figure 4.2. The uniformity within the possible working area (PWA) of capsule could be considered as high if it is within half of the coil radius (r). However, the overall H-field uniformity could be considered poor within a large region ($y = \pm 0.75r$) in which patient body will be exposed. The exposed area needs to be well considered to protect the body tissues from high field area. In this regard, a large region of uniform within the PTC will be advantageous.

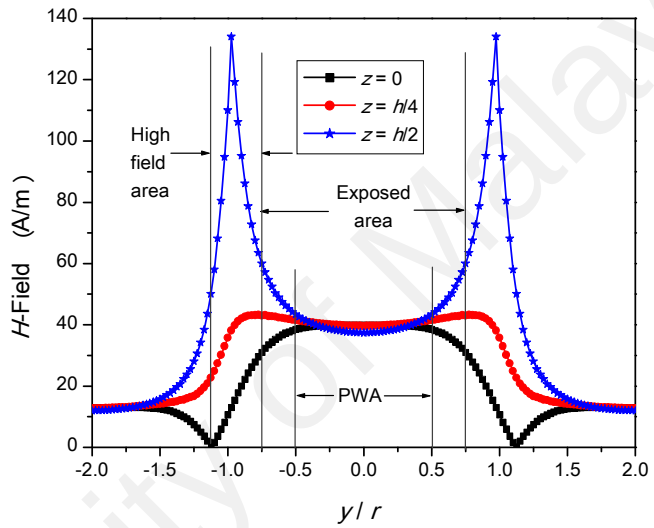

Figure 4.2: *H*-field distribution in a typical Helmholtz coil (THC) perpendicular to the *z*-axis and co-centric with Cartesian coordinate system, the *H*-field has been generated with 26 Ampere-turns (Basar *et al*., 2015).

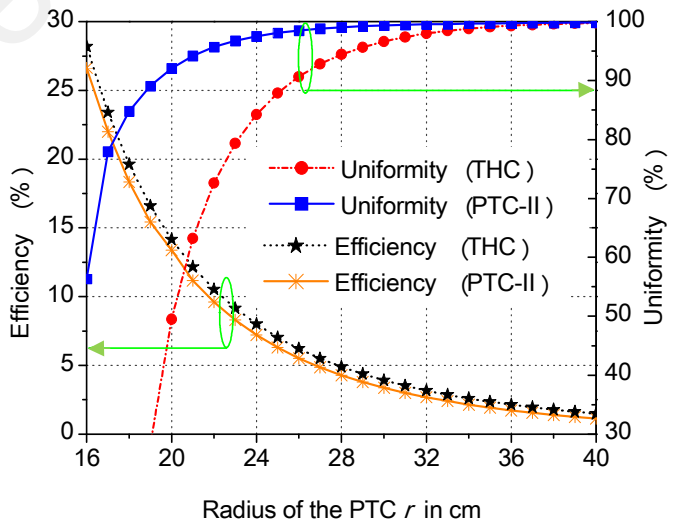

Figure 4.3: Variation of inductive link efficiency and magnetic field uniformity with the radius *r* of the PTC, uniformity was considered within a region of Ø 30 cm x height 20 cm inside the PTC (Basar *et al*., 2017).

University of Malaya

Although, the uniformity of *H*-field generated by a THC can be increased by simply enlarging its radius (*r*), however, the efficiency is almost inversely exponential function of *r* as illustrated in Figure 4.3. Referring to the Figure 4.3, both of the coils can ensure high uniformity with bigger *r* where efficiency is low. In addition, bigger diameter of PTC is always undesirable to use. Thus, increasing *r* in the THC is not always the best solution. In this regards, the proposed PTC-II can be utilized to overcome the aforementioned problems. Since the proposed PTC-II offers more than 90% uniformity with the *r* lower than 20 cm.

4.3.2 Configuration of the proposed PTC-II

In order to obtain a uniform magnetic field within the working region of the capsule, a new configuration of PTC has been proposed as shown in Figure 4.4. This PTC has been innovated from a THC and named as "PTC-II".

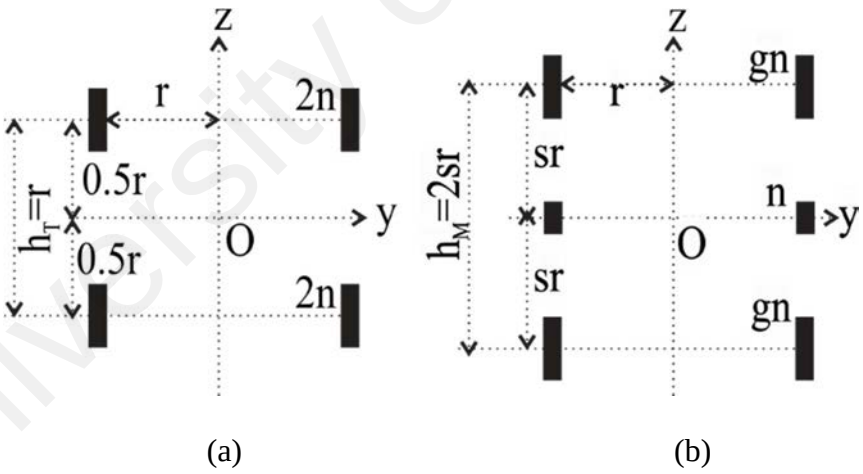

Figure 4.4: Crossectional view with desing specification of: (a) typical Helmholtz coil (THC), and (b) the proposed PTC-II (Basar *et al*., 2017).

This PTC-II has been enhanced with incorporation of an auxiliary coil segment placed at the middle. Identical *r* has been used for all the coil segments. In order to obtain optimum parameters for the PTC-II, it has considered that the outer coils (i.e. side coils) has been spaced from the middle coil by the distance of *sr* and the turn ratio between the outer to the middle coil has been set to *g*:1.

4.3.3 Optimization of *s* and *g* of the proposed PTC-II

In order to optimize the *s* and *g* of proposed PTC-II, the *H*-field has been calculated using Biot-Savart's Law (Beiranvand, 2013) and compared with that of THC. In this calculation, both PTCs (THC and PTC-II) have been considered concentric with the Cartesian coordinate and perpendicular to the *z*-axis. Due to the symmetrical distribution, *H*-field has been analyzed only on the *y*-*z* plane at $x = 0$. According to the Biot-Savart's Law, the *H*-field at any point on the *y*-*z* plane at $x = 0$ generated by a tightly wound solenoid coil having *n* turns and carrying *I* ampere current can be calculated by

$$\vec{H}_z(y,z) = H_{Yz}(y,z)\hat{j} + H_{Zz}(y,z)\hat{k}, \tag{4.2}$$

where
$$\begin{cases} H_{Yz}(y,z) = H_0(n)\displaystyle\int_0^{2\pi} \frac{zSin(\theta)}{\left[y^2 + z^2 + r^2 - 2yrCos(\theta)\right]^{\frac{3}{2}}} d\theta \\ H_{Zz}(y,z) = H_0(n)\displaystyle\int_0^{2\pi} \frac{r - yCos(\theta)}{\left[y^2 + z^2 + r^2 - 2yrCos(\theta)\right]^{\frac{3}{2}}} d\theta \end{cases}$$

$$\text{and } H_0(n) = \frac{Irn}{4\pi}.$$

Considering (4.2), the *H*-field generated by the THC (in Figure 4.4a) can be given by

$$H_{zTHC}(y,z) = H_0(2n) * H_z(y, z + \frac{r}{2}) + H_0(2n) * H_z(y, z - \frac{r}{2}). \tag{4.3}$$

Similarly, the *H*-field generated by the PTC-II (in Figure 4.4b) can be obtained using

$$H_{zMHC}(y,z) = H_0(gn) * H_z(y, z + s) + H_0(gn) * H_z(y, z - s) + H_0(n) * H_z(y,z). \tag{4.4}$$

The uniformity of *H*-field at any point on *y*-*z* plane with respect to the field at the origin has been computed using (3.22). In order to obtain optimum values of *s* and *g*, the uniformity of field within a region $-0.75r \le y \le 0.75r$ and $-0.5r \le z \le 0.5r$ in PTC-II can be formulated as

$$\gamma_{PTC-II}(s,g)=\left(1-\frac{\left|H_{z,PTC-II}(0,0,s,g)-H_{z,PTC-II}(y,z,s,g)\right|}{H_{z,PTC-II}(0,0,s,g)}\right). \quad (4.5)$$

The variation of $\gamma_{PTC-II}(s,g)$ over the s and g has been shown in Figure 4.5. The $\gamma_{PTC-II}(s,g)$ becomes maximum when: s=0.73 and g=1.8. To simplify coil fabrication and to avoid possible fractional value in number of turns approximated values of s and g: s = 0.75 or ¾ and g = 2 have been used. Therefore, 3r/4 and 2:1 have been nominated as an optimum separation and turn ratio between the outer to the middle coil, respectively.

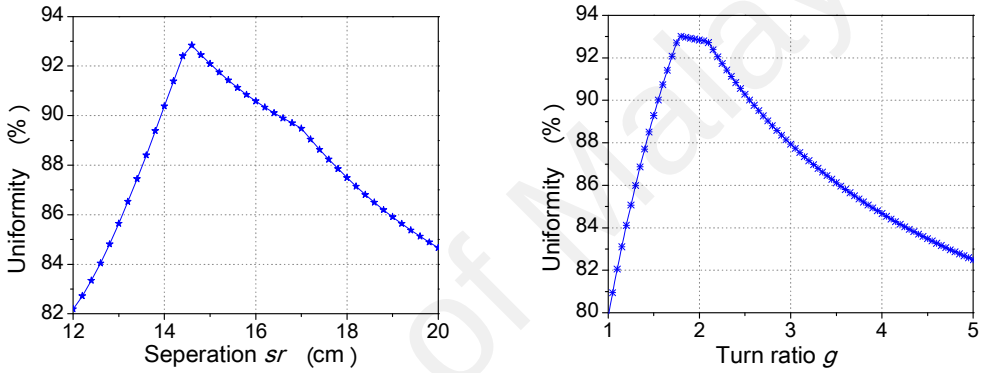

(a) (b)

Figure 4.5: Variation of $\gamma_{PTC-II}(s,g)$ with the: a) separation *sr* between outer to middle coil, and b) turn ratio *g*: within the region $-15cm \leq y \leq 15$ cm and $-10\ cm \leq z \leq 10$ cm inside the PTC (Basar *et al.*, 2017).

4.3.3.1 Analysis of *H*-field and its uniformity

Based on the above calculations, normalized *H*-fields generated by THC and PTC-II within a relatively large region considering $-0.75r \leq y \leq 0.75r$ and $-0.5r \leq z \leq 0.5r$ have been compared in Figure 4.6. As shown in the Figure 4.6, the proposed PTC-II has achieved relatively constant level of *H*-field as compared to the THC. Thus, PTC-II can provide more stable power to the load because it is closely related to the H-field. More interestingly, the proposed PTC-II suppresses the undesired peak electromagnetic exposure by around 26% as compared to the THC, considering a practical scenario where the average transverse diameter of human body is around 75% of the PTC diameter.

University of Malaya

The *H*-field uniformity in the PTCs has been compared along the radial (*y*-axis) lines at $z = 0$ and $z = 0.5r$ (Figure 4.7). As shown in Figure 4.7, considering the two lines, uniformity of $H_{zPTC\text{-}II}$ (generated by PTC-II) has been improved by 11.32% and 47.98%, respectively as compared to the THC. Within the larger region, the minimum uniformity of *H*-field attained by our PTC-II was 91.13% this was an improvement by 41.66%. Whereas it was merely 49.47% in the THC.

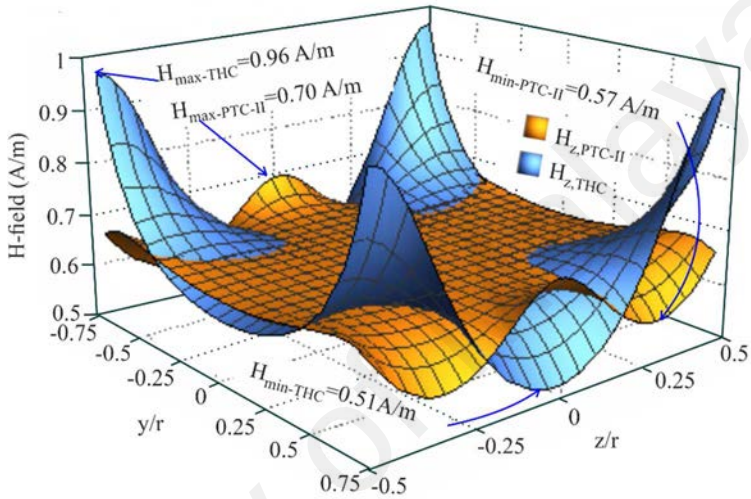

Figure 4.6: Comparison of normalized *H*-field (on *y*-*z* plane at *x* = 0) generated by the proposed PTC-II and the conventional THC: *n* = 6 and *r* = 20 cm are used for both of the coils (Basar *et al*., 2017).

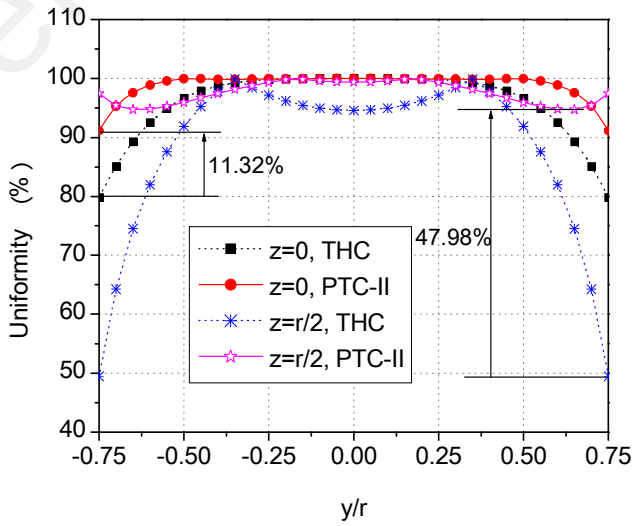

Figure 4.7: Comparison of *H*-field uniformity of THC and PTC-II along the radial axis at *z* = 0 and *z* = *r*/2 (Basar *et al*., 2017).

University of Malaya

This uniformity was irrespective of the total number of turns used in the THC or PTC-II as long as the recommended turn ratio and separation distance among the coils are followed.

4.3.3.2 Analysis of quality factor

In order to analyze for an optimum *Q*, a lumped model of PTC-II as shown in Figure 4.8 was used. In this model, each of the coil segment consists of: an inductance (L_{self}), a series AC resistance (R_{ac}), and a parallel stray capacitance (C_{stray}) (Ke *et al.*, 2015; RamRakhyani *et al.*, 2011). Based on this lumped model and the model of *Q* descripted in section 3.3.3.3, the Q of PTC-II can be given by

$$Q_t(n,f) = \frac{\omega L_t(n,f)}{R_t(n,f)} = \frac{2\pi f \sum_{i=1}^{b} \dfrac{L_{self,i}(n)}{1-(2\pi f)^2 L_{self,i}(n) C_{stray,i}(n)}}{\sum_{i=1}^{b} \dfrac{R_{ac,i}(n,f)}{\left[1-(2\pi f)^2 L_{self,i}(n) C_{stray,i}(n)\right]^2}}, \tag{4.6}$$

where the number of coil segment, *b*=3 for PTC-II and *b*=2, for THC.

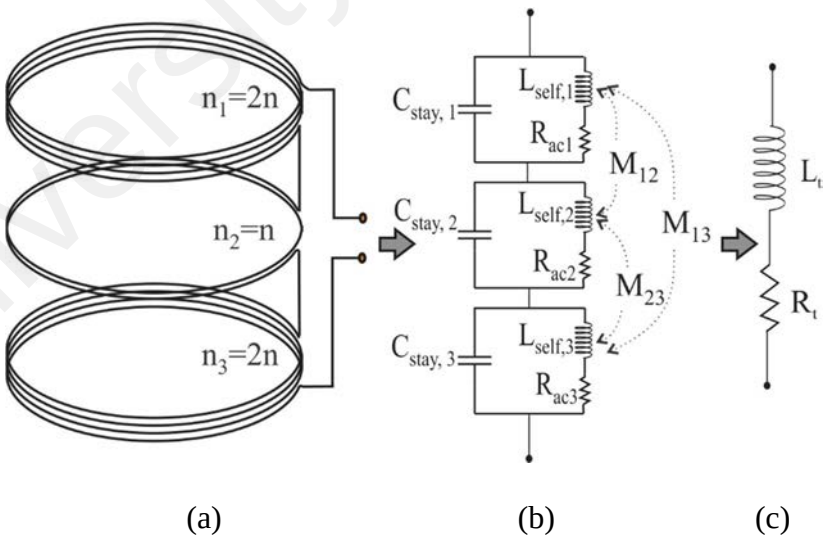

Figure 4.8: (a) Modified Helmholtz coil based PTC, (b) lumped model, and (c) simplified lumped model (Basar *et al*., 2017).

Considering the mutual induction among the individual coil segments, L_{self} of individual coil segment can be given: for the THC,

$$L_{self,i} = \sum_{u=1}^{n_i} L_u(r,a) + \sum_{u=1}^{n_i}\sum_{v=1}^{n_i} M(r_u, r_v, d_{uv}) * (1-\delta_{uv}) + 0.5\sum_{u=1}^{n_i}\sum_{w=1}^{n_i \pm 1} M(r_u, r_w, d_{uw}). \quad (4.7)$$

Similarly for PTC-II,

$$L_{self,i} = \sum_{u=1}^{n_i} L_u(r,a) + \sum_{u=1}^{n_i}\sum_{v=1}^{n_i} M(r_u, r_v, d_{uv}) * (1-\delta_{uv}) + 0.5\sum_{w=1}^{n_i}\sum_{u=1}^{n_i \pm 1} M(r_w, r_u, d_{wu}) + 0.5\sum_{x=1}^{n_i}\sum_{u=1}^{n_i \pm 1} M(r_x, r_u, d_{xu}), \quad (4.8)$$

where $d_{uv} = |u-v|d$, $d_{uw} = r + |u-w|d$, $d_{wu} = d_{xu} = 0.75r + |w-u|d$ for i=3 otherwise, $d_{wu} = 0.75r + |w-u|d$ and $d_{xu} = 1.5r + |x-u|d$. And d is the diameter of Litz wire. δ_{uv} = 1 for the $u = v$, otherwise δ_{uv} = 0.

i. Calculated quality factor

The calculated Q_t of PTC-II is plotted over frequency and number of turn in Figure 4.9. It can be noted from Figure 4.9 that for each value of n number of turns, there is a corresponding frequency which gives maximum Q_t.

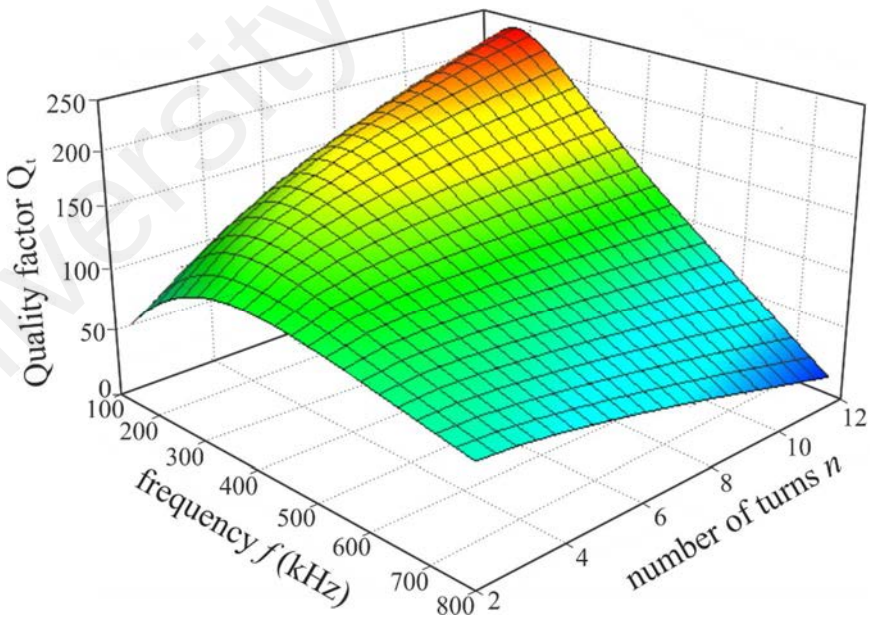

Figure 4.9: The Q_t of the PTC-II over the frequency and the number of turns. Coil specification: r = 20 cm, coil conductor was AWG 42 Litz wire with 270 strands (Basar *et al*., 2017).

University of Malaya

The Q_t significantly increases with n whereas the corresponding frequency of maximum Q_t slightly reduces. It happens at the frequency remarkably below the self-resonance of the PTC. Because, at lower frequencies, the increase of L_t with n dominates over the increases of R_t, therefore, the Q_t has been increased. While, the Q_t has abruptly been reduced when the frequency approaches to the self-resonance of the PTC. Because, the R_t has abruptly been increased at the frequency close to the self-resonance of PTC that reduces the Q_t.

ii. Comparison of quality factor

The Q_t of PTC-II and THC are plotted over frequencies in Figure 4.10. As it can be noted, the proposed PTC-II gives slightly higher Q_t when the value of n has equal value in both of the coils. The equal n results the total number of turns in the PTC-II and THC to be 5n and 4n, respectively. If the value of n is increased in the THC only to make the total number of turns equal to that of PTC-II, the Q_t of THC will be slightly increased. However, the optimum selection of n for maximum PTE follows the characteristics of PRC and power amplifier as well.

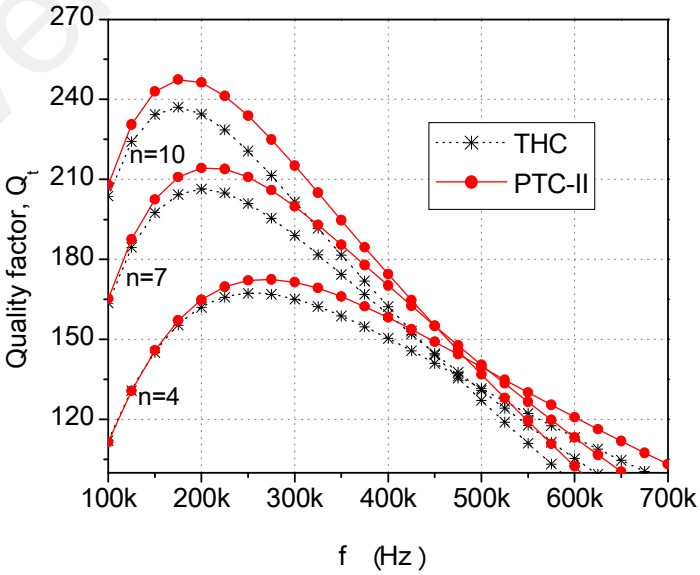

Figure 4.10: The Q_t of THC and PTC-II for different n. Coil specification: r = 20 cm, coil conductor is AWG 42 Litz wire with 270 strands (Basar *et al*., 2017).

University of Malaya

4.3.4 Analysis of Mixed Resonance Scheme

Although, the concept of mixed resonance scheme (MRS) is not new, however, it is important to analyze the use of this technique along with other common schemes in order to explore the full benefit in a given application (Chen *et al.*, 2013; Xue *et al.*, 2013). To the best of my knowledge, a complete analysis of MRS has never been performed in WPT system in WCE platform, hence this resonance scheme has been analyzed in this research along with the other two common schemes namely: parallel resonance scheme (PRS), and series resonance scheme (SRS).

From (4.1), the maximum power transfer can be achieved under optimum load factor (α) that is when $\alpha = Z_L/\mathrm{re}|Z_{RC}| = 1$. With optimum Q_r, the receiving coil impedance depends on the resonance scheme used with PRC. Typically, two different types of resonance schemes have been employed in WPT system: i) parallel resonance scheme (PRS) (Cheon *et al.*, 2011; Ahn & Hong, 2014) and ii) series resonance scheme (SRS) (Sample *et al.*, 2011; Qingwei, *et al.*, 2015) as shown in Figure 4.11, where $\mathrm{re}|Z_{RC}|$ can be determined as

$$\text{for PRS:} \quad re|Z_{RC}| \cong \frac{R_r}{(1-\omega^2 L_r C_p)^2}, \text{and} \tag{4.9}$$

$$\text{for SRS:} \quad re|Z_{RC}| \cong R_r. \tag{4.10}$$

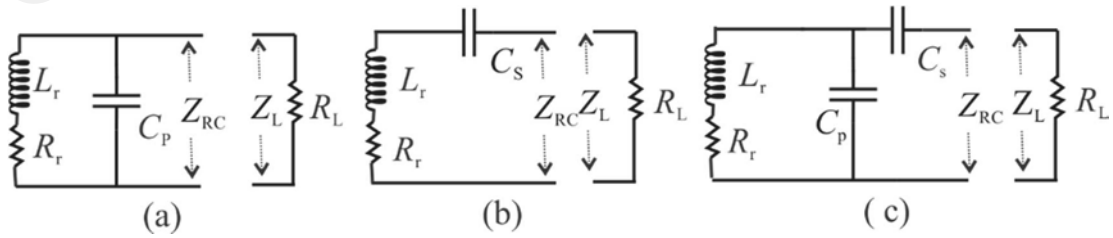

Figure 4.11: **PRC resonance scheme: (a) PRS, (b) SRS, and (c) MRS (Basar *et al.*, 2017).**

University of Malaya

At resonance ($\omega^2 L_r C_P \sim 1$), the PRS has resulted a high value of re$|Z_{RC}|$ that causes α to be lower than unity, thus, this resonance scheme is suitable for low power WPT system where Z_L is high (few hundred ohm or above) and R_r is relatively lower (Ahn & Hong, 2014). From (4.10), the re$|Z_{RC}|$ in SRS is approximately equal to R_r (Sample *et al.*, 2011) which is low at high Q_r and around 10 Ω in existing design (Carta *et al.*, 2009, 2010). Provided that the robotic capsule demands an average power of 300 mW at 3 V supply (Carta *et al.*, 2011; Xin *et al.*, 2010), the average Z_L should be around 30Ω. Although, in this circumstance the SRS can perform better than the PRS (Ma *et al.*, 2007), but both of these resonance schemes could not always ensure a unity load factor (α = 1). Therefore to address this problem, a mixed resonance scheme (MRS) has been utilized (Chen *et al.*, 2013). The schematic of MRS is shown in Figure 4.11c. For resonance, the values of the parallel and the series capacitors (C_P and C_S) of MRS are calculated by

$$C_P = \frac{\sqrt{R_r^2 + \omega^2 L_r^2} - R_L}{\omega R_L \sqrt{R_r^2 + \omega^2 L_r^2}}, \text{ and} \tag{4.11}$$

$$C_S = \frac{\left(1 - \omega^2 L_r C_P\right)^2 + \left(R_r \omega C_P\right)^2}{\omega^2 \left[L_r \left(1 - \omega^2 L_r C_P\right) - R_r^2 C_P\right]}. \tag{4.12}$$

The performance of these three resonance schemes have been compared in a WPT model designed using PSpice circuit solver as shown in Figure 4.12. The received power (V_{R3}^2 / R_3) for the PRS, SRS and MRS have been compared in Figure 4.13. The results have indicated that the MRS can increase the transferred power up to around 500 mW while the other two schemes performed lower. Therefore the MRS scheme has been chosen in this study.

University of Malaya

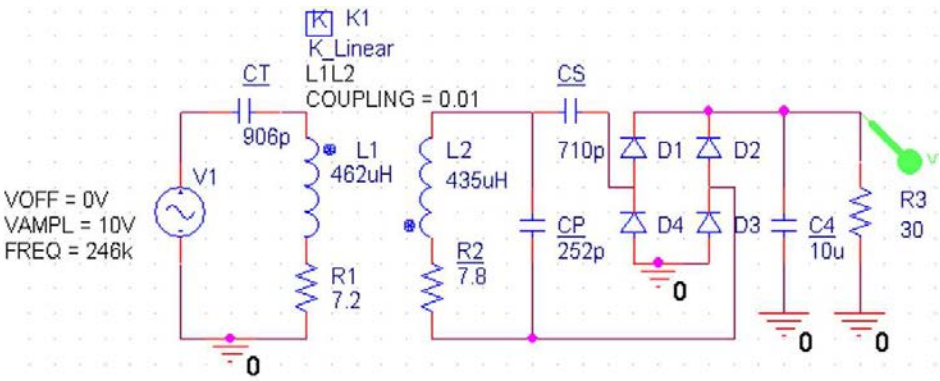

Figure 4.12: Simulation model of WPT system to verify the performance of MRS, SRS and PRS (the connection of CP and CS were adjusted for SRS and PRS) (Basar *et al*., 2017).

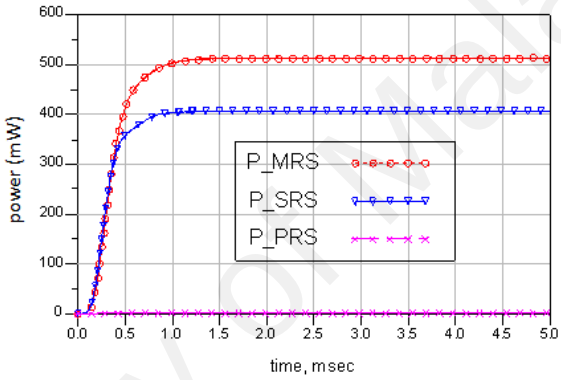

Figure 4.13: Power delivery to the load by the MRS, SRS and PRS for the WPT setup shown in Figure 4.12 (Basar *et al*., 2017).

4.3.5 Implementation of the Proposed PTC-II and MRS based WPT System

Based on the design and analysis described above, a prototype of WPT system has been designed and implemented for WCE platform. The prototype of the proposed PTC-II and MRS based system are shown in Figure 4.14 which consists of: a) the PTC-II, b) a 3D PRC with MRS and a full bridge power conversion circuit (PCC), and c) a class-E driving amplifier circuit.

University of Malaya

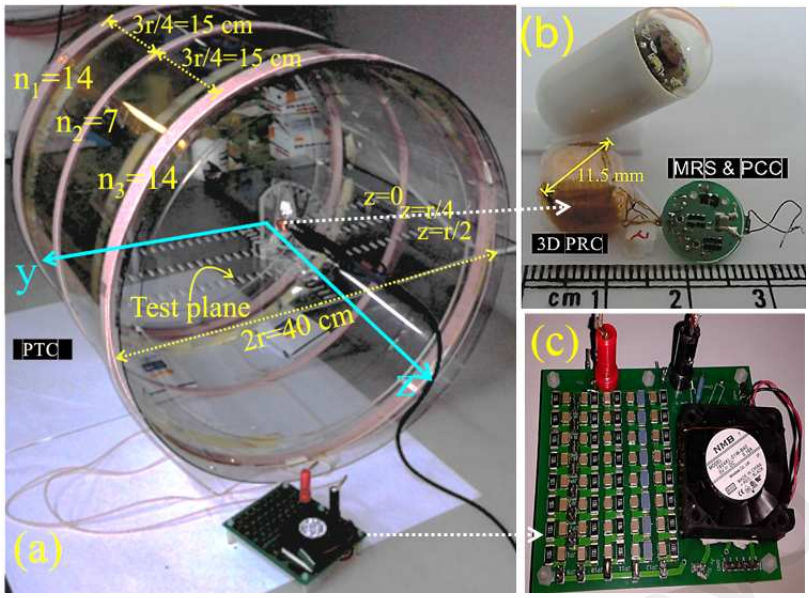

Figure 4.14: A prototype of the proposed WPT system: (a) proposed PTC-II, (b) 3D PRC with mixed resonance scheme (MRS) and power conversion circuitry (PCC), and (c) class E driving amplifier circuit (Basar *et al*., 2017).

4.3.5.1 Implementation of the PTC-II

The implemented prototype of proposed PTC-II is illustrated in Figure 4.14a. In order to obtain high *H*-field uniformity as described above, a non-magnetic coil frame (using polymethyl methacrylate and polycarbonate sheet) has been fabricated using computer numerical control (CNC) machine where identical coil radius and coil separation are precisely controlled. The coil frame can be modified to be attached to a fabric so that it is more comfort to the user and offers patient mobility. For the purpose of measurement, a polymethyl methacrylate sheet was used with the coil frame to indicate the measurement point on the *y*-*z* plane (named as test plane). Considering system portability and to cover major patient group in Malaysia, a 40 cm coil diameter was chosen. The diameter of PTC was adjustable to fit a specific patient. The PTC can also be implemented with a textile frame to increase patient's mobility and comfort level. In this chapter, a rigid coil structure is considered in testing the proof of concept. Such structure can be useful for robotic capsule endoscopy (RCE) where the patient normally required to stay in a healthcare facility. In order to maximize Q_t by minimizing R_t, a twisted Litz wire of AWG 42 with 270 strands has been used to implement the proposed PTC. Generally, from (1)

high Q_t improves the PTE and the Q_t has been increased with the number of turns in the PTC (see Figure 4.9). However, to determine optimum number of turns, the input impedance of driving circuit needs to be in consideration. The input impedance abruptly increases with n in the PTC (Ke *et al.*, 2015) which reduces the performance of the transmitter. Moreover, to determine the optimum operating frequency, the frequency characteristics of PRC also need to be considered. Operating WPT system at the frequency of maximum Q_t can ensure high transmission efficiency. For optimum receiving efficiency, PRC must be tuned at its optimum frequency. Considering these factors, $n = 7$ has been used in the implemented PTC and system has been operated at 246 kHz. For $n = 7$, the total number of turns ($N = 2n+n+2n$) was 35 in the PTC-II.

For comparison, three different THCs have been implemented. The configurations of the implemented THCs are: i) THC_1: having $h_T = r$ and $N = 28$, which was based on optimum design, ii) THC_2: having $h_T = r$, $N = 36$ which was to equalize N in THC and PTC-II, and iii) THC_3*: having $h_T = 1.5r$, $N = 36$ which was to equalize z-region (i.e. height of the coil) and N in THC and PTC-II. For the implemented PTCs, the calculated and the measured electrical parameters at the frequency of 246 kHz are given in Table 4.1. The Q_t slightly varies in the THCs where THC_2 possesses higher Q_t. Because Q_t increases with the number of turns while THC_2 consists of higher number of turns than that in THC_1. Although, the number of turns in THC_2 and in THC^*_3 are equal, nonetheless, the larger h_T causes the Q_t lower in the THC^*_3. Overall comparison indicates that the optimum design of PTC-II achieved the highest Q_t. This achievement is due to the optimum combination of number of turns and separation of coil segments.

4.3.5.2 Implementation of the PRC with MRS

The implemented PRC and the associated circuit are shown in Figure 4.14b. The size of the PRC is kept small enough (11.5 mm diameter and 10 mm height) to fit within an

Table 4.1: Electrical Specification of the PTCs (Basar *et al*., 2017).

Particulars		Calculated	Measured
In PTC-II	$L_{t\ (\mu H)}$	557.05	544.47
	R_t (Ω)	4.07	4.18
(h_M = 1.5r, N	Q_t	211.48	201.50
	f_{self} (MHz)	1.55	1.57
In THC_1	$L_{t\ (\mu H)}$	449.22	435.26
	R_t (Ω)	3.44	3.52
(h_T = r, N =	Q_t	201.72	191.13
	f_{self} (MHz)	1.59	1.60
In THC_2	$L_{t\ (\mu H)}$	583.32	568.39
	R_t (Ω)	4.47	4.53
(h_T = r, N =	Q_t	205.16	197.29
	f_{self} (MHz)	1.46	1.46
In THC_3*	$L_{t\ (\mu H)}$	580.05	564.71
	R_t (Ω)	4.46	4.51
(h_T = 1.5r, N	Q_t	204.52	196.65
	f_{self} (MHz)	1.47	1.48
* By the definition, the THC_3* can not be considered as a typical Helmholtz coil because the h_T is not exactly equal to r.			

existing commercial capsule. In order to improve the power receiving efficiency the PRC has been designed with high permeability core materials. A rounded cubic core (8 mm side length) of a ferromagnetic material (MnZn, 3E6 model) supplied by Ferroxcube Ltd. has been used as the core of the PRC. This material has high initial permeability, approximately 7500 at the frequency of 246 kHz. A multi-strands Litz wire has been wound on the core to form a 3D PRC. The number of turns and strands in the 3D PRC need to be adjusted within the limited usable space in the capsule. An eight strands Litz wire of AWG 44 has been used for multilayer 3D PRC. The measured electrical parameters of three different coils in 3D PRC are given in Table 4.2. In order to obtain unity load factor with MRS, the value of C_p and C_s have been calculated using (4.11) and (4.12) for tuning. The optimum values of C_p and C_s for 30 Ω load are given in Table 4.2. A full wave bridge rectifier with an ultra-low dropout voltage (V_{th}, 220 mV at 100 mA forward current) Schottky barrier rectifier diode PMEG2005AEL has been used to minimize power conversion loss.

University of Malaya

Table 4.2: Specification of the PRCs and resonance circuit.

Parameters	Coil 1	Coil 2	Coil 3
n_r	150	142	135
$L_{r\ (\mu H)}$	435.2	416.1	405.5
R_r (Ω)	7.8	7.5	7.4
Q_r	86.24	85.75	84.69
C_p (pF)	206	205	205
C_s (pF)	756	801	827

4.3.5.3 Implementation of the PTC Driver

The implemented driver is shown in the Figure 4.14c. Class-E amplifier scheme has been chosen for its high power conversion efficiency which theoretically can approach up to 100% (Narendra & YewKok, 2014a, 2014b). The driving circuit has been implemented with IRF3710ZPBF MOSFET from International Rectifier, which has high drain current 59 A and small turn on resistance 18 mΩ. A high voltage multilayer ceramic capacitor 302S43W33KV4E from Johanson Dielectrics has been used to resonate the PTC. Multiple capacitors are connected in series to enhance the capability of driver to cope with high voltage that appears across the capacitors due to the high Q_t. A number of series capacitor tracks also used in parallel to tune the PTC at desired frequency. The driver circuit was able to cope with ~8 kVrms and supply current 2 Arms. The used series and parallel capacitor bank was made it possible to tune within the range of 412.5 pF - 1.65nF.

4.4 Results and Discussion

4.4.1 Experimental results on the PTC-II and MRS based WPT system

Performance of the implemented prototype has been evaluated by measuring the DC output voltage V_L across the 30 Ω load resistance R_L. The voltage V_L for the different coordinates inside the PTC-II was measured to find the power stability. The measured V_L value was converted to output power P_L as follows

University of Malaya

$$P_L(y,z) = \frac{V_L^2(y,z)}{R_L}. \tag{4.13}$$

From the P_L, the position stability of received power ($P_{L,\,PS}$) and PTE were calculated as follows

$$P_{L,PS}(y,z) = \left(1 - \frac{\left|P_L(y,z) - P_L(0,0)\right|}{P_L(0,0)}\right) \times 100\,\% \text{ and} \tag{4.14}$$

$$PTE(y,z) = \frac{P_L(y,z)}{P_{in}} \times 100\,\%, \tag{4.15}$$

where P_{in} is input power. Multiplying the input DC current by the input DC voltage to the driving circuit gives the P_{in}. The V_L was measured in 1 cm interval along radial y-axis through $z = 0$ and $z = 0.5r$.

4.4.1.1 Output power with variation of PRC position

The P_L values for different positions of PRC are shown in Figure 4.15 when THC_1 and the PTC-II have been used as PTCs. It can be noted that in the PTC-II based PTC the P_L was almost stable with respect to the positions of PRC. This stability of P_L is attained by the highly uniform H-field that was generated by the PTC-II. The optimal separation of outer coils in PTC-II withhold the excessive increment of H-field, as well as P_L along the y-axial lines pass through the $z = r/2$. Whereas, the optimum number of turns and the placement of middle coils compensate the reduction of H-field, as well as P_L along the y-axial lines pass through the $z = 0$. As a result, the overall P_L becomes stable in PTC-II based WPT system. In this PTC, the P_L was at least 534 mW even when the PRC was positioned within a large working region $-0.75r \leq y \leq 0.75r$ and $-0.5r \leq z \leq 0.5r$. Over the given positions of the PRC, the P_L significantly varied in the THC_1 based WPT system. This was mainly due to less uniform H-field generated by the THC_1. The concentrated number of turns in the coil windings cause the H-field excessively increased at the regions near the THC_1 windings.

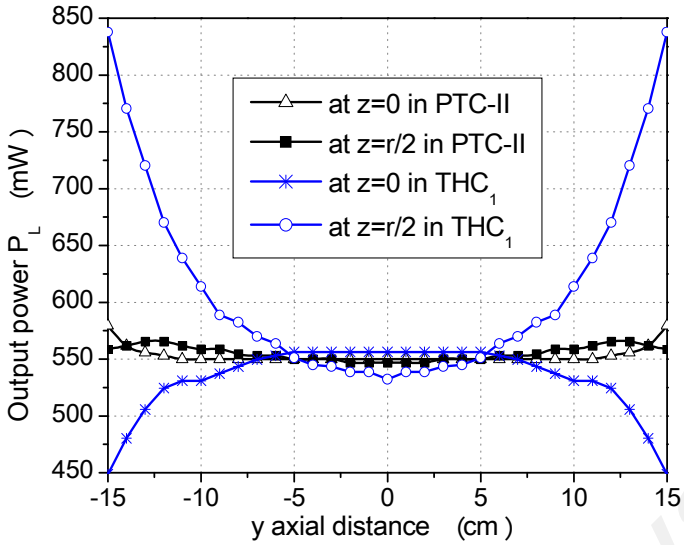

Figure 4.15: Output power measured at the different position of PRC inside the PTCs: the positon of PRC varies along *y*-axial lines through at *z* = 0 and *z* = *r*/2 with 1 cm interval (Basar *et al*., 2017).

Whereas, the large gap on the mid-plane of the THC_1 causes the level of *H*-field drops on the mid-plane at the regions away from the center. This non-uniform *H*-field of THC_1 results the P_L varies in the THC_1 based WPT system within the range 450 mW to 840 mW.

4.4.1.2 Stability of output power with variation of PRC position

Stability of P_L ($P_{L,\,PS}$) with respective to the position of PRC is clearly illustrated in Figure 4.16. The $P_{L,\,PS}$ is converted from measured P_L using (4.14). Then the $P_{L,\,PS}$ is also compared with that of the calculated values. As shown in Figure 4.16, the proposed PTC-II based PTC has improved the power stability by 13.94% along the radial line at $z = 0$ (Figure 4.16a). The PTC-II has tremendously improved the $P_{L,\,PS}$ along radial line at $z = 0.5r$ (Figure 4.16b). Along this line the $P_{L,\,PS}$ were improved by 47.82%. Along both of the lines, the measured $P_{L,\,PS}$ was very close to the calculated value. The region of this improvement has clearly been discussed in the above section (section 4.4.1.1).

University of Malaya

4.4.1.3 Performance comparison

The minimum level of P_L, $P_{L,\,PS}$, and PTE attained by the different PTCs and resonance schemes (such as SRS and MRS) have been compared in Table 4.3. It can be noted form the Table 4.3 that the PTC-II has transferred the highest amount of power and obtained the highest PTE. The PTC-II also attained maximum $P_{L,\,PS}$.

Table 4.3: Performance comparison of WPT system based THCs, PTC-II, SRS and MRS (Basar *et al*., 2017).

($-0.75r \leq y \leq 0.75r$, $-0.5r \leq z \leq 0.5r$)	PTC-II	THC_1	THC_2	THC^*_3
P_{L_min} (mW)	547.03	448.72	472.09	289.88
$P_{L,\,PS\text{-}min}$ (%)	**94.62**	49.47	49.47	74.61
$PTE_{SRS\text{-}min}$ (%)	3.55	2.86	2.95	1.89
$PTE_{MRS\text{-}Min}$(%)	**4.93**	4.01	4.12	2.61

Thus, the PTC-II has performed the best contribution by its higher Q_t and H-field uniformity. Among the different THCs, the PTE obtained by the THC_2 was better than that of THC_1 and THC_3*. Although, the $P_{L,\,PS}$ obtained by the THC_3* was remarkably higher than that of THC_1 and THC_2, nonetheless, the PTE of THC_3* was the worst. For all of these PTCs, the MRS has always performed better than SRS. The PTE of proposed PTC-II and THC_2 with two different resonance schemes have further been compared in Figure 4.17 for different positions of the PRC in y- direction at $x = 0$ and $z = 0$. As it can be seen from Figure 4.17, the proposed PTC-II with MRS based system has improved the PTE by 1.95%. The improvement of the PTE was significantly contributed by the MRS that used to resonate the PRC to ensure optimum load factor. Using the MRS, the PTE was improved by 1.37% as compared to the SRS. The PTE has further been improved by the utilization of the proposed PTC-II. In the conventional THC, the PTE decreased along the radial axis at $z = 0$. However, the proposed PTC-II compensates this reduction where it can improve the minimum PTE by 0.58%.

University of Malaya

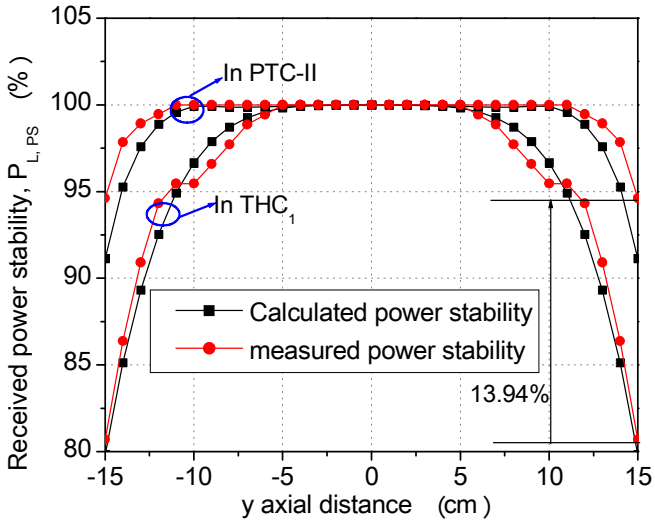

(a)

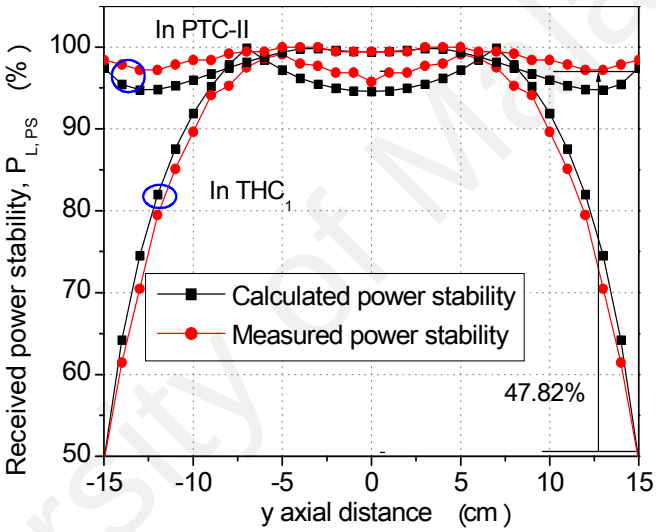

(b)

Figure 4.16: Received power stability over the positions of PRC varies along *y*-axial lines through at: a) *z* = 0, and b) *z* = *r*/2 (Basar *et al*., 2017).

The overall performances of the proposed PTC-II and MRS based WPT systems are also compared with the most recently published works in Table 4.4. To make a fair comparison, for each case, the P_L and the PTE are taken when the PRC was located at the center of the PTC. Based on this comparison, proposed design has substantially improved the PTE and the power stability. It is worth mentioning here that, the WPT system in this application causes patient body tissues to be exposed to a certain level of magnetic field generated by the PTC. Therefore, a careful evaluation of the electromagnetic exposure

University of Malaya

effect is important. These findings have indicated that the proposed technique helps to minimize the unnecessary exposure level through improving PTE and the uniformity of the generated magnetic field.

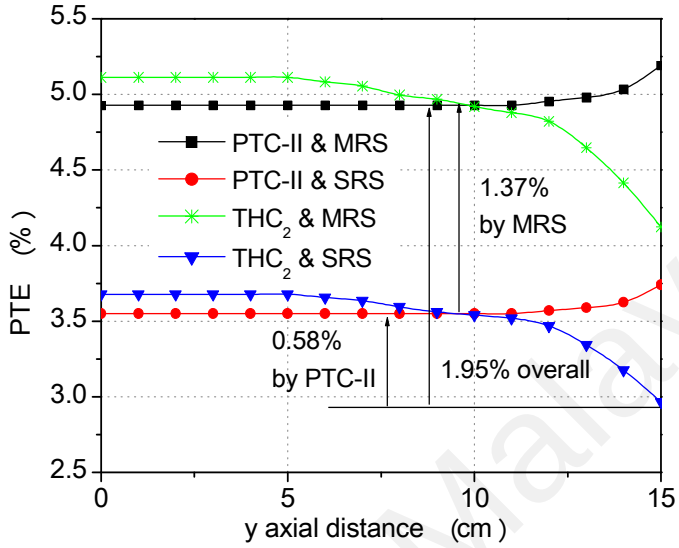

Figure 4.17: Comparison of PTE attained by the PTC-II and THC_2 under two resonance schemes (MRS and SRS) with PRC: position of PRC varies in *y* direction where *x* = 0 and *z* = 0 (Basar *et al*., 2017).

Table 4.4: Performance comparison of the proposed WPT systems with existing system (adopted from Basar *et al*., 2017).

Reff.	PTC/PRC, cm	*f* (MHz)	P_L (mW)	PTE (%)	$P_{L,PS}$(%)
(Xin *et al*., 2010)	65/1.2	0.4	790	3	82.1
(Sun *et al*., 2012)	48/1.1	13.56	24	3.04	--
(Na *et al*., 2015)	22/0.9	16.470	26	0.02	--
(He *et al*., 2015)	50/14	0.218	600	2	--
(Ke *et al*., 2016)	69/0.95	0.22	750	3.55	--
(Ding *et al*., 2016)	1.33, 15.9	433.9	47.55	1.21	--
[This work$_{PTC-II}$]	40/1.1	0.246	534	**4.93**	**94.62**

4.5 Conclusion

Stable and high-efficiency wireless power transfer system using PTC-II (modified Helmholtz coil) and Mixed Resonance Receiver has been presented in this chapter. A modified Helmholtz coil based PTC-II has been introduced and its performance was analyzed with comparison with a typical Helmholtz coil having the same diameter. The

comparison has shown that the performance of modified Helmholtz coil outweighs that of typical Helmholtz coil. The proposed modified Helmholtz coil was able to provide a better *H*-field uniformity which in turn improved power stability by 45.15% and interestingly minimized the unnecessary peak electromagnetic exposure level by 26%. In addition, to ensure optimum load factor, utilization of mixed resonance scheme (MRS) has improved the PTE. The proposed design was validated through rigorous experiments. The experimental results indicated that the proposed system attained at least 94.62 % power stability and 4.9 % PTE when 534 mW power was delivered to the load.

University of Malaya

CHAPTER 5: OVERALL PERFORMANCE IMPROVEMENT OF WPT SYSTEM

5.1 Introduction

The previous chapters illustrated two new power transmission coils PTC-I and PTC-II for the improvement of power transfer efficiency (PTE) and position stability of received power, respectively. The performance of these PTCs has been analyzed mathematically, tested experimentally and compared with the performance of others existing PTCs. This chapter introduces wireless power transfer (WPT) system with a compact wearable form of PTC to improve the system portability. The overall improvement of PTE and stability of WPT system are shown in this chapter by several techniques. The contribution made in this chapter includes: i) PTC-III to further improve the *H*-field uniformity for compact WPT system, ii) comparative study among all the proposed PTCs, iii) adopting multi-coil inductive link for WPT system in wireless capsule endoscopy (WCE) platform, iv) improvement of PRC configuration for better orientation stability of received power, v) overall implementation and experimental testing of WPT system in air and in saline water, and vi) electromagnetic safety analysis with compact wearable PTCs.

5.2 Literature Review

Most of the existing WPT systems for WCE proposed in literature with a large size (∅ 60-75 cm) of PTC that did not allow free movement of patient during the operation (Carta *et al.*, & Xin *et al.*, 2010; Pan *et al.*, 2011; Jourand *et al.*, 2012). Because this large size of PTC is incompatible for a portable WPT system. Although a few portable systems have been presented in the literature (Uehara & Hoshina, 2003; Shi *et al.*, 2015) with a simple configuration of wearable PTC, however, the obtained PTE of these systems were not more than 2.8%. In addition, the *H*-field uniformity of compact PTC and resultant receiving power stability and electromagnetic exposure were not fully investigated. Thus,

University of Malaya

this study bridges this gap with proposing a portable system using the newly proposed PTCs. In addition, the 2-coils inductive link was widely used approach for WPT where PTC and power receiving coil (PRC) would directly connect to the source and load, respectively. In this approach, the source and load resistance affect the loaded quality factor of PTC and PRC, respectively. In order to minimize this effect and maximize the power transfer efficiency (PTE), multi-coils inductive link such as 4-coils and 3-coils have also been presented in the literature (RamRakhyani *et al.*, and Kiani *et al.*, 2011). Based on the literature the 4-coils based system attains relatively higher inductive link efficiency (RamRakhyani *et al.* 2011). However, this investigation was performed with small size of coil set (∅ 6.4 – 2.2 cm). An analysis by Kiani *et al.* (2011) with a medium size of coil set(∅ 16.8-10.5 cm) indicated that the 4-coils based inductive link fails to attain high power delivery to the load (PDL) though it obtains high efficiency. Thus, Kiani *et al.* (2011) proposed a 3-coils inductive link to obtain high PDL. However, the 4-coils or 3-coils based indicative link has not been analyzed for WCE platform where a large coil (around ∅ 40 cm) in transmitting side and tiny coil (around ∅1 cm) in receiving side are deployed. Thus, this analysis is important to be included in this chapter. Besides, this chapter illustrated the improvement of orientation stability of received power ($P_{L,}$os) through the power combining technique in the orthogonal receiving coil set, where the parallel configuration of 3D PRC (Carta *et al.*, & Xin *et al.*, 2010; Pan *et al.*, 2011) was commonly used in the existing studies.

5.3 Materials and Methods

5.3.1 Configuration of PTC-III

In order to improve the *H*-field uniformity in the region away from the center, another new configuration of PTC has been proposed which named as PTC-III. The configuration of proposed PTC-III is illustrated in Figure 5.1. The configuration of PTC-III mainly

differs from the two other proposed PTCs (PTC-I and PTC-II) because it consists of four coil segments instead of three. These four coil segments have improved the *H*-field uniformity beyond the $y = \pm 0.75r$ lines which is advantageous for compact wearable PTC. As shown in Figure 5.1, the PTC-III consists of two auxiliary coil segments (2 and 3) placed in between the two main coil segments (1 and 4). All these coil segments have the same radius (*r*) and stacked coaxially i.e. their centers are on a common axis (*z*-axis). These coil segments have been connected in series. In this design, the main and the auxiliary coil segments have been separated from the mid plane by optimum distances of 3*r*/4 and 3*r*/16, respectively. The optimum turn ratio between the main coil and the auxiliary coil to obtain maximum *H*-field uniformity was 3:1. These design parameters have been optimized by the same methods illustrated in section 4.3.3.

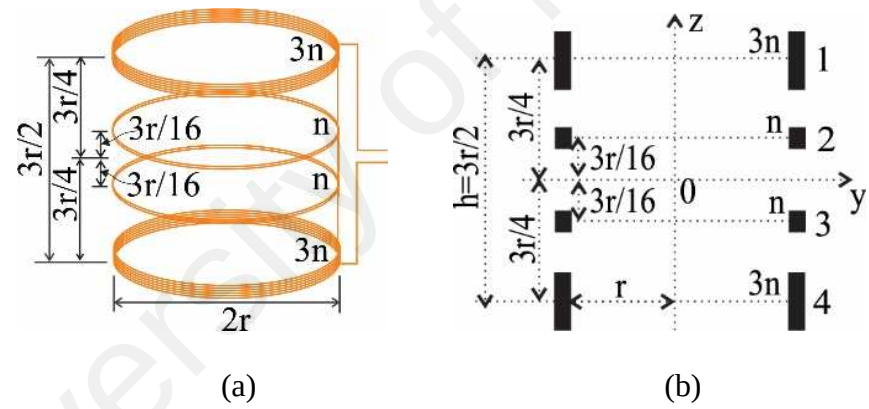

Figure 5.1: Design specification of PTC-III: (a) schematic view and (b) cross sectional view (Basar *et al.*, 2016b).

The performance of the proposed PTC-III has been compared with the typical Helmholtz coil (THC) that used in the WPT system proposed by (Carta *et al.*, 2010; Xin *et al.*, 2010). Among the existing coils, the THC was known to give higher uniformity, especially around the center (Beiranvand, 2013). The calculation of *H*-fields intensity that generated by the THC (H_{THC}) and others proposed PTCs has been shown in the previous chapter. The *H*-fields intensity generated by the proposed PTC-III ($H_{PTC\text{-}III}$) has been calculated using the formula given below

$$H_{PTC-III}(y,z) = \frac{Ir}{4\pi} * \sum_{i=1}^{4} \left[N \int_0^{2\pi} \frac{r - y\cos(\theta) + (z+s)\sin(\theta)}{\left[y^2 + (z+s)^2 + r^2 - 2yr\cos(\theta)\right]^{\frac{3}{2}}} d\theta \right]. \quad (5.1)$$

Where $N = \begin{cases} 3n & \text{for } i = 1 \text{ and } 4 \\ n & \text{for } i = 2 \text{ and } 3 \end{cases}$, and $s = \begin{cases} 3r/4 & \text{for } i = 1 \\ 3r/16 & \text{for } i = 2 \\ -3r/16 & \text{for } i = 3 \\ -3r/4 & \text{for } i = 4 \end{cases}$.

In this calculation, both PTCs are considered concentric with the Cartesian coordinate and perpendicular to the *z*-axis. Due to the symmetrical distribution, *H*-field has been analyzed only on the *y*-*z* plane at *x*=0.

The calculated normalized *H*-fields of PTC-III and THC have been compared in Figure 5.2 (a). As it can be seen from the Figure 5.2 (a), within a region enclosed by the lines $y = \pm 0.75r$ and $z = \pm 0.5r$, the level of *H*-field generated by the PTC-III was much uniform. Based on the (4.5), the uniformity (γ) of *H*-field attained by the PTC-III was 94% which was 45% improvement in comparison to the 49% of γ attained by the THC. The γ of PTC-III also has been compared with that of PTC-II in Figure 5.2 (b). This comparison shows that within the region enclosed by the lines $y = \pm 0.8r$ and $z = \pm 0.5r$, the PTC-III improves the γ around 9%.

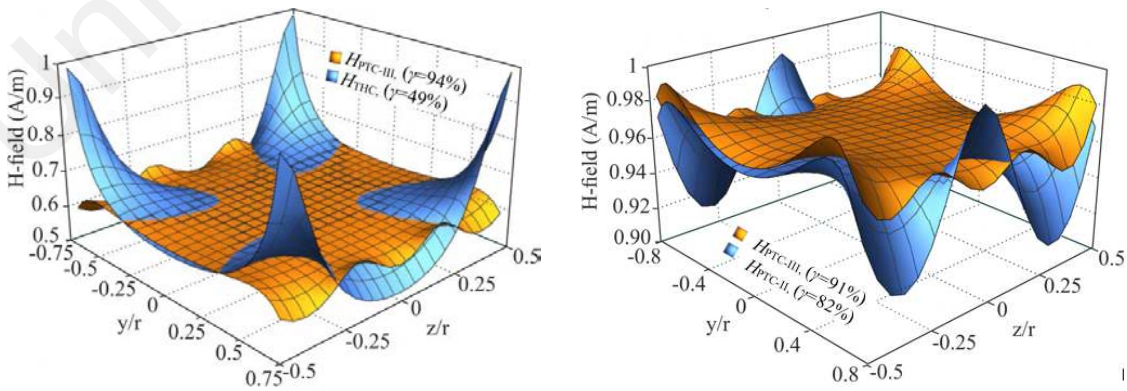

(a) (b)

Figure 5.2: Comparison of calculated normalized *H*-field intensity generated by the proposed PTC-III and: a) THC (Basar *et al.*, 2016b), and b) PTC-II.

5.3.2 Performance Comparisons of PTC-I, PTC-II and PTC-III

In this section, the overall performance of all the proposed PTCs (PTC-I, PTC-II, and PTC-III) have been compared to access their suitability. The performances have mainly been compared by the minimum level of *H*-field uniformity (γ), and link efficiency (η). Within the considered region, the γ and η of the proposed PTCs have been shown in Table 5.1. The given η has been computed with an equal number of turns and diameter of PTCs with an identical PRC. Among the proposed PTCs in Table 5.1, it can be seen that the PTC-I attains the highest η. However, this PTC results relatively low γ which will lead to lower position stability of received power and higher electromagnetic exposure. Considering the issues of electromagnetic exposure and position stability of received power, the PTC-II and PTC-III provide better solution since, these PTCs attain higher uniformity of *H*-field. Within axial line to $y = 0.5r$, these PTCs attain around 96 % of γ.

Table 5.1: Performance comparison of proposed PTCs.

WPT with	z region within	γ in % (within y = ± 0.5r, ± 0.8r),	η in % (within y = ± 0.5r)
PTC-I	± 0.4r	88, 67	36
PTC-II	± 0.5r	96, 82	14
PTC-III	± 0.5r	96, 91	13
* Minimum level of efficiency (η_{min}) of all the TPCs are given for an identical PRC.			

However, considering a compact PTC size in wearable from, if the region of uniform field had increased up to $y = \pm 0.8r$ lines then the PTC-III would performed the best for higher uniformity. Within this region, the γ obtained by the PTC-III was 91%. Thus, PTC-III could be the most advantageous one for wearable WPT system to improve the position stability of received power and level of peak exposure. However, PTC-I was the best option for high η.

University of Malaya

5.3.3 Overview of multi-coil inductive power link in WCE platform

In order to analyze the η of multi-coil inductive link, a 4-coil system has been used. Figure 5.3 presents the simplified schematic and lumped element model of 4-coils based WPT system for analysis. This 4-coils based system has used two additional coils with the conventional 2-coils based system. The additional coils are named as driving coil (coil 1) and load coil (coil 4) deployed in transmitting and receiving sides, respectively.

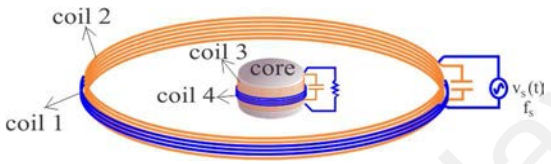

(a)

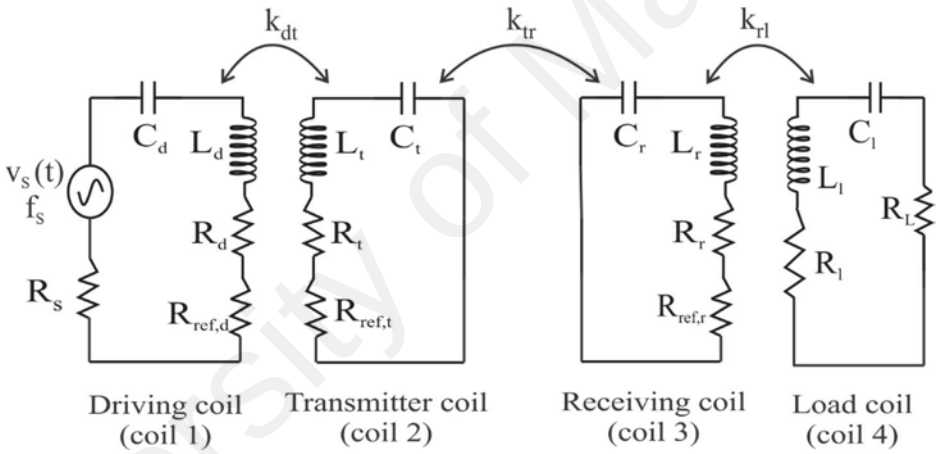

(b)

Figure 5.3: Simplified 4-coil based inductive link: (a) schematic view, and (b) lumped element model.

For the purpose of analysis, this 4-coils inductive power transfer link could be transformed into 3-coils or 2-coils based link by excluding one or both of the additional coils. Generally, the highest link efficiency is attained when all the coils are resonated at the same operating frequency. At the resonance, the effect of receiving side to corresponding transmitting side could be represented by the reflected resistance. For a *m*-coils system, where coil 1 is connected to the source and coil *m* is connected to the load, the reflected resistance at any stage can be given by (Kiani *et al.* 2011)

University of Malaya

$$R_{\text{ref i}} = k_{i,i+1}\omega L_i Q_{i+1}. \tag{5.2}$$

And the loaded quality factor of the driving coil, any middle coil, and load coil can be given by (Kiani *et al.* 2011)

$$Q_{1,\text{L}} = \frac{\omega L_1}{R_1 + R_s + R_{\text{ref 1}}}, Q_{\text{i,L}} = \frac{\omega L_i}{R_i + R_{\text{ref i}}}, \text{and } Q_{m,L} = \frac{\omega L_m}{R_m + R_L} \tag{5.3}$$

For the loaded Q_{L}, the efficiency of 2-coil (transmitting and receiving coils), 3-coils (transmitting, receiving, and load coils), and 4-coil (driving, transmitting, receiving, and load coils) based inductive link of Figure 5.3 can be given by (Kiani *et al.*, 2011; Cook *et al.*, 2013)

$$\eta_{\text{2-coils}} = \frac{k_{tr}{}^2 Q_{t,L} Q_{r,L}}{[1 + k_{tr}{}^2 Q_{t,L} Q_{r,L}]} * \frac{R_L}{R_r + R_L} \tag{5.4}$$

$$\eta_{\text{3-coils}} = \frac{k_{tr}{}^2 Q_{t,L} Q_{r,L} * k_{rl}{}^2 Q_{r,L} Q_{l,L}}{[1 + k_{rl}{}^2 Q_{r,L} Q_{l,L}] * [1 + k_{tr}{}^2 Q_{t,L} Q_{r,L} + k_{rl}{}^2 Q_{r,L} Q_{l,L}]} * \frac{R_L}{R_l + R_L} \tag{5.5}$$

$$\eta_{\text{4-coils}} = \frac{k_{dt}{}^2 Q_{d,L} Q_{t,L} * k_{tr}{}^2 Q_{t,L} Q_{r,L} * k_{rl}{}^2 Q_{r,L} Q_{l,L}}{[(1 + k_{dt}{}^2 Q_{d,L} Q_{t,L})(1 + k_{rl}{}^2 Q_{r,L} Q_{l,L}) + k_{tr}{}^2 Q_{t,L} Q_{r,L}] * [1 + k_{tr}{}^2 Q_{t,L} Q_{r,L} + k_{rl}{}^2 Q_{r,L} Q_{l,L}]} * \frac{R_L}{R_l + R_L} \tag{5.6}$$

Based on the above relations, the simulated η of the inductive links consisting different number of coils for WCE application is shown in Figure 5.4. It can be seen from the Figure 5.4 that the 3-coils based WPT system has attained the maximum efficiency which was slightly higher than that of 4-coil based system. In comparison with the 2-coils system, the load coil of the 3-coils system compensates the effect of load resistance on the loaded quality factor of receiving coil. In the 3-coils based system, the load resistance was not directly connected to the receiving coil that allows to obtain high loaded quality factor of receiving coil that has compensated the weak coupling between transmitting and receiving coil (k_{tr}) and helps to improve the efficiency. Similarly, the driving coil in 4-coils system could be advantageous for the system that is derived with a source having high resistance (around R_{S} = 50Ω). Since, PTC has been derived by a driving amplifier

having low output resistance, thus R_S can be considered low and there is less effect on the loaded quality factor of PTC. Therefore, the 4-coils based system is not advantageous over the 3-coils system in this particular application. In addition, the large dimension and high quality factor of transmitting coil result relatively high reflected resistance at the driving coil as well as low loaded quality factor. Thus, in this application platform, the 4-coils system has degraded the performance than 3-coils based system.

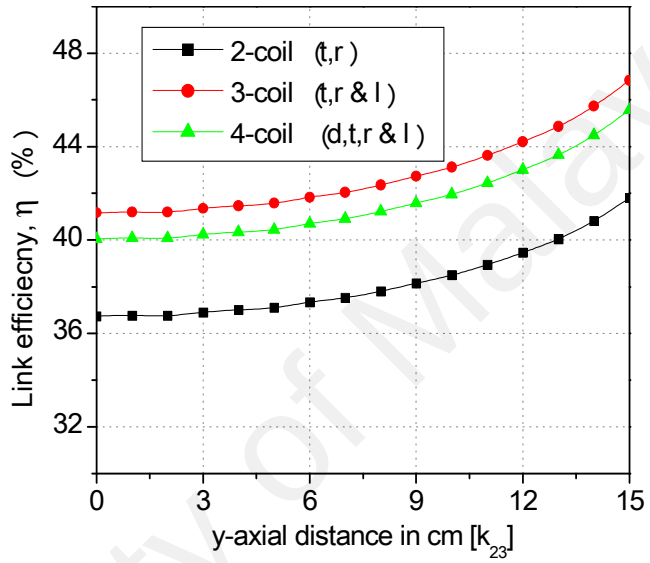

Figure 5.4: Comparison of simulated link efficiency of 2-coils, 3-coils, and 4-coils based inductive link in WCE platform.

5.3.4 Improved Power Receiving Scheme and Orientation Stability

For the 3-coils system, power delivery to the load (P_L) can be given by (Kiani *et al.*, 2011)

$$P_L = \frac{V_s^2}{2R_2} * \frac{k_{tr}{}^2 Q_{t,L} Q_{r,L} * k_{rl}{}^2 Q_{r,L} Q_{l,L}}{(1 + k_{tr}{}^2 Q_{t,L} Q_{r,L} + k_{rl}{}^2 Q_{r,L} Q_{l,L})^2} * \frac{R_L}{R_l + R_L}. \tag{5.7}$$

In existing designs, receiving coil set of 3D PRC was connected in parallel to the load through the full wave bridge rectifier as shown in Figure 5.5. In this configuration, the output power is offered by the coil (among L_{rx}, L_{ry}, and L_{rz}) which received the maximum power. In this configuration, the P_L can be given by

$$P_L = \mathrm{MAX}(P_{L,Lx}, P_{L,Ly}, P_{L,Lz}). \tag{5.8}$$

However, during the operation, the PRC continuously changes the orientation that causes misalignment between the PTC-PRC. In the worst case of misalignment, it could happen that none of the receiving coils of 3D PRC are perfectly aligned with the PTC as the misalignment model shown in Figure 5.6.

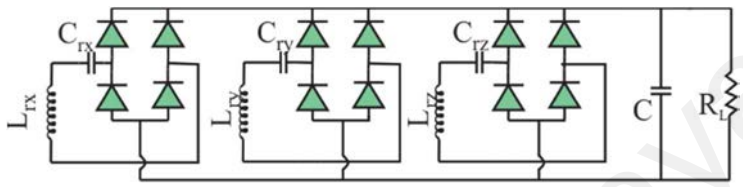

Figure 5.5: Typical configuration of power receiver.

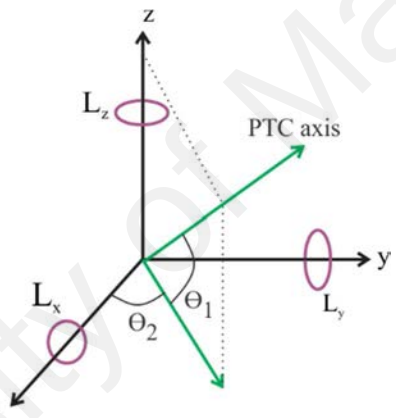

Figure 5.6: Relative orientation (misalignment) model between PRC and PTC axis.

Based on the misalignment model shown in Figure 5.6, the $P_{L,\,Lx}$, $P_{L,\,Ly}$ and $P_{L,\,Lz}$ can be calculated as

$$P_{L,Lx}(\theta_1,\theta_2) = \frac{V_s^2}{2R_t} * \frac{(k_{tr}Cos\theta_1 Cos\theta_2)^2 Q_{t,L}Q_{r,L} * k_{rl}{}^2 Q_{r,L}Q_{l,L}}{(1+(k_{tr}Cos\theta_1 Cos\theta_2)^2 Q_{t,L}Q_{r,L} + k_{rl}{}^2 Q_{r,L}Q_{l,L})^2} * \frac{R_L}{R_l + R_L}. \tag{5.9}$$

$$P_{L,Ly}(\theta_1,\theta_2) = \frac{V_s^2}{2R_2} * \frac{V_s^2}{2R_t} * \frac{(k_{tr}Cos\theta_1 Sin\theta_2)^2 Q_{t,L}Q_{r,L} * k_{rl}{}^2 Q_{r,L}Q_{l,L}}{(1+(k_{tr}Cos\theta_1 Sin\theta_2)^2 Q_{t,L}Q_{r,L} + k_{rl}{}^2 Q_{r,L}Q_{l,L})^2} * \frac{R_L}{R_l + R_L}. \tag{5.10}$$

$$P_{L,Lz}(\theta_1) = \frac{V_s^2}{2R_2} * \frac{V_s^2}{2R_t} * \frac{(k_{tr}Sin\theta_1)^2 Q_{t,L}Q_{r,L} * k_{rl}{}^2 Q_{r,L}Q_{l,L}}{(1+(k_{tr}Sin\theta_1)^2 Q_{t,L}Q_{r,L} + k_{rl}{}^2 Q_{r,L}Q_{l,L})^2} * \frac{R_L}{R_l + R_L}. \tag{5.11}$$

The P_L has been varied with θ_1 and θ_2 for a given set of Q, k, and R_L. The P_L become maximum when PTC axis was in line with any of the x-axis or y-axis or z-axis. Similarly,

University of Malaya

the P_L become minimum when $\theta_2 = 45^0$ or 135^0 or 225^0 or 315^0 with $\theta_1=35^0$ or 145^0 or 215^0 or 325^0. For an analytical model of 3-coil inductive link having $Q_{t,L}=255$, $Q_{r,L}=56$, $Q_{l,L}=0.25$, $k_{tr}=0.011$, and $k_{rl}=0.72$, the maximum and minimum P_L within the possible orientation of PRC were $P_{L\text{-Max}} = 681$ mW and $P_{L\text{-Min}} = 245$ mW. Based on the orientation stability of P_L can be given as

$$P_{L,OS} = \left(1 - \frac{P_{L,Max} - P_{L,Min}}{P_{L,Max}}\right) * 100\%, \tag{5.12}$$

the P_L can obtain 40% of $P_{L,}$os in conventional parallel connection of 3D PRC (as shown in Figure 5.5). This orientation stability of P_L could be considered very low. The overall stability of P_L, considering orientation and position stability, even lower. In this work, the position stability was improved with highly uniform *H*-field resulted by the proposed PTCs. Thus, to improve the orientation stability of P_L, a power combining configuration of 2-3D PRC has been used (Figure 5.7). In this configuration, two sets of 3D coils have been used as shown in Figure 5.7 (a). Where three receiving and three load coils were reeled on a common core. Load coils have been reeled on the receiving coil (where three receiving coils are perpendicular to each other or aligned in three axis *x*, *y*, and *z*). The load coils $L_{l,x}$, $L_{l,y}$, and $L_{l,z}$ have been connected to the load R_L through the resonating capacitor and full wave bridge rectifier.

Therefore, in this power combining series configuration, all the coils can contribute power to the load if the coil receives the power above the threshold level of the bridge rectifier. Thus, the overall load power can be given by

$$P_L = P_{L,Lx}(\theta_1,\theta_2) + P_{L,Ly}(\theta_1,\theta_2) + P_{L,Lz}(\theta_1). \tag{5.13}$$

Although, the rectifier loss in this configuration was higher than the conventional parallel configuration, nonetheless, this configuration tremendously improves the $P_{L,OS}$ and $P_{L,\text{ Min}}$.

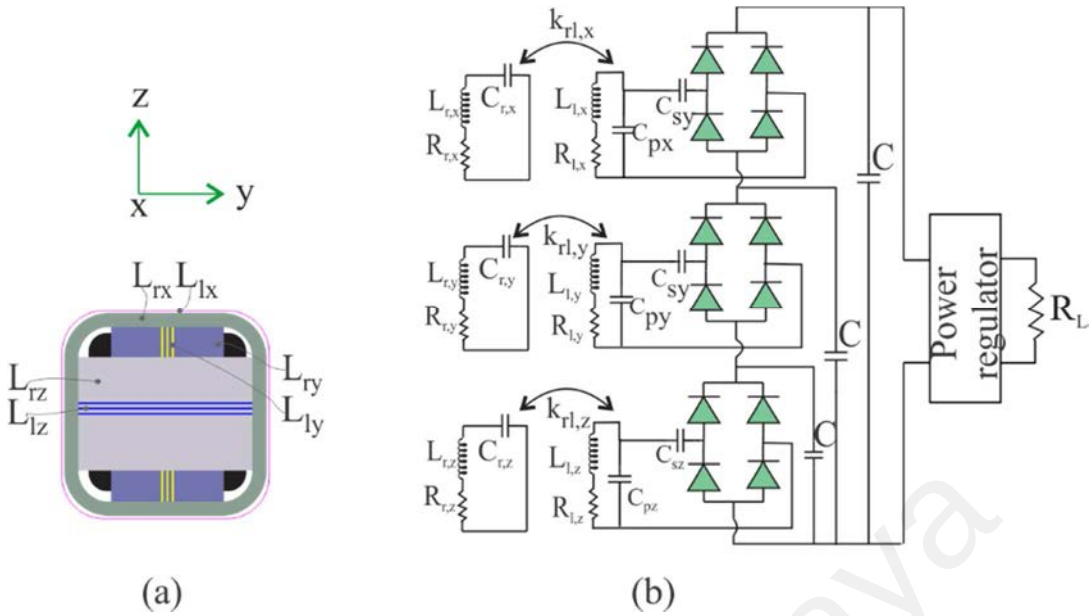

Figure 5.7: (a) configuration of 2-3D PRC, (b) power combining configuration of 2-3D PRC.

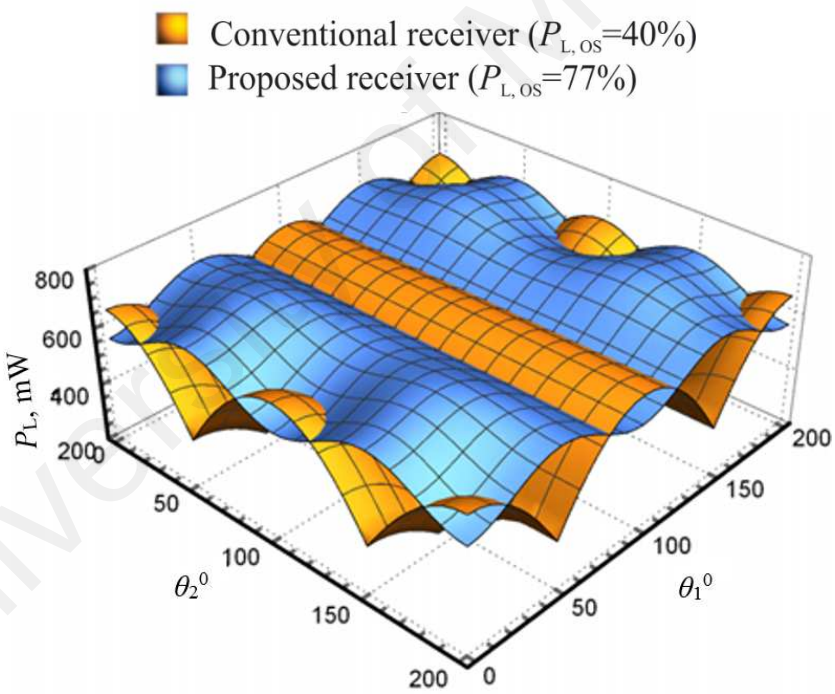

Figure 5.8: Variation of load power P_L with the relative orientation of PRC in conventional parallel configuration and power combining configuration used in this study.

The variation of received power over the possible orientation of PRC is illustrated in Figure 5.8. The proposed series connection of 2-3D PRC results $P_{L\text{-Min}}$ = 563 mW when PTC axis was in line with any of the *x*-axis, *y*-axis or *z*-axis. Whereas, the $P_{L\text{-Max}}$ = 730 mW when $\theta_2 = 45^0$ or 135^0 or 225^0 or 315^0 with θ_1=35^0 or 145^0 or 215^0 or 325^0. Based on

(5.7), this $P_{L\text{-}Max}$ and $P_{L\text{-}Min}$, results the $P_{L,OS}$ =77%. Thus, in comparison to the conventional parallel connection of PRC, the power combining series connection almost double the orientation stability.

5.3.5 Prototype Implementation

The prototype of above design WPT system has been implemented for experimental testing. The implemented PTC and experimental setup are shown in Figure 5.9 (a). The setup consists of PTCs, power receiver, and driver/power amplifier. All these parts are discussed in the following subsections.

5.3.5.1 Implementation of Wearable PTCs

In order to improve the system portability and compactness, wearable form of PTC-I and PTC-III have been implemented based on the comparison of PTC performance (see Table 5.1). The implemented wearable PTC-I and PTC-III are shown in Figure 5.9 (b) and (c), respectively. These PTCs have been implemented with textile where a diameter of 35 cm was chosen to be adjusted with a free size Mannequin. This diameter can be adjusted with different patient group, though, the larger diameter causes the lower PTE. Two wearable waist belts having equal length of 115 cm, thickness of 3.5 cm and different heights 28 cm and 19 cm have been prepared to fix the PTC to the patient body.

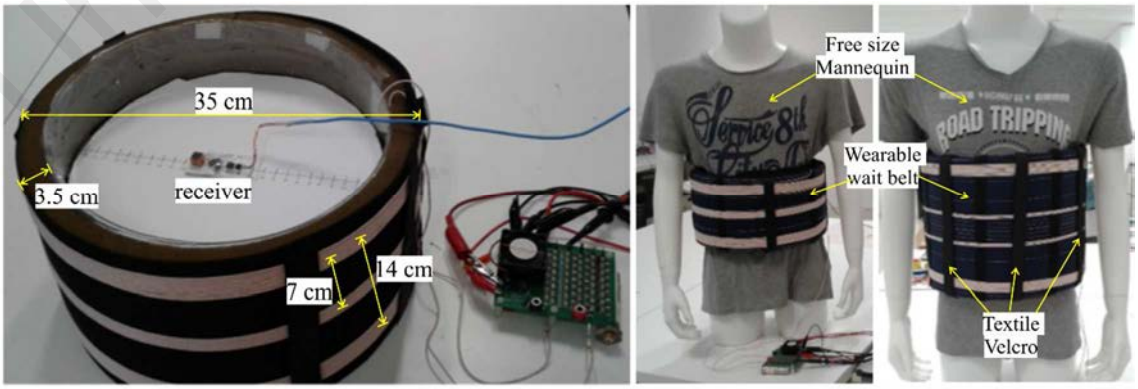

(a) (b) (c)

Figure 5.9: (a) Experimental setup for measurement of power and efficiency, (b) PTC-I, and (c) PTC-III set with the free size mannequin.

University of Malaya

The waist belts have been papered with textile cloth, semi-rigid polyurethane foam, and Velcro. The waist belt can be easily worn and taken off. The foam was used between the coil and the body to isolate the body from strong reactive *H*-field that is produced in very close vicinity to the PTCs' coil segments. The PTCs are fixed with the wearable waist belt using Velcro. The specifications of implemented PTCs are summarized in Table 5.2.

Table 5.2: Specification of implemented wearable PTCs

Particulars	PTC-I	PTC-III
Number of turns	32 (12+8+12)	32(12+4+4+12)
Diameters (cm)	35	35
Inductance, L_t (μH)	412.50	342.28
Resistance, R_t (Ω)	1.28	1.18
Quality factor ($Q_{t,UL}$)	506.21	452.23

5.3.5.2 Implementation of improved power receiving system

The implemented power receiver unit is shown in Figure 5.10. The Figure 5.10a shows the 1D PRC of 3-coils link that consists of receiving and load coil. The load coil (L_l) has been reeled on the receiving coil (L_r). In order to cope with the misalignment problem, the 1D coil has been converted to 3D PRC which is shown in Figure 5.10b. This 3D PRC consists of two sets of three orthogonal coils aligned in *x*, *y*, and *z*-direction, one for receiving coil and another for load coil, therefore, it is named as 2-3D PRC. The electrical specifications of this implemented 2-3D PRC are given in Table 5.3. In 2-3D PRC set, it is important to have identical properties of each of the coils in *x*, *y*, and *z*-direction to ensure an equal amount of received power by the individual coil for a common alignment, thus this improves the orientation stability. Therefore, the coils need to be carefully implemented to obtain about equal specifications of coils. As it can be seen from the Table 5.3, all the implemented the coils have almost similar specifications of inductance, resistance and quality factor. The selection of number of turns, in receiving coil has been

University of Malaya

optimized for high Q_r. Whereas, the selection of number of turns in the load coil needed to be optimized for optimal Q_l of load coil and coupling k_{rl}. The high Q_l and k_{rl} cause high reflected impedance at receiving coil which decreases the loaded $Q_{r,L}$ of receiving coil and power transfer efficiency. On the other hand, low k_{rl} causes the low efficiency between the receiving and load coil as well as in the overall link. Taking account of these effects an optimal number of 3 turns was used for the load coil. The final shape of implemented 2-3D PRC was a cubic with the average diameter of 12 ±0.1 mm. This size of the PRC was small enough to fit in an existing commercial capsule with the length of 27.9 mm and diameter of 13 mm (Li *et al.*, 2008).

The associated power combining circuit with LED load and 30 Ω resistive load have been shown in Figure 5.10c and Figure 5.10d, respectively. In order to test the orientation stability, a miss-aligner was made with PMMA sheet shown in Figure 5.10e. It can rotate the PRC in θ_1 and θ_2 directions. The coaxial cable shown in Figure 5.10f was used for measuring the voltage across the load using an oscilloscope.

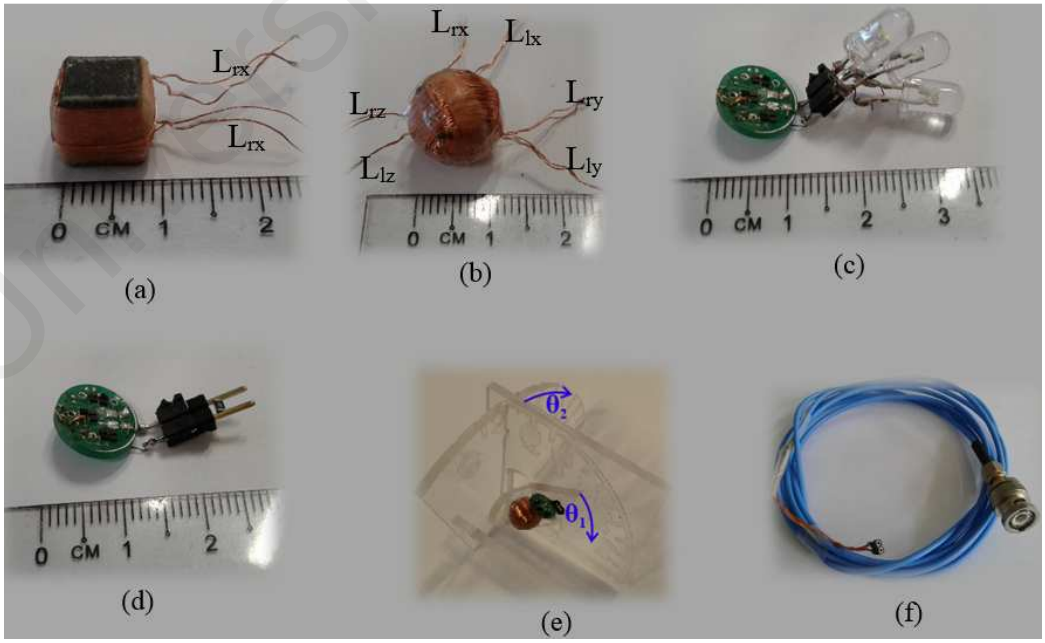

Figure 5.10: Implemented: (a) 1D PRC, (b) 2-3D PRC, (c) power conversion circuit loaded with LEDs, (d) power receiving circuit with 30 Ω load, (e) custom made 2-3D PRC orientation controller, (f) calibrated coaxial cable for power measurement.

Table 5.3: Specification of 2-3D PRC.

Specification	L_{rx}	L_{ry}	L_{rz}	L_{lx}	L_{ly}	L_{lz}
Number of turns	140	142	141	3	3	3
Wire gauge and strands	AWG 42, 8 strands					
Inductance (μH)	415.5	416.1	415.7	0.328	0.349	0.322
Resistance (Ω)	7.5	7.5	7.6	0.215	0.22	0.242
Quality factor (Q_{uL})	87.25	85.75	85.49	2.39	2.49	2.09

5.3.5.3 Driving circuit with fine tuning capability

Implementation of class E driver has been illustrated in the previous chapter. This chapter presents the same class E driver with incorporation of a better tuning mechanism consist of series capacitance that allows driving the PTC of different values of inductance at different operating frequencies. In order to allow fine tuning, a high voltage variable capacitor SGNMNC31006 (supplied by Sprague-Goodman Electronics) was used in parallel with the main capacitor bank as shown in Figure 5.11. The variable capacitor itself allows fine tuning within the range of 10-100 pF with the maximum voltage tolerance 6000 V (6 kV). The variable capacitor and series parallel capacitor bank together has provided overall tuning within the range of 10pF to 2162.5 pF.

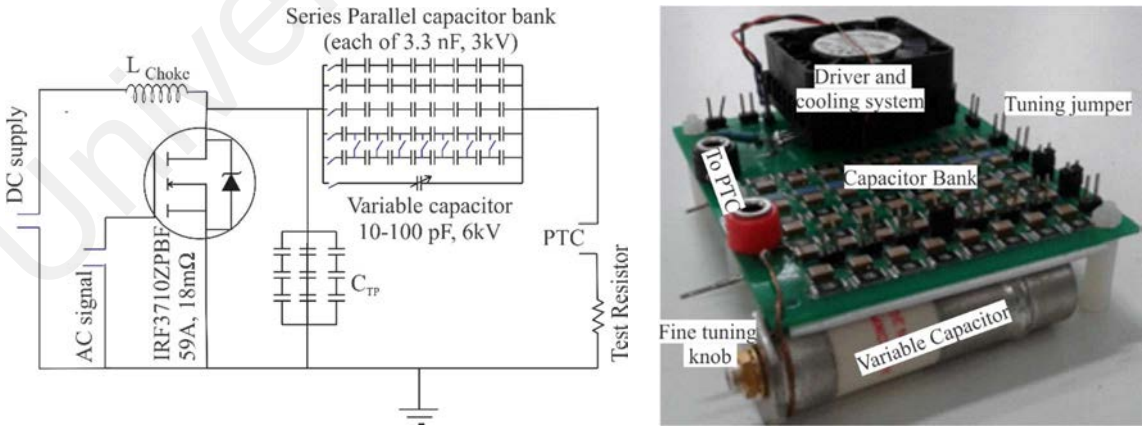

(a) (b)

Figure 5.11: Class E driver with improved tuning circuit: (a) schematic diagram, and (b) implemented driver.

University of Malaya

5.4 Results and Discussion

5.4.1 Experimental test of implemented WPT system

The performance of the implemented systems have been tested by measuring voltage across the 30 Ω load. Then the measured voltage has been converted to the received power (P_L) and PTE from source to load using (4.13) and (4.15), respectively. The P_L and PTE of PTC-I and PTC-III based WPT systems are shown in Figure 5.12. The P_L and PTE are shown within a region enclosed by the lines y = ± 13 cm (around 75% of coil radius). It can be seen from the Figure 5.12 that the P_L and PTE obtained by the PTC-I based system were remarkably higher than that was obtained by the PTC-III based system. The PTC-I based WPT system attained the minimum P_L of 758.48 mW when PRC was located at y = 0, z = 0.

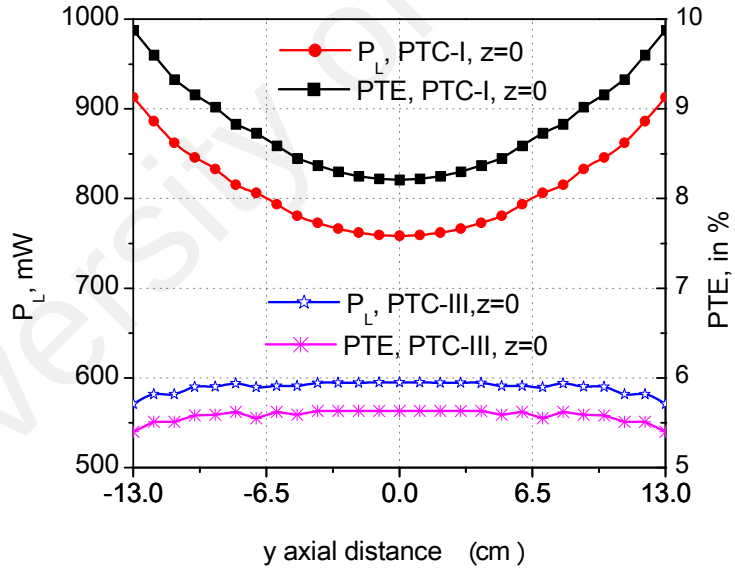

Figure 5.12: Measured P_L and PTE of implemented 3-coils WPT system with PTC-I and PTC-III.

At this location of PRC, the PTC-I based system has attained the PTE of 8.21 %. Whereas, the minimum 570.96 mW of power has been transferred by the PTC-III based system with the PTE of 5.4% when the PRC was located at y = ±13 cm, z = 0. Although, the P_L and PTE obtained by the PTC-III based system were lower than that of PTC-I based system, nonetheless, the position stability of received power ($P_{L,pS}(y, z)$) attained in the

PTC-III was relatively higher than that in the PTC-I. Based on the (4.14), the $P_{L,pS}$ (y, z) attained by the PTC-III was 96.98% whereas it was around 83.08% in PTC-I. The $P_{L,pS}$ (y, z) of PTC-III based WPT system was higher due to its capability of generating highly uniform H-field. Whereas, the PTE of PTC-I based WPT system was higher due to the high quality factor and coupling coefficient of PTC-I. Thus, the PTC-I would be the good choice to attain high PTE, while PTC-III was the best option for higher $P_{L,pS}$ (y, z).

5.4.2 Experimental test of with orientation of 2-3D PRC

The variation of received power with the orientation of 2-3D PRC is shown in Figure 5.13. As illustrated in section 5.3.4, the variation of P_L with θ_1 was maximum when $\theta_2 = 45^0$ or 135^0 or 225^0 or 315^0 and minimum when $\theta_2 = 0^0$ or 90^0 or 180^0 or 270^0. Thus, the variation of P_L with θ_1 has been shown for $\theta_2 = 0^0$ and 45^0. As it can be seen from the Figure 5.13, the P_L varies with the θ_1 and θ_2 within around $P_{L,max}$ = 913 mW to $P_{L,min}$ = 750 mW, that has been resulted around 81.64% of $P_{L,os}$.

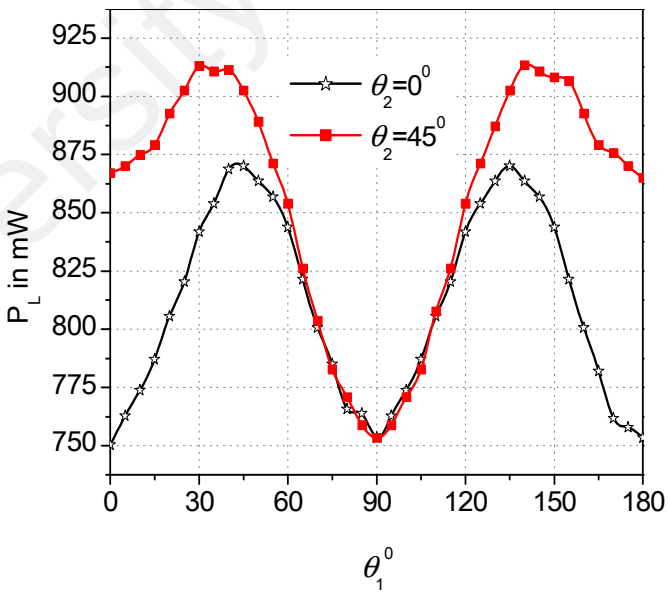

Figure 5.13: **Variation of received power with the orientation of the PRC.**

5.4.3 Experimental test of WPT system in saline water

Since the WPT system for WCE works in biological tissue environment, it was important to test power transfer in tissue environment. In the previous chapter, the power

transfer has been tested with slaughtered biological tissue, where it was noticed that placing the PRC in deep tissue reduces the efficiency around 3%. However, the slaughtered tissue contains less fluid thus it might cause less effect than that of actual living tissue which consists of blood which has some electrical conductivity. Thus, power transfer efficiency has also been tested in saline water which has electrical conductivity. The transferred powers in air and that in saline water has been shown in Figure 5.14. As can be seen in the Figure 5.14, the brightness of LED reduced in the saline water. The power transfers in air and that in saline water have also been compared by measuring the PTE across the 30 Ω load. The comparison of PTE has been shown in Figure 5.15. The Figure 5.15 shows that the saline water has reduced the PTE to 7.6% from 8.21 % in air. This reduction of PTE was 0.61% which was around 7.4% of the PTE obtained in air.

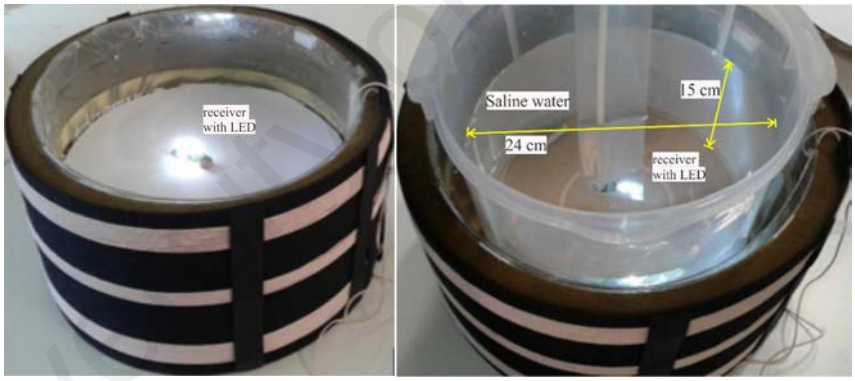

Figure 5.14: Comparison of transfer power in air (left) and in saline water (right) through the LED intensity.

This reduction of PTE was higher than that of in slaughtered tissue having less conducting fluid (blood). Based on this observation, it was assumed that the reducing of PTE in real field application with living tissue will be in between the effect of slaughtered tissue and saline water.

5.4.4 Electromagnetic exposure effect

The electromagnetic effect has been analyzed for the compact wearable PTCs where the smaller diameter of PTCs (35 cm) was used. The details of simulation setup was

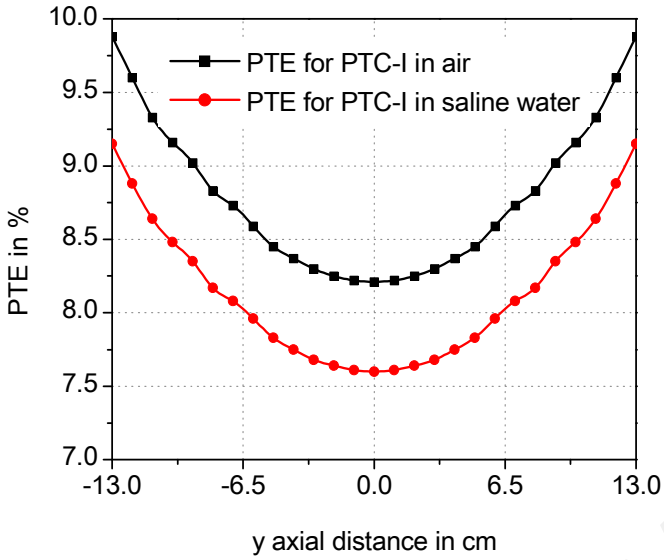

Figure 5.15: Comparison of measured PTE in air and in saline water.

shown in the previous chapter. The simulated induced current density *J*, A/m^2 in the WPT system with PTC-I and PTC-III is shown in Figure 5.16 for the equal amount of power transfer. As indicated in Figure 5.16, the peak point *J* induced near the PTC-III was around 2.23 A/m^2 which was lower than 2.39 A/m^2 that induced near the PTC-I at 250 kHz frequency. This was because of more uniform *H*-field in PTC-III that has reduced the peak point *J*. In both of the cases, the *J* near the PRC were 2.46 A/m^2 which was just below of ICNIRP limit 2.5 A/m^2 at 250 kHz.

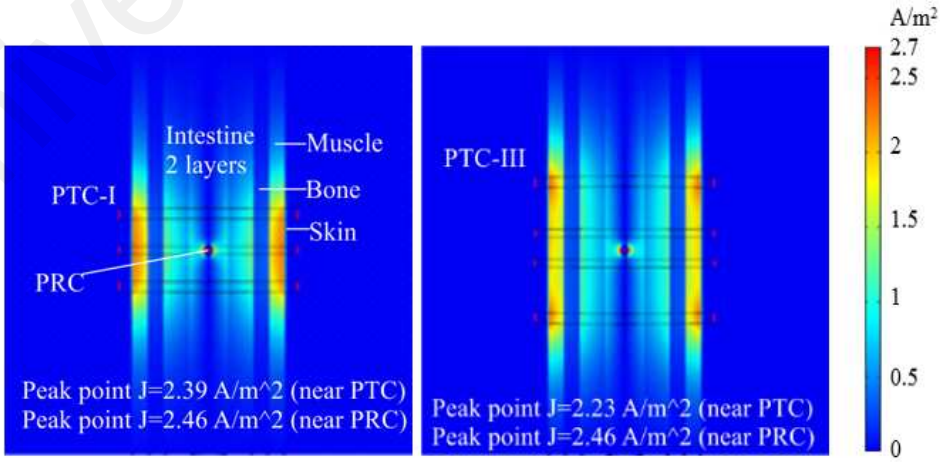

Figure 5.16: Simulated induced current density (*J*, A/m^2) in the biological tissues for the WPT system with PTC-I (left) and PTC-III (right).

University of Malaya

Thus, for the equal amount of power transfer (200 mW), the PTC-III minimized the *J* in the tissues proximity to the PTC. Whereas the peak point *J* in the tissues near the PRC was similar in both of the cases.

5.5 Conclusion

A 3-coil inductive WPT system with the wearable form of PTC and 2-3D PRC using power combining configuration has been presented in this chapter. The analysis and experimental results have shown that the proposed WPT system tremendously improve the PTE and received power stability. The PTC-I based wearable system attained the best PTE which was around 8.21% when at least 758 mW power being transferred. While the PTC-III based system obtained the best position stability of the received power which was around 96.9% within the region of 0.75 times of PTC radius. The PTC-III also minimized the peak point current density in the tissues near the PTC. The orientation stability of received power also improved up to 81.6% by the 2-3D PRC.

University of Malaya

CHAPTER 6: CONCLUSIONS AND RECOMMENDATIONS

6.1 Introduction

Finally, this chapter presents the major conclusions based on the contributions that have been made in this thesis. The chapter begins with an overall conclusion then highlights the major contributions. The chapter ends with the declaring the limitations of this study with suggestions and recommendations for future work.

6.2 Conclusions

The design of wireless power transfer (WPT) system for high power transfer efficiency (PTE) and received power stability (RPS) have been presented in this thesis for wireless capsule endoscopy (WCE) application. The overall design has shown tremendous improvement of WPT system performance in terms of PTE and RPS. The PTE obtained by the optimum design was 8.12% which was remarkably higher than 3.55% of PTE obtained by the best existing design (Ke *et al.*, 2015). The optimum proposed design also has attained overall RPS of 79.2% whereas only 33.9% of RPS obtained by the best existing design (Xin *et al.*, 2010). The performance of the proposed system has been improved with three new configurations of power transmitting coil (PTC), referred to PTC-I, PTC-II, and PTC-III for better *H*-field uniformity, quality factor, and coupling coefficient. Along with these PTCs, the power receiver has also been improved with optimization of number of strands in power receiving coil (PRC), design of mixed resonance scheme, power combining scheme with 2-3D PRC, full wave bridge rectifier with ultra low voltage Schottky diode. In addition, 3-coils inductive link has been designed and proposed to improve the PTE by minimizing the loading effect. Finally, wearable PTC has been designed for compact WPT system. In addition, this research has enabled analysis of electromagnetic exposure effect with incorporation of PRC using high permeability ferrite core. The analysis reveals that the induced current density was

University of Malaya

relatively higher in the body tissues near the PRC in comparison to the tissues that near to the PTC. In accordance with the guideline of ICNIRP, induced current density exceeded the limit when more than 200 mW of power was transferred. The proposed WPT system has been presented for wireless capsule endoscopy application, however, it could be also advantageous in other applications where power receiver system is moving within a certain region.

6.3 Summary of Major Contributions

The following are the list of major contributions made by this thesis.

i. Performance analysis and optimization with mathematical model

The existing studies on the WPT system for WCE platform have limited analysis and optimization on key design parameters. Therefore, a complete mathematical model has been introduced in this work to analyze and optimize the performance of WPT system. With the introduced mathematical model, the relationship between key design parameters such as coil configuration, coil size, number of turns etc. and key performance indices such as *H*-field uniformity, coil's quality factor, coupling coefficient, inductive link efficiency, and received power stability have been analyzed and optimized.

ii. New configuration of PTC

Three new power transmission coils have been proposed in this research. The proposed coils were named as PTC-I, PTC-II and PTC-III, respectively. The performance of these coils in terms of *H*-field uniformity, coil's quality factor, coupling coefficient, inductive link efficiency, and received power stability have been analyzed and compared with that of available power transmitting coils used in existing research work. The comparison indicated that the proposed three coils outweigh the existing conventional coils. Among the proposed three coils the PTC-I works the best to obtain

University of Malaya

higher efficiency and the PTC-III performs the best for improvement of position stability of received power. The PTC-III was more compatible to minimize peak point exposure, therefore this coil is more suitable for wearable power transfer system.

iii. 3-Coil inductive link for wireless power transfer

A 3-coils (transmitting, receiving and load coil) inductive link has been designed and proposed to improve the power transfer efficiency by minimizing loading effect. The performance of proposed 3-coil inductive link has been compared with that of 2-coils and 4-coils inductive link, where the 3-coils link performs the best in WCE platform. Because in WCE platform, the power transfer system works with a source having low resistance and the load having high resistance in compare to the internal resistance of the coils. The 2-coil link suffers from high loading effect at the receiving coil, whereas the 4-coils link suffers from high reflected impedance in the driving coil. Thus, both of these 2-coils and 4-coils link fail to attain maximum efficiency.

iv. 2-3D PRC with power combining configuration

With the 3-coils link, a new configuration of power receiver with 2-3D PRC and power combining technique has been proposed. The proposed 2-3D PRC has consisted of two coil sets (receiving and load coils). In each of receiving and load coil set, three orthogonal coils (three coils are perpendicular to each other or aligned in three axis *x*, *y*, and *z*) have been used. The three receiving coils were reeled orthogonally on a common ferrite core materials. Then, the load coils were reeled on each of receiving coil. The receiving coil formed a closed loop by connecting to the resonating capacitor. The load coils were connected to the load through the resonating capacitor and full wave bridge rectifier in power combining configuration. In this configuration, the load is not directly connected to the receiving coil, thus the effect of load resistance to the receiving coil is minimized and it ensures the high quality factor of receiving coil as

University of Malaya

well as high power transfer efficiency. On the other hand, all the load coils are connected to the load in series. Thus, each of three load coils offers power to the load if the received power is above the threshold level of rectifier. This configuration has tremendously improved the orientation stability of received power.

v. Improvement of received power stability

The overall received power stability ($P_{L,S}$) has been tremendously improved by the new configuration of PTC and power combining technique. The total stability of received power has two types: i) position stability ($P_{L,}$ ps); which was improved by the uniform *H*-field generated by the PTC, and ii) orientation stability ($P_{L,}$os); which was improved by the power combining technique applied to the load coils. The improvement has been compared with that of existing results in Table 6.1. As it can be seen in the Table 6.1, this work attained $P_{L,S}$ around 79.2% which was 45.3% higher than the $P_{L,S}$ attained by Xin *et al.* (2010). This improvement will be higher if the $P_{L,}$ps of this work is measured within 0.5 times of PTC radius like that in (Xin *et al.* 2010). However, for a compact wearable PTC, the $P_{L,}$ps of this work is measured within 0.75 times of PTC radius. The overall $P_{L,S}$ is compared with one of previous works because, among the existing papers, only Xin *et al.* (2010) presented the full figure of $P_{L,S}$.

Table 6.1: Comparison of received power stability.

	($P_{L,}$ ps) in %	**($P_{L,}$ os) in %**	**($P_{L,}$ s) in %**
(Xin *et al.*, 2010)	82.1	41.3	33.9
This work	96.9	81.6	79.2

vi. Improvement of PTE

The overall PTE of proposed WPT system has been remarkably improved by this research work. To improve the PTE, several techniques have been used. The used techniques were : i) optimization of number of strands in the PRC, ii) new configuration PTC, iii) mixed resonance scheme, iv) 3-coil inductive link, and v) 2-

3D PRC with power combining series configuration. The optimization of number of strands in the PRC within the given space minimizes the resistive loss in the PRC. In addition, the new configuration of PTC improves the quality factor and coupling coefficient that contribute for high PTE. Additionally, the mixed resonance scheme allows maximum power delivering to the load. The 3-coils link has also minimized the effect of load resistance on the receiving coil to ensure the high quality factor. Moreover, the 2-3D PRC and power combining configuration compensate the low power in worst misalignment cases. Thus, all of these techniques contribute to improve the PTE. The final design of wearable WPT system with the above techniques has attained the overall PTE of 8.21%. This PTE is remarkably higher than that were attained by the other works as shown in Table 6.2.

Table 6.2: Comparison of PTE attained by the proposed and existing system.

Work/study	Size of PTC, PRC in cm	PTE in %
(Xin *et al.*, 2010)	65, 1.2	3
(Sun *et al.*, 2012)	48, 1.1	3.04
(Na *et al.*, 2015)	22, 0.9	0.02
(He *et al.*, 2015)	50, 1.4	2
(Ke *et al.*, 2016)	69, 0.95	3.55
(Ding *et al.*, 2016)	1.33, 15.9	1.21
This study	35, 1.2	8.21

vii. Analysis of electromagnetic effect with incorporation of ferrite core

The electromagnetic exposure effect of patient's body tissues has been assessed in other studies (Xin *et al.*, 2010; Zhiwei *et al.*, 2011) using only PTC and a human body model, where the PRC and ferrite core have not been included. However, the high permeability ferrite core densifies the magnetic flux in and around it, therefore, the investigation of electromagnetic effect on the tissue proximity to the core was important. In this study, the electromagnetic effect has been analyzed with incorporation of PRC and high permeability ferrite core. This analysis reveals that the

University of Malaya

induced current density is relatively higher in the tissues proximity to the PRC with high permeability ferrite core than the tissue proximity to the PTC. That reduced the amount of power that could be transferred with following the ICNIRP guideline. The analysis of current density in this research indicates that within the ICNIRP guideline, around 200 mW of power could be transferred with the proposed WPT system.

6.4 Limitation of the Study

This thesis has mainly focused on improvement of the PTE and RPS. The experiments of this thesis have been conducted with manual tuning at transmitting side. Although, a fine tuning circuit has been adjusted which can compensate very small level of detuning, however, incorporation of an auto-tuning system will make the proposed system more practical. In addition, the electromagnetic safety analysis has been performed with multi-layer homogeneous body model to access induce current density. The simulation of current density with high-resolution heteronomous body model or investigation of long-term effect in the animal body will provide more clear evidence on electromagnetic safety.

6.5 Recommendations for Future Works

The research work reported in this thesis can be further extended as listed below:

i. Investigation on single side auto tuning circuit that can work with high voltage and high quality inductive coil for compensation of any detuning in wireless power transmission link

This research work has been carried out mainly on the performance improvement of the inductive power link with rigorous analysis and characterization of different coil configuration. It would be interesting to investigate on single side auto tuning circuit. The power receiver in this application of WPT system works inside the human body,

University of Malaya

therefore, the implemented tuning circuit in receiving side is not practical. Whereas it could be applied in transmitting side. The auto tuning circuit would be able to compensate any detuning of the resonance frequency in the power transmission link and ensure the expected performance not fall down. However, the effect of tuning circuit itself on the resonant power transmission link should be minimum as much as possible. In addition, the tuning circuit needs to be able to work in high voltage (several kV) environment.

ii. Investigation of using the proposed PTCs where high H-field uniformity is important such as magnetic resonance imaging.

Uniform magnetic field is important for many different areas such as magnetic resonance imaging, sensors calibration, and some other industrial applications. However, the advantage of highly uniform magnetic field of proposed PTCs especially PTC-III is evaluated for WPT application. Therefore, the effectiveness of PTC-III could be evaluated for other applications.

iii. Investigation on the long term electromagnetic exposure effect in animal.

The electromagnetic exposure effect of WPT system has been analyzed in this study by the simulation of current density with looking at the guideline provided by the ICNIRP. According to ICNIRPT guideline, the WPT system was safe for a certain amount of power transfer, nonetheless, analysis of long term effect in animal body will be an interesting topic, since in this application high power is required to transfer energy for long period of time.

University of Malaya

REFERENCES

Adler, S. N., & Hassan, C. (2013). *Colon Capsule Endoscopy: Quo Vadis?*: Intech Open Access Publisher.

Ahn, D., & Hong, S. (2014). Wireless power transmission with self-regulated output voltage for biomedical implant. *IEEE Transactions on Industrial Electronics, 61*(5), 2225-2235.

Aldhaher, S. (2014). Design and optimization of switched-mode circuits for inductive links. (Unpublished doctoral dissertation). Cranfield University, Cranfield, UK.

Arai, S., Miura, H., Sato, F., Matsuki, H., & Sato, T. (2005). Examination of circuit parameters for stable high efficiency TETS for artificial hearts. *IEEE transactions on magnetics, 41*(10), 4170-4172.

Barman, S. D., Reza, A. W., Kumar, N., Karim, M. E., & Munir, A. B. (2015). Wireless powering by magnetic resonant coupling: Recent trends in wireless power transfer system and its applications. *Renewable and Sustainable Energy Reviews, 51*, 1525-1552.

Beiranvand, R. (2013). Analyzing the uniformity of the generated magnetic field by a practical one-dimensional helmholtz coils system. *Review of Scientific Instruments, 84*(7), 1-11.

Carta, R., & Puers, R. (2011). Wireless power and data transmission for robotic capsule endoscopes. *18th IEEE Symposium on Communications and Vehicular Technology in the Benelux*.

Carta, R., Sfakiotakis, M., Pateromichelakis, N., Thoné, J., Tsakiris, D. P., & Puers, R. (2011). A multi-coil inductive powering system for an endoscopic capsule with vibratory actuation. *Sensors and Actuators A: Physical, 172*(1), 253-258.

Carta, R., Thoné, J., & Puers, R. (2009). A 3D Ferrite Coil Receiver for Wireless Power Supply of Endoscopic Capsules. *Procedia Chemistry, 1*(1), 477-480.

Carta, R., Thoné, J., & Puers, R. (2010). A wireless power supply system for robotic capsular endoscopes. *Sensors and Actuators A: Physical, 162*(2), 177-183.

Chen, L., Liu, S., Zhou, Y. C., & Cui, T. J. (2013). An optimizable circuit structure for high-efficiency wireless power transfer. *IEEE Transactions on Industrial Electronics, 60*(1), 339-349.

University of Malaya

Cheon, S., Kim, Y.-H., Kang, S.-Y., Lee, M. L., Lee, J.-M., & Zyung, T. (2011). Circuit-model-based analysis of a wireless energy-transfer system via coupled magnetic resonances. *IEEE Transactions on Industrial Electronics, 58*(7), 2906-2914.

Christ, A., Douglas, M., Nadakuduti, J., & Kuster, N. (2013). Assessing human exposure to electromagnetic fields from wireless power transmission systems. *Proceedings of the IEEE, 101*(6), 1482-1493.

Cook, N. P., Widmer, H., & Sieber, L. (2013). Antennas and their coupling characteristics for wireless power transfer via magnetic coupling: Google Patents.

Ding, K., Yu, Y., Lin, H., & Xie, J. (2016). Wireless Power Transfer at Sub-GHz frequency for Capsule Endoscope. Progress In Electromagnetics Research C, 66, 55-61.

Drug, V. L. (2002). Wireless capsule endoscopy--a novel technique for visualising the gut. *Rev Med Chir Soc Med Nat Iasi, 106*(4), 845-847.

Ge, Z. Z., Hu, Y. B., Gao, Y. J., & Xiao, S. D. (2003). Clinical application of wireless capsule endoscopy. *Chinese Journal of Digestive Diseases, 4*(2), 89-92.

Ghoshal, U. C. (2013). Capsule Endoscopy: A New Era of Gastrointestinal Endoscopy *Endoscopy of GI Tract*. Rijeka: InTech

Ghotbi, I., Najarzadegan, M., Ashtiani, S., Shoaei, O., & Shahabadi, M. (2015) 3-Coil Orientation Insensitive Wireless Power Transfer for Capsule Endoscope. *23rd Iranian Conference on Electrical Engineering*, 1249-1254.

Guanying, M., Guozheng, Y., & Xiu, H. (2007). Power transmission for gastrointestinal microsystems using inductive coupling. *Physiological Measurement, 28*(3), 9-18.

International Commission on Non-Ionizing Radiation Protection. (1998). Guidelines for limiting exposure to time-varying electric, magnetic, and electromagnetic fields (up to 300 GHz). *Health Phys, 74*(4), 494-522.

He, S., Yan, G.-Z., Ke, Q., Wang, Z.-W., & Chen, W.-W. (2015). A wirelessly powered expanding-extending robotic capsule endoscope for human intestine. *International Journal of Precision Engineering and Manufacturing, 16*(6), 1075-1084.

University of Malaya

Hui, S. Y. R., Zhong, W., & Lee, C. K. (2014). A critical review of recent progress in mid-range wireless power transfer. *IEEE Transactions on Power Electronics, 29*(9), 4500-4511.

Iddan, G., Meron, G., Glukhovsky, A., & Swain, P. (2000). Wireless capsule endoscopy. *Nature, 405*(6785), 417-417.

Japan Society of Medical Electronics and Biological Engineering. (2002). *Basic Knowledge and Safety Management of Medical and Biological Engineering, 4th edn (Tokyo: Nankodo Co. Ltd)*, 42-60.

Jegadeesan, R., Nag, S., Agarwal, K., Thakor, N. V., & Guo, Y.-X. (2015). Enabling Wireless Powering and Telemetry for Peripheral Nerve Implants. *IEEE journal of biomedical and health informatics, 19*(3), 958-970.

Jia, Z., Yan, G., Shi, Y., & Zhu, B. (2012). A wireless power transmission system for an active capsule endoscope for colon inspection. *Journal of Medical Engineering & Technology, 36*(5), 235-241.

Jia, Z., Yan, G., Shi, Y., & Zhu, B. (2012). A wireless power transmission system for an active capsule endoscope for colon inspection. *Journal of medical engineering & technology, 36*(5), 235-241.

Jia, Z. W., Yan, G. Z., Liu, H., Wang, Z. W., Jiang, P. P., & Shi, Y. (2012). The optimization of wireless power transmission: design and realization. *International Journal of Medical Robotics and Computer Assisted Surgery, 8*(3), 337-347.

Jonah, O., Georgakopoulos, S. V., & Tentzeris, M. M. (2013). *Orientation insensitive power transfer by magnetic resonance for mobile devices.* IEEE Wireless Power Transfer, 5-8.

Jourand, P., & Puers, R. (2012). A Class-E driven inductive power delivery system covering the complete upper body. *Sensors and Actuators A: Physical, 183*(0), 132-139.

Ju, X., Dong, L., Huang, X., & Liao, X. (2015). Switching Technique for Inductive Power Transfer at High-Regimes. *IEEE Transactions on Industrial Electronics, 62*(4), 2164-2173.

Jusoh, M., Kamarudin, M. R., Basar, M. R., Jack, S. P., Sabapathy, T., & Azir, K. N. F. K. (2015). Synthesis of a Biasing Circuit for a Reconfigurable WiMAX Antenna

University of Malaya

(RWA) at 2.3 GHz *Theory and Applications of Applied Electromagnetics*, 145-153.

Ke, Q., Luo, W., Yan, G., & Yang, K. (2016). Analytical Model and Optimized Design of Power transmission coilfor Inductively Coupled Endoscope Robot. *IEEE Transactions on Biomedical Engineering, 63*(4), 694-706.

Koulaouzidis, A., & Dabos, K. J. (2013). Looking forwards: Not necessarily the best in capsule endoscopy? *Annals of Gastroenterology, 26*(4), 365-367.

Lee, S. H., Lee, J., Yoon, Y. J., Park, S., Cheon, C., Kim, K., & Nam, S. (2011). A wideband spiral antenna for ingestible capsule endoscope systems: experimental results in a human phantom and a pig. *IEEE Transactions on Biomedical Engineering, 58*(6), 1734-1741.

Lenaerts, B., & Puers, R. (2005). Inductive powering of a freely moving system. *Sensors and Actuators A: Physical, 123–124*(0), 522-530.

Lenaerts, B., & Puers, R. (2007). An inductive power link for a wireless endoscope. *Biosens Bioelectron, 22*(7), 1390-1395.

Li, C.-y., Zhang, B.-l., Chen, C.-x., & Li, Y.-m. (2008). OMOM capsule endoscopy in diagnosis of small bowel disease. *Journal of Zhejiang University SCIENCE B, 9*(11), 857-862.

Li, H., Yan, G., & Ma, G. (2008). An active endoscopic robot based on wireless power transmission and electromagnetic localization. *The International Journal of Medical Robotics and Computer Assisted Surgery, 4*(4), 355-367.

Lin, J. C. (2006). A new IEEE standard for safety levels with respect to human exposure to radio-frequency radiation. *IEEE Antennas Propag. Magazine 48*(1), 157-159.

Liu, G., Yan, G., Xu, W., & Kuang, S. (2015). Dual-head wireless powered video capsule based on new type of receiving coils. *Journal of medical engineering & technology, 39*(4), 246-252.

Liu, H., Shao, Q., & Fang, X. (2016). Modeling and Optimization of Class-E Amplifier at Subnominal Condition in a Wireless Power Transfer System for Biomedical Implants. *IEEE Transactions on Biomedical Circuits and Systems,* 11(1), 35-43.

University of Malaya

Mavrogenis, G., Coumaros, D., Renard, C., Bellocq, J. P., Defta, D., Charneau, D., & Leroy, J. (2011). Jejunal gastrointestinal stromal tumor missed by three capsule endoscopies. *Endoscopy, 43*(8), 735-736.

Moglia, A., Menciassi, A., Dario, P., & Cuschieri, A. (2009). Capsule endoscopy: progress update and challenges ahead. *Nature Reviews Gastroenterology & Hepatology, 6*(6), 353-362.

Mustafa, B. F., Samaan, M., Langmead, L., & Khasraw, M. (2013). Small bowel video capsule endoscopy: An overview. *Expert Review of Gastroenterology and Hepatology, 7*(4), 323-329.

Myer, P. A., Mannalithara, A., Singh, G., Singh, G., Pasricha, P. J., & Ladabaum, U. (2013). Clinical and economic burden of emergency department visits due to gastrointestinal diseases in the United States. *American Journal of Gastroenterology, 108*(9), 1496-1507.

Na, K., Jang, H., Ma, H., & Bien, F. (2015). Tracking Optimal Efficiency of Magnetic Resonance Wireless Power Transfer System for Biomedical Capsule Endoscopy. *IEEE Trans. Microw. Theory Tech., 63*(1), 295-304.

Nakamoto, H., Yamazaki, D., Yamamoto, T., Kurata, H., Yamada, S., Mukaida, K., . . . Gotoh, K. (2006). *A passive UHF RFID tag LSI with 36.6% efficiency CMOS-only rectifier and current-mode demodulator in 0.35/spl mu/m FeRAM technology.* Paper presented at the IEEE International Solid-State Circuits Conference.

Narendra, K., & YewKok, T. (2014a). A design technique to improve harmonic suppression in high efficiency wideband Class E RF power amplifier. *IEICE Electronics Express, 11*(3), 1-6.

Narendra, K., & YewKok, T. (2014b). Optimised high-efficiency Class E radio frequency power amplifier for wide bandwidth and high harmonics suppression. *IET Circuits, Devices & Systems, 8*(2), 82-89.

O'Driscoll, S., Poon, A. S., & Meng, T. H. (2009). *A mm-sized implantable power receiver with adaptive link compensation.* Paper presented at the IEEE International Solid-State Circuits Conference-Digest of Technical Papers.

Pan, G., & Wang, L. (2011). Swallowable wireless capsule endoscopy: progress and technical challenges. *Gastroenterology research and practice,* 1-5.

University of Malaya

Pan, G. B., Xin, W. H., Yan, G. Z., & Chen, J. L. (2011). A video wireless capsule endoscopy system powered wirelessly: design, analysis and experiment. *Measurement Science & Technology, 22*(6).

Puers, R., Carta, R., & Thone, J. (2011). Wireless power and data transmission strategies for next-generation capsule endoscopes. *Journal of Micromechanics and Microengineering, 21*(5).

Qingwei, Z., Yanjie, G., Lifang, W., Chenglin, L., & Fang, L. (2015). Improving the Misalignment Tolerance of Wireless Charging System by Optimizing the Compensate Capacitor. *IEEE Transactions on Industrial Electronics, 62*(8), 4832-4836.

RamRakhyani, A. K., Mirabbasi, S., & Chiao, M. (2011). Design and Optimization of Resonance-Based Efficient Wireless Power Delivery Systems for Biomedical Implants. *IEEE Trans. Biomed. Circuits Systs., 5*(1), 48-63.

Roes, M. G., Duarte, J. L., Hendrix, M. A., & Lomonova, E. A. (2013). Acoustic energy transfer: a review. *IEEE Transactions on Industrial Electronics, 60*(1), 242-248.

Ryu, M., Kim, J. D., Chin, H. U., Kim, J., & Song, S. Y. (2007). Three-dimensional power receiver for in vivo robotic capsules. *Medical & Biological Engineering & Computing, 45*(10), 997-1002.

Sample, A. P., Meyer, D., & Smith, J. R. (2011). Analysis, experimental results, and range adaptation of magnetically coupled resonators for wireless power transfer. *IEEE Transactions on Industrial Electronics., 58*(2), 544-554.

Schuylenbergh, K. V., & Puers, R. (2009). Inductive powering: basic theory and application to biomedical systems. Netherlands: Springer Science & Business Media.

Shi, Y., Yan, g., Jia, Z., & Zhu, B. (2012). *The Design and Implementation of the Wireless Power Transmission System of Video Capsule Endoscopy.* Paper presented at the International Conference on Biomedical Engineering and Biotechnology.

Shi, Y., Yan, G., Zhu, B., Liu, G., Liu, F., Lee, D.-H., . Kumar, S. (2015). A portable wireless power transmission system for video capsule endoscopes. *Bio-Medical Materials and Engineering, 26*(s1), S1721-S1730.

Shiba, K., & Higaki, N. (2009, 12-16 Jan. 2009). *Analysis of SAR and Current Density in Human Tissues Surrounding an Energy Transmitting Coil for a Wireless Capsule*

University of Malaya

Endoscope. Paper presented at 20th International Zurich Symposium on the Electromagnetic Compatibility.

Shiba, K., Morimasa, A., & Hirano, H. (2010). Design and Development of Low-Loss Transformer for Powering Small Implantable Medical Devices. *IEEE Transactions on Biomedical Circuits and Systems, , 4*(2), 77-85.

Shiba, K., Nagato, T., Tsuji, T., & Koshiji, K. (2008a). Energy transmission transformer for a wireless capsule endoscope: analysis of specific absorption rate and current density in biological tissues. *IEEE Trans Biomed Eng, 55*(7), 1864-1871.

Shiba, K., Nagato, T., Tsuji, T., & Koshiji, K. (2008b). Energy Transmission Transformer for a Wireless Capsule Endoscope: Analysis of Specific Absorption Rate and Current Density in Biological Tissues. *IEEE Transactions on Biomedical Engineering, 55*(7), 1864-1871.

Shibuya, T., & Shiba, K. (2013). *Externally-coupled transcutaneous energy transmission for a ventricular assist device-Miniaturization of ferrite core and evaluation of biological effects around the transformer*. Paper presented at the 2013 IEEE Biomedical Circuits and Systems Conference.

Sumin, Y., Kihyun, K., & Sangwook, N. (2010). Outer-Wall Loop Antenna for Ultrawideband Capsule Endoscope System. *IEEE Antennas and Wireless Propagation Letters, 9*, 1135-1138.

Sun, T., Xie, X., & Wang, Z. (2013). *Wireless power transfer for medical microsystems*: Springer.

Sun, T. J., Xie, X., Li, G. L., Gu, Y. K., Deng, Y. D., & Wang, Z. H. (2012). A Two-Hop Wireless Power Transfer System With an Efficiency-Enhanced Power Receiver for Motion-Free Capsule Endoscopy Inspection. *IEEE Transactions on Biomedical Engineering, 59*(11), 3247-3254.

Swain, P. (2008). The future of wireless capsule endoscopy. *World Journal of Gastroenterology, 14*(26), 4142-4145.

Uehara, & Hoshina. (2003). Capsule endoscope NORIKA system. *Minim Invasive Ther Allied Technol, 12*(5), 227-234.

Vandevoorde, G., & Puers, R. (2001). Wireless energy transfer for stand-alone systems: a comparison between low and high power applicability. *Sensors and Actuators A: Physical, 92*(1), 305-311.

University of Malaya

Wang, G., Liu, W., Sivaprakasam, M., Weiland, J. D., & Humayun, M. S. (2005). *High efficiency wireless power transmission with digitally configurable stimulation voltage for retinal prosthesis.* Paper presented at 2nd International IEEE EMBS Conference on Neural Engineering.

Westerhof, J., Koornstra, J. J., Hoedemaker, R. A., Sluiter, W. J., Kleibeuker, J. H., & Weersma, R. K. (2012). Diagnostic yield of small bowel capsule endoscopy depends on the small bowel transit time. *World Journal of Gastroenterology, 18*(13), 1502-1507.

Xiang, X., Guolin, L., Baoyong, C., XueYi, Y., Chun, Z., & Zhihua, W. (2005). *Micro-system Design for Wireless Endoscopy System.* Paper presented at 27th Annual International Conference of the Engineering in Medicine and Biology Society IEEE-EMBS.

Xin, W., Yan, G., & Wang, W. (2010). Study of a wireless power transmission system for an active capsule endoscope. *Int J Med Robot, 6*(1), 113-122.

Xin, W. H., Yan, G. Z., & Wang, W. X. (2010). A stable wireless energy transmission system for gastrointestinal microsystems. *J Med Eng Technol, 34*(1), 64-70.

Xue, R. F., Cheng, K. W., & Je, M. (2013). High-efficiency wireless power transfer for biomedical implants by optimal resonant load transformation. *IEEE Transactions on Circuits and Systems I: Regular Papers, 60*(4), 867-874.

Xuelin, F., Hao, L., Guiyang, L., Qi, S., & Hongyi, L. (2011). *Wireless power transfer system for capsule endoscopy based on strongly coupled magnetic resonance theory.* Paper presented at International Conference on Mechatronics and Automation (ICMA).

Yadong, H., Jianfeng, W., Tianjia, S., Xiang, X., Guolin, L., Yingke, G., & Zhihua, W. (2013a). *An efficiency-enhanced wireless power transfer system with segmented transmitting coils for endoscopic capsule.* Paper presented at the IEEE International Symposium on Circuits and Systems

Yan, L., Lee, S., Kim, Y., Kim, H., Kim, B., & Yoo, H.-J. (2009). *A 5.2 mW self-configured wearable body sensor network controller and a 12μW 54.9% efficiency wirelessly powered sensor for continuous health monitoring system.* Paper presented at the IEEE International Solid-State Circuits Conference-Digest of Technical Papers.

University of Malaya

Yan, L., Wang, T., Liu, D., Peng, J., Jiao, Z., & Chen, C.-Y. (2015). Capsule Robot for Obesity Treatment With Wireless Powering and Communication. *IEEE Trans. Ind. Electron.*, *62*(2), 1125-1133.

Yang, Z., Liu, W., & Basham, E. (2007). Inductor modeling in wireless links for implantable electronics. *Magnetics, IEEE Transactions on*, *43*(10), 3851-3860.

Ye, D., Yan, G., Wang, K., & Ma, G. (2008). Development of a micro-robot for endoscopes based on wireless power transfer. *Minim Invasive Ther Allied Technol*, *17*(3), 181-189.

Yu, X., & Zhang, J. (2013). Gastric cancer with large bowel obstruction as the first presentation: A case report. *Oncology Letters*, *6*(5), 1377-1379.

Zhiwei, J., Guozheng, Y., Jiangpingping, Zhiwu, W., & Hua, L. (2011). Efficiency optimization of wireless power transmission systems for active capsule endoscopes. *Physiol Meas*, *32*(10), 1561-1573.

Zhu, B., Yan, g., Jia, Z., & Shi, Y. (2012). *Portable Wireless Power Transmission System of a Video Capsule Endoscopy: Design and Realization.* Paper presented at the International Conference on Biomedical Engineering and Biotechnology.

University of Malaya

LIST OF PUBLICATIONS AND PAPERS PRESENTED

Journal Papers

Basar, M. R., Ahmad, M. Y., Cho, J., & Ibrahim, F. (2014a). Application of Wireless Power Transmission Systems in Wireless Capsule Endoscopy: An Overview. *Sensors*, *14*(6), 10929-10951: (Q1, IF: 2.033, ISI-Indexed).

Basar, M. R., Ahmad, M. Y., Cho, J., & Ibrahim, F. (2017). Stable and High-efficiency Wireless Power Transfer System for Robotic Capsule Using a Modified Helmholtz Coil. *IEEE Transactions on Industrial Electronics*, 64(2), 1113-1122: (Q1, IF: 6.383, ISI-Indexed)

Basar, M. R., Ahmad, M. Y., Cho, J., & Ibrahim, F. (2016a). Resonant wireless power transfer system with optimum coil configuration for capsule endoscopy. *Sensors and Actuators A: Physical*, 249 (1 October 2016). 207-216: (Q1, IF: 2.201, ISI-Indexed).

Mateen, H., Basar, M. R., Ahmed, A. U., Ahmad, M. Y., (2017). Localization of Wireless Capsule Endoscope: A Systematic Review. *IEEE Sensors Journal*, 17(5), 1197-1206: (Q2, IF: 1.889, ISI-Indexed).

Conference Papers

Basar, M. R., Ahmad, M. Y., Cho, J., & Ibrahim, F. (2014b). A wireless power transmission system for robotic capsule endoscopy: Design and optimization. In *IEEE RF and Wireless Technologies for Biomedical and Healthcare Applications (IMWS-Bio)*, 1-3.

Basar, M. R., Ahmad, M. Y., Cho, J., & Ibrahim, F. (2015). Performance evaluation of power transmission coils for powering endoscopic wireless capsules. In *IEEE Engineering in Medicine and Biology Society (EMBC)*, 2263-2266.

Basar, M. R., Yazed, A. M., Cho, J., & Fatimah, I. (2016b). *Resonant Inductive Power Transfer System for Freely Moving Capsule Endoscope with Highly Uniform Magnetic Field.* Paper presented at IEEE Industrial Electronics and Applications Conference (IEACon), Sabah, Malaysia.

Basar, M. R., Yazed, A. M., Cho, J., & Fatimah, I. (2017). *A 3-coil Inductive Wireless Power Transfer System with Fine Tuned Power Amplifier for Biomedical Application* Submitted to IEEE Industrial Electronics and Applications Conference, Kuala Lumpur, Malaysia.

University of Malaya

University of Malaya

ERROR: syntaxerror
OFFENDING COMMAND: --nostringval--

STACK:

/Title
()
/Subject
(D:20170531124006+08’00’)
/ModDate
()
/Keywords
(PDFCreator Version 0.9.5)
/Creator
(D:20170531124006+08’00’)
/CreationDate
(WPT1)
/Author
-mark-

University of Malaya